Residual lifetime assessment of uPVC gas pipes

Roy Visser

RESIDUAL LIFETIME ASSESSMENT OF UPVC GAS PIPES

Roy Visser

De promotiecommissie is als volgt samengesteld:

Voorzitter en secretaris:
prof.dr. F. Eising — Universiteit Twente

Promotoren:
prof.dr.ir. R. Akkerman — Universiteit Twente
prof.dr.ir. M. Wolters — Universiteit Twente

Assistent promotor:
dr.ir. L.E. Govaert — Technische Universiteit Eindhoven

Leden (in alfabetische volgorde):
prof.dr.ir. A. de Boer — Universiteit Twente
dr.ir. T.C. Bor — Universiteit Twente
prof.dr. R.W. Lang — Johannes Kepler Universität Linz
prof.dr. G.J. Vancso — Universiteit Twente

This research project is financially supported by Cogas Infra en Beheer, Enexis, Liander and Stedin.

Residual lifetime assessment of uPVC gas pipes
Visser, Hendrikus Antonius
PhD Thesis, University of Twente, Enschede, The Netherlands
December 2009

ISBN 978-90-365-2958-7
DOI 10.3990/1.9789036529587

Printed by PrintPartners Ipskamp B.V, Enschede, the Netherlands

Cover: photographs of beach animals. These creatures live on wind and are made from PVC pipes by Theo Jansen (more information: www.strandbeest.com). Front: the Percipiere family at the beach of IJmuiden. Back: close-up of the Animaris Percipiere Primus. Both photographs were taken by Loek van der Klis (www.loekvanderklis.com) and are used with permission.

RESIDUAL LIFETIME ASSESSMENT OF UPVC GAS PIPES

PROEFSCHRIFT

ter verkrijging van
de graad van doctor aan de Universiteit Twente,
op gezag van de rector magnificus,
prof.dr. H. Brinksma,
volgens besluit van het College voor Promoties
in het openbaar te verdedigen
op vrijdag 22 januari 2010 om 15.00 uur

door

Hendrikus Antonius Visser

geboren op 6 februari 1980

te Amersfoort

Dit proefschrift is goedgekeurd door de promotoren:

prof.dr.ir. R. Akkerman
prof.dr.ir. M. Wolters

en door de assistent promotor:

dr.ir. L.E. Govaert

Summary

The Dutch gas distribution network consists of about 20% (22,500 km) of unplasticised poly(vinyl chloride) (uPVC) pipes, most of which have been installed from the mid-sixties up to the mid-seventies of the previous century and have been in service ever since. In the next decade the specified service lifetime of 50 years will be reached for these pipes. Replacing the uPVC gas pipes exactly after this specified service lifetime will lead to a costly and extremely labour intensive project. Postponing the replacement is only an option when this can be done without compromising the integrity of the network. It is therefore of great value for the network operators to have full knowledge on the condition of the pipes in their network. In this thesis the framework for a method that can determine the condition, and therewith the residual lifetime, of uPVC gas pipes is developed.

Recent failure data shows that the majority of the failures in uPVC gas pipes is caused by excavation activities (third-party damage). The risk of life threatening situations after such a failure is considerably higher for a brittle fracture than for ductile failure behaviour of the pipe. Brittle uPVC gas pipes should therefore be replaced, which makes the impact behaviour the limiting factor for the service lifetime of these pipes. A review of the degradation mechanisms occurring during the lifetime of uPVC pipes shows that physical ageing is expected to be the most important mechanism that causes embrittlement. During physical ageing the polymer chains move towards their thermodynamically favoured positions, causing an increase in resistance against plastic deformation. Moreover the deformation behaviour localises, causing embrittlement on a macroscopic scale. The focus of this thesis is therefore on the influence of physical ageing on the mechanical behaviour of uPVC gas pipes. The procedure of determining the residual lifetime is based on these findings and is split into four aspects: the choice of a measure for the condition of the pipe material, characterisation of the change of the condition in time (its ageing kinetics), determining the critical condition and development of a method of measuring the current condition. Each of these aspects is individually described in consecutive chapters.

The yield behaviour is selected as the measure for the condition of uPVC gas pipes, as the yield stress is a direct measure for the thermodynamic state (i.e. the age) and can also be linked to the impact behaviour of the material. The yield stress behaviour of uPVC is characterised using short-term tensile tests (at a wide range of strain rates and temperatures) in Chapter 1. The yield behaviour is accurately described by a pressure-modified Eyring relation that links the applied deformation rate to the yield stress and, vice versa, the applied stress to the plastic deformation rate. By hypothesising that failure occurs at a constant value of the accumulated plastic strain, the pressure-modified Eyring relation can be used to predict the failure time of loaded glassy polymers. This engineering approach is successfully applied to predict the time-to-failure of both polycarbonate and uPVC specimens. The predicted influence of stress level, temperature, loading geometry and thermal history of the specimens on the time-to-failure is in excellent quantitative agreement with experimentally obtained failure data. Furthermore, it is shown that the engineering approach can also be employed to predict the failure time for a pipe subjected to a constant internal pressure. This approach makes it possible to determine the long-term hydrostatic strength (LTHS) based on short-term tests only, and eliminates the necessity to carry out expensive long-term pressurised pipe tests (under the assumption that slow crack growth failure does not limit the LTHS).

As already stated, physical ageing is expected to be the most important ageing process during the lifetime of uPVC gas pipes. The influence of physical ageing on the yield behaviour of uPVC is characterised and modelled in Chapter 2. The engineering approach presented in Chapter 1 is extended to include this ageing behaviour. The resulting approach is employed to predict experimentally obtained long-term failure data for tensile specimens and pipe segments subjected to a constant load. Some of these data sets reveal a so-called endurance limit caused by the ageing induced change in deformation behaviour. The good quantitative agreement between predictions and the experimental data is a strong indication that the physical ageing kinetics of the yield stress is described successfully. Moreover, the engineering approach is applied to the failure of tensile specimens subjected to a dynamic stress signal. The influence of both the frequency and the stress ratio of the signal has been proven to be correctly accounted for. The predictions of the failure times are rather conservative as the influence of physical ageing is somewhat underestimated for dynamic stress signals. At lower levels of dynamic stresses a second type of failure kinetics becomes apparent: fatigue crack growth failure. Preliminary results on fatigue crack growth failure show that slow crack growth failure can be ruled out as a limiting factor during the service life of uPVC gas pipes. These results confirm that physical ageing can indeed be expected to be the critical embrittlement process for uPVC gas pipes.

The residual lifetime of the uPVC pipes can only be determined when the critical thermodynamic state at which the pipe should be taken out of service is known. As mentioned before, the fracture behaviour upon an impact load, such as those encountered during excavation activities, is a limiting factor for safe deployment of uPVC gas pipes. A direct relation between a critical yield stress and the ductile-to-brittle transition temperature ($T_{d\rightarrow b}$, a measure for the impact behaviour of the material) is hypothesised in Chapter 3. The influence of physical ageing on the $T_{d\rightarrow b}$ of uPVC pipe material is determined employing instrumented falling weight tests on specimens taken from a uPVC water pipe at a range of thermodynamic states. The uPVC water pipe grade used in the experiments shows only a small increase in $T_{d\rightarrow b}$ for the range of thermodynamic states investigated. The measured increase is in reasonable agreement with the prediction that follows from the proposed relation between the constant critical yield stress, $T_{d\rightarrow b}$ and the ageing kinetics of this water pipe grade. Applying the ageing kinetics of the gas pipe grade, which differs significantly from that of the water pipe grade, shows that a more pronounced increase in $T_{d\rightarrow b}$ can be expected from the gas pipe grade during its service life. This indicates that uPVC gas pipes can be expected to embrittle during their service life, as a result of physical ageing.

The last aspect that is studied is in which way the condition of the pipes can be determined in a non-destructive way. Micro-indentation measurements were performed to probe the condition of uPVC pipes by relating the hardness that follows from the indentation curve with the yield stress of the material. The hardness proves to behave similarly as a function of time and temperature as the yield stress. In fact, a linear relation between hardness and yield stress is found within the range of thermodynamic states investigated. The rather low resolution of the lifetime assessment procedure is mainly caused by the scatter of the experimental data around the linear relation between the hardness and the yield stress. Decreasing the influence of local effects on the indentation measurement might decrease the scatter and improve the resolution of the procedure.

With all four aspects of the lifetime assessment method considered, important steps towards a non-destructive condition measurement procedure for uPVC gas pipes are taken.

Samenvatting

Het Nederlandse gasdistributienetwerk verschilt van de gasnetwerken van andere landen doordat er naast het meer gebruikte polyethyleen ook poly(vinyl chloride) (PVC) leidingen toegepast zijn. Vanaf de jaren zestig tot midden jaren zeventig werd hard (ongeplastificeerd) PVC gebruikt. Daarna werd slagvast PVC het voorkeursmateriaal voor lage druk gasleidingen. Momenteel is er nog ongeveer 22.500 km hard PVC leidingen in gebruik in de lage druk (100 mbar) gasdistributiesystemen. Initiëel is de levensduurverwachting van de hard PVC leidingen op 50 jaar geschat. Gezien de leeftijd van de eerste generatie hard PVC leidingen wordt er in de komende 10 jaar een vervangingsgolf voorzien wanneer de netbeheerders besluiten de hard PVC leidingen op basis van anciënniteit te vervangen. Hierbij is een tweetal problemen te verwachten. Ten eerste zijn de kosten van dit vervangingsproces exorbitant hoog en ten tweede is er niet genoeg specialistisch personeel om het uit te voeren. Uitstellen is echter alleen mogelijk wanneer de veiligheid van het netwerk niet in gevaar komt. Daarom is vanuit vier Nederlandse gasnetbeheerders een onderzoek gestart naar het ontwikkelen van een techniek waarmee de restlevensduur van hard PVC gasleidingen op een niet-destructieve manier bepaald kan worden. Met behulp van een dergelijke meetmethodiek kunnen de netbeheerders in de toekomst hun vervangingsbeleid afstemmen.

Uit een analyse van recente storingdata van het gasnetwerk blijkt dat hard PVC leidingen even betrouwbaar zijn als nieuwere typen leidingmaterialen. Tevens kan uit deze gegevens worden afgeleid dat het falen van hard PVC leidingen meestal veroorzaakt wordt door graafwerkzaamheden. De kans op het ontstaan van een gevaarlijke situatie hangt bij dit soort falen sterk af van de manier waarop de leiding breekt. Wanneer de leiding op een brosse manier breekt, zal de gasuitstroom moeilijker te stelpen zijn dan bij een taaie breuk. Bovendien is een brosse leiding minder bestand tegen stootbelastingen. Het is een bekend fenomeen dat amorfe thermoplasten, zoals hard PVC, verbrossings verschijnselen kunnen vertonen. Daarom is het van belang om te weten welke verouderingsprocessen tijdens het gebruik tot verbrossing van het materiaal kunnen leiden. Analyse van de verouderingsprocessen die kunnen optreden in hard

PVC leidingen leert dat fysische veroudering de belangrijkste bijdrage levert aan het verbrossen van hard PVC gasleidingen. Met het fysische verouderen komen de koolstofketens in het materiaal dichter bij elkaar te liggen, waardoor het materiaal dichter bij haar thermodynamische evenwicht komt te liggen. Hierdoor neemt de weerstand tegen plastische deformatie toe en zal dientengevolge de deformatie op lokalere schaal plaatsvinden, waardoor het materiaal zich brosser zal gedragen. De invloed van dit proces op de mechanische eigenschappen van hard PVC is in dit proefschrift nader bestudeerd om een methodiek te ontwikkelen waarmee de restlevensduur van de hard PVC gasleidingen kan worden bepaald. Het onderzoek is opgesplitst in vier onderdelen welke elk in een afzonderlijk hoofdstuk beschreven zijn. Eerst is er een graadmeter voor de conditie gekozen waaruit kan worden opgemaakt in welke mate het materiaal fysisch is verouderd. Vervolgens is de evolutie van de conditie van de leidingen in de tijd gekarakteriseerd. In het derde hoofdstuk is een relatie tussen deze evolutie en het verbrossen van het materiaal gelegd. Tot slot is er gezocht naar een niet-destructieve meetmethode welke in situ ingezet kan worden en informatie geeft over de huidige conditie van het materiaal. Door de vier onderdelen te combineren kan de restlevensduur van de hard PVC leiding bepaald worden.

De vloeispanning van het materiaal is geselecteerd als graadmeter voor de conditie van de hard PVC gasleidingen. Deze vloeispanning is direct te relateren aan de thermodynamische toestand waarin het materiaal zich bevindt en daarmee met de "schijnbare leeftijd"[1] van het materiaal. Het vloeigedrag van hard PVC is gekarakteriseerd middels trekproeven bij verschillende reksnelheden en temperaturen en beschreven met een Eyring-relatie. Door de drukafhankelijkheid van het vloeigedrag in deze relatie mee te nemen kan de vloei in verschillende (eenvoudige) 3D spanningstoestanden beschreven worden. Deze relatie is gecombineerd met de hypothese dat een polymeer faalt wanneer de plastische rek tot een kritische waarde accumuleert. Op deze wijze kan de tijd tot falen voor statisch belaste hard PVC proefstukken worden voorspeld. De aanpak is getoetst op zowel hard PVC als polycarbonaat proefstukken, binnen een breed temperatuurbereik, voor verschillende belastingtoestanden en -niveaus en voor proefstukken met verschillende thermodynamische toestanden. De voorspellingen bleken in alle gevallen nauwkeurig en ook data van langeduur barstdrukproeven kunnen correct voorspeld worden met de gepresenteerde aanpak. Hiermee wordt aangetoond dat dure, langdurende barstdrukproeven in de toekomst wellicht overbodig kunnen worden wanneer vloei uiteindelijk falen inleidt.

[1] Onder het begrip schijnbare leeftijd wordt hier de leeftijd van het materiaal op de gebruikstemperatuur van de gasleidingen verstaan. Op hogere temperaturen vindt fysische veroudering versneld plaats, waardoor een korte periode op een hoge temperatuur overeenkomt met een langere periode op een lagere temperatuur. De schijnbare leeftijd is een vertaling van de temperatuurhistorie die het materiaal heeft ondervonden naar de leeftijd op de gebruikstemperatuur van de hard PVC gasleiding.

Zoals eerder genoemd, levert fysische veroudering de belangrijkste bijdrage aan de verbrossing van hard PVC gasleidingen. Daarom is de invloed van dit proces op de vloeispanning van het materiaal nader bestudeerd door trekproeven uit te voeren op proefstukken die met een warmtebehandeling tot verschillende schijnbare leeftijden zijn verouderd. Naast een verhoging in de temperatuur zorgt een aangelegde spanning ook voor een versnelling van het verouderingsproces. Zowel de temperatuur- als de spanningsafhankelijkheid zijn gekarakteriseerd en modelmatig beschreven. Deze beschrijving is getoetst door de tijd tot falen te voorspellen voor een kruipexperiment waarin de proefstukken tijdens de meting verouderden (progressieve veroudering). Voor een statische belasting stemmen de voorspellingen kwantitatief overeen met de experimenteel bepaalde waarden. Worden de proefstukken echter dynamisch belast, dan is de voorspelling enigszins conservatief. Het is opvallend dat er bij dynamisch belaste proefstukken een tweede faalmechanisme optreedt, waar dat bij statisch belaste proefstukken niet het geval is. Dit tweede faalmechanisme is langzame scheurgroei onder invloed van vermoeiing. Het is bekend dat langzame scheurgroei ook onder invloed van statische belasting op kan treden. Conservatieve voorspellingen laten echter zien dat langzame scheurgroei falen in hard PVC niet optreedt tijdens de verwachte levensduur van hard PVC gasleidingen.

Om de restlevensduur te kunnen bepalen is het noodzakelijk dat er een bepaalde minimale slagvastheidseis vastgelegd wordt om een veilig functioneren in de praktijk te garanderen. In hoofdstuk 3 wordt de slagvastheid van hard PVC gekoppeld aan de schijnbare leeftijd van het materiaal. Hard PVC zal onder invloed van een slagbelasting taai of bros falen. Bij lage temperaturen zal het eerder op een brosse manier breken, terwijl bij hogere temperaturen taai falen preferent optreedt. Er is dus een temperatuur aan te wijzen waarop het materiaal overgaat van voornamelijk brosse naar voornamelijk taaie breuk. Deze taai-bros overgangstemperatuur neemt toe met de leeftijd van hard PVC leidingen als gevolg van fysische veroudering. Door geïnstrumenteerde valproeven op verschillende temperaturen uit te voeren en gebruik te maken van proefstukken die in verschillende mate verouderd zijn, is er een relatie gelegd tussen de taai-bros overgangstemperatuur en de leeftijd van het materiaal. Voor de hier beproefde hard PVC waterleiding[2] was de toename in de taai-bros overgangstemperatuur, ook voor proefstukken met een erg hoge schijnbare leeftijd, marginaal. Op basis van de eerder bepaalde verouderingskinetiek van het hard PVC gebruikt voor gasleidingen is te verwachten dat de effecten voor dit type leidingmateriaal uitgesprokener zullen zijn.

[2]Voor de geïnstrumenteerde valproef is veel materiaal nodig. Omdat er onvoldoende uniform hard PVC gasleidingmateriaal beschikbaar is, zijn er nieuw geproduceerde hard PVC waterleidingen voor de valproeven gebruikt.

Vanuit de opgebouwde kennis is de vloeispanning van het materiaal te relateren aan de slagvastheid en is bovendien de evolutie van de vloeispanning en dus de slagvastheid bekend. Om de restlevensduur van hard PVC gasleidingen te kunnen bepalen is er alleen nog een meetmethode nodig om de vloeispanning van de leidingen te kunnen bepalen. Deze meetmethode is bij voorkeur niet destructief, omdat bij een destructieve meting alsnog tot vervanging overgegaan dient te worden. Door op hele kleine schaal het materiaal te laten vloeien met een micro-indentatiemeting, is het mogelijk om de vloei-eigenschappen te meten zonder dat de meting op macroscopische schaal destructief is. De verandering van de met micro-indentatie bepaalde hardheid als gevolg van fysische veroudering volgt eenzelfde kinetiek als de in hoofdstuk 2 bepaalde verouderingskinetiek van de vloeispanning. Er wordt daarmee een lineaire relatie gevonden tussen de met micro-indentatie bepaalde hardheid en de vloeispanning van hard PVC. De resolutie van de vertaalslag van de meting naar de vloeispanning en de uiteindelijke restlevensduur zal echter in de toekomst nog verbeterd moeten worden voordat de meetmethodiek in de praktijk toegepast kan worden. Hiermee zijn er in deze studie belangrijke stappen gezet naar de ontwikkeling van een niet-destructieve, in situ meetmethodiek voor de restlevensduurbepaling van hard PVC gasleidingen.

Nomenclature

Roman symbols:

A	Pre-exponential factor in Paris law	[-]
A_p	Projected area of contact	[m^2]
a	Crack size	[m]
$a_{d,age}$	Acceleration of the ageing kinetics for one cycle defined in Equation (2.12)	[-]
$a_{d,\dot{\tilde{\gamma}}}$	Acceleration of the deformation kinetics for one cycle, defined in Equation (2.10)	[-]
a_σ	Stress induced acceleration factor defined in Equation (2.7)	[-]
a_T	Temperature induced acceleration factor defined in Equation (2.6)	[-]
B	Pre-exponential factor used in Equation (2C.1)	[-]
b_0	Pre-exponential factor in ageing kinetics	[s^{-1}]
b_1	Exponent in ageing kinetics	[-]
d_0, d_1	Fit factors in Equation (3.8)	[-]
D	Outer diameter	[m]
E	Absorbed energy	[J]
E_{max}	Absorbed energy up to the point of maximum force	[J]
E_{frac}	Absorbed energy up to the point of fracture	[J]
F	Force	[N]
f	Frequency	[s^{-1}]
H	Hardness	[Pa]
h	Indentation depth	[m]
K	Stress intensity factor	[$Pa \cdot m^{0.5}$]
K_{Ic}	Critical stress intensity factor for mode I failure (opening)	[$Pa \cdot m^{0.5}$]
ΔK	Range of the stress intensity factor ($= K_{max} - K_{min}$)	[$Pa \cdot m^{0.5}$]
m	Exponent in power law functions such as the Paris law	[-]
m	Mass of falling weight	[kg]

N	Cycles	[-]
n	Constant in Equation (2C.1)	[-]
p	Hydrostatic pressure	[Pa]
p_i	Internal pressure	[Pa]
R	Stress ratio ($= \sigma_{min}/\sigma_{max}$)	[-]
R	Universal gas constant	[J/(mol · K)]
S	Contact stiffness	[Pa]
s	Displacement	[m]
T	Temperature	[K]
$T_{d\rightarrow b}$	Ductile-to-brittle transition temperature	[K]
t	Time	[s]
t	Wall thickness	[m]
t_0	Constant with the value 1 s	[s]
$t_{contact}$	Time at contact between tup and specimen	[s]
v	Speed of the tup	[m/s]
w	Width of a specimen	[m]
Y	Geometrical factor used for calculating the stress intensity factor	[-]

Greek symbols:

ΔH_{th}	Activation energy used in Equation (2C.1)	[J/mol]
ΔU	Activation energy	[J/mol]
$\dot{\epsilon}$	Strain rate	[s^{-1}]
γ	Constant in Equation (2C.1)	[J/mol]
$\bar{\gamma}$	Equivalent plastic strain	[-]
$\dot{\gamma}$	Shear strain rate	[s^{-1}]
$\dot{\bar{\gamma}}$	Equivalent plastic strain rate	[s^{-1}]
μ	Pressure dependence	[-]
v^*	Activation volume	[m^3/mol]
σ	(Tensile) stress	[Pa]
τ	Shear stress	[Pa]
$\bar{\tau}$	Equivalent stress	[Pa]

Subscripts:

0	Used to refer to a pre-exponential factor
α	Refers to α-relaxation
a	Annealing
amp	Amplitude

β	Refers to β-relaxation
c	Contact
cr	Critical
e	Elastic
eff	Effective
f	Failure
h	Hoop
I	Refers to mode I failure (opening)
IT	Indentation
ini	Initial or initiation
l	Longitudinal
m	Mean
max	Maximum
min	Minimum
p	Plastic or permanent
$prop$	Propagation
r	Radial
ref	Reference
vm	Von Mises equivalent
y	Yield

Abbreviations:

3D	Three dimensional
ESC	Environmental stress cracking
erf	Error-function
LEFM	Linear elastic fracture mechanics
LTHS	Long-term hydrostatic strength
PC	Polycarbonate
(HD)PE	(High density) polyethylene
PMMA	Poly(methyl methacrylate)
PVC	Poly(vinyl chloride)
uPVC	Unplasticised poly(vinyl chloride)

Contents

Introduction

The history of the Dutch gas network

In the early morning of July the 22nd, 1959 at 6:33 am a test drill of the Slochteren I tower proved successful. It struck a very large gas field that is now known as the Slochteren or Groningen gas field. At the time of its discovery it was the second largest discovered natural gas field in the world, but it took several years before its size and value were fully understood. The proven amount of natural gas was only about 5% of the currently known initial field size of 2,800 billion m^3_n, when the Dutch government proposed a bill on the exploitation of the Groningen gas field. In those days nuclear energy was believed to take over the role of fossil fuels before the millennium, which was an important reason for the Dutch government to exploit the Slochteren gas field as fast as possible. On June 25, 1963 the exploitation of the Groningen gas field officially started [1]. It was decided to focus the gas sales on the domestic market, with the advantage that the gas could be sold for a better price. Consequently a national transportation network was required to transport the gas from the Groningen gas field to the customers. An ambitious plan was proposed to interconnect the existing regional gas networks[1] to form a national gas transportation and distribution network. In 1964 about 450 km of gas transport pipe was installed within 8 months. The installation included several passways through large rivers like the IJssel, Waal and Maas. In the same year about 3,000 km of gas pipe for local distribution networks was installed to increase the number of households connected to the gas network. In parallel all burners of the privately owned gas appliances, such as cookers and heaters, were adapted to burn natural gas instead of town gas. The success of implementing the use of natural gas in the daily life of Dutch citizens led to a densification of the Dutch gas network, evolving to its current form where more than 99% of the Dutch households are connected to the gas network.

[1] These existing regional gas networks were originally in use for the distribution of town gas, a gas produced by either carbonisation or gasification of coal.

Structure of the network

The Dutch gas network is divided into the national transportation network and the local distribution network. The national transportation network operates under a maximum pressure of either 67 bar or 40 bar and has a length of approximately 12,000 km [2]. This network feeds about 350 large industrial plants and the distribution network via 1,100 pressure reduction stations, where the pressure is reduced to 8 bar. The gas distribution network has a total length of approximately 125,000 km [2] and can be split into a high pressure network (1 to 8 bar) and a low pressure network (mainly operated at 100 mbar). These two distribution networks are linked by about 10,000 district stations. The low pressure network distributes the gas to consumers with a small gas demand (mainly households). The network consists of a large number of branches and interconnections to ensure gas supply to the customer even in case of (local) failure(s) in the network. Each customer is connected to the gas distribution network via a service line. These service lines are connected to the mains via a so-called saddle and run to the gas meters in the consumer's house. The focuss of this thesis is on the gas distribution network.

This research project is supported by four Dutch gas network operators that supply natural gas to approximately 4.7 million households (about 90% of all customers in the Netherlands). The material composition of this part of the distribution network is shown in Figure 1. The low pressure distribution network consists mainly of plastic pipes, whereas steel is the most used material for the high pressure distribution network. Three types of polymers are used in the distribution network: polyethylene (PE), unplasticised poly(vinyl chloride) (uPVC) and ductile poly(vinyl chloride) (PVC). In the mid-fifties uPVC was the

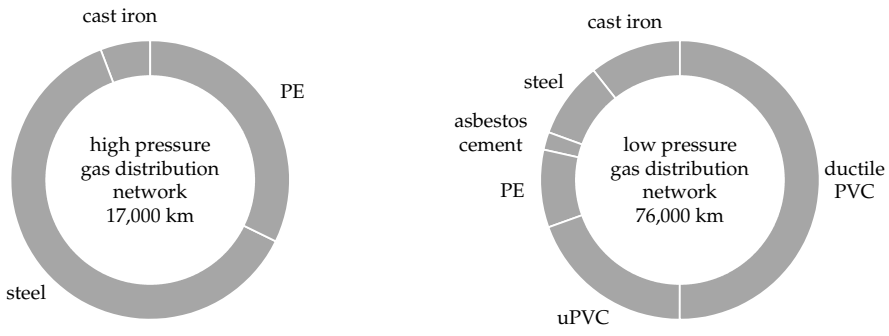

Figure 1 *Material composition of the gas distribution network operated by the participating network companies (data originate from 2005) [3].*

first polymer that was applied in the local (city) gas distribution networks, for example in Ootmarsum [4]. The positive experiences [5] with these uPVC pipes led to a more extensive use during the national expansion of the network in the mid-sixties. At the same time the first generation of PE gas pipes was introduced in the gas network. These pipes were more resistant to impact loads and could also be applied in the high pressure gas distribution network. In the mid-seventies another type of PVC, ductile (impact-modified) PVC, was introduced in the gas distribution network and this material has been the preferred material for most of the Dutch network operators since. This type of PVC contains modifiers such as chlorinated polyethylene (CPE) or acrylate modifiers, resulting in an improved impact performance compared to uPVC.

Problem definition

Still almost 20% of the current low pressure gas distribution network consists of uPVC pipes, although no uPVC pipe systems were installed anymore after the mid-seventies. Most of these pipes will reach their initially specified service life of 50 years within the next decade. As a large part of the distribution network was installed in densely populated areas, a replacement policy that is based on the specified service lifetime leads to costly and labour intensive projects. Problems can be expected especially on the labour side as most of the qualified personnel have retired. Postponing some of the replacements to spread out the project over a larger period of time is therefore favourable, but only acceptable without concessions to safety. Recent failure data of the Dutch gas distribution network [2] suggests that the quality of uPVC is still on an acceptable level. The number of failures in uPVC pipes accounts for only 8% of the total number of failures in the distribution network, which is comparable to the percentages of (more recently installed) ductile PVC and PE. Though the failure rate of uPVC is still low, it would be highly beneficial for the network operators to have a tool that can detect a decrease in integrity of the network prior to failure. In the ideal case it would enable the network providers to postpone replacement up to the day prior to failure. Such tools are readily available for gas transportation networks [6, 7], but not for dense, branched polymer networks like the Dutch gas distribution network. The goal of this thesis is to develop a framework for a method that can determine the residual lifetime of uPVC gas pipes in a non-destructive way. Such a method van only be developed when it is known which component and which (material) property limit the lifetime of the network. These aspects are considered in the next section.

Limitation of the service life

A uPVC pipe system consists of more components than just pipes; other components such as joints and saddles are required to form a branched, leak-proof network. The first uPVC pipes were interconnected with joints that were glued to the pipes. This glue is now known to deteriorate the impact performance of uPVC [8], leading to brittle fracture behaviour at the joints. Most of these connections have therefore been replaced and in the last years most of the failures in the uPVC network originate from the pipes (about 75%) [2]. Consequently, the present study focuses on the uPVC pipes only and the failure of other components is not taken into account.

The failure data [2] also shows that spontaneous failure hardly occurs and the cause of failure of uPVC can be ascribed to third-party damage in 50% of the cases. Other important causes of failure are subsidence of the ground and inadequate installation of the pipe. The percentage of uPVC pipe that fail as a result of third-party damage is relatively high compared to the percentage found for steel, cast iron and asbestos cement (up to 15%). It shows that, like the other polymers in the network, uPVC is susceptible to impact loads resulting from digging activities. For a risk assessment of the gas distribution network it is of importance in which way a uPVC pipe fails upon impact loading; whether it fails in a ductile or a brittle way. There are two important differences between these failure modes. Firstly, significantly more energy is absorbed before ductile failure occurs, when compared to brittle failure. A ductile uPVC pipe can therefore survive stronger impact events than a brittle pipe. Secondly, it is easier to stop the gas flowing from a ductile rupture than from a brittle fracture. Generally, a relatively large part of a pipe is instantly destroyed after brittle fracture, resulting in a sharp, irregular fracture surface. This makes it more difficult to plug the gas flow. Moreover, there is a risk of crack propagation at the moment the pipe segment is plugged. For these two reasons, the probability of (fatal) incidents after third-party damage is higher for brittle pipes than for pipes that behave in a ductile manner. As already stated, most of the uPVC gas pipes are installed in densely populated areas, which further increases the probability on fatalities [9]. Consequently, brittle failure behaviour of uPVC gas pipes cannot be tolerated. From this reasoning it is concluded that embrittlement limits the service life of uPVC pipes used in gas distribution networks.

Factors that affect the mechanical properties

The uPVC pipes are required to have a good impact performance during their entire service life and not just during installation, since third-party damage can occur at any moment in service. Therefore, the following sections discuss in

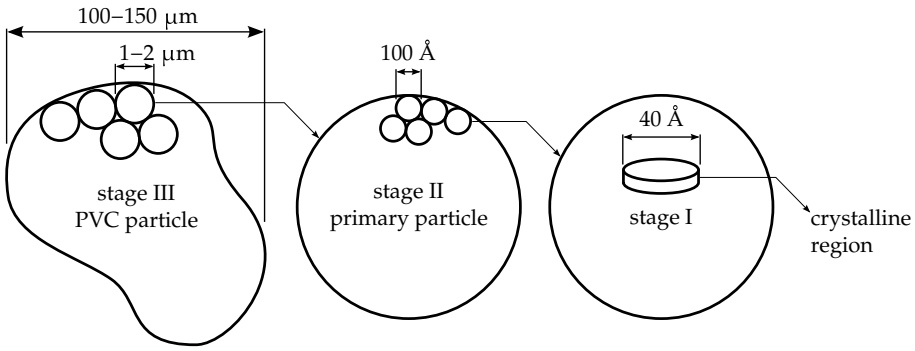

Figure 2 *Schematic representation of the structure of PVC particles [10].*

which way the impact behaviour is influenced during each stage in the lifetime of a uPVC pipe.

Processing

The raw material used in the extrusion of uPVC pipes is PVC powder, which is mostly produced using suspension polymerisation, but also emulsion or mass polymerisation processes have been applied. A schematic representation of a working model for the particulate structure of these PVC particles as proposed by [10] is shown in Figure 2. The PVC grains (stage III) consist of primary particles (stage II) of about 1-2 μm. These particles are believed to contain basic polymer units formed during polymerisation (stage I particles), which contain small crystalline regions. The crystallinity of PVC is generally up to about 8-10% [10, 11]. The mechanical properties of the uPVC match those of amorphous polymers, rather than semi-crystalline polymers. Therefore, PVC is referred to as an amorphous or glassy polymer throughout this thesis.

The particulate structure of the PVC powder should be destroyed during the production process to obtain a homogeneous product. For most other polymers, thermal energy is used as an effective way to break down the particulate structure of the virgin polymer. The crystalline structure in PVC will, however, only completely break up at a temperature of around 265 °C, which is far above the degradation temperature of PVC (∼200 °C). As a result, PVC pipes cannot be extruded from a melt and the particulate structure is destroyed by applying high shear rates instead. The use of a counter rotating twin screw extruder ensures a low distribution of the residence time of the uPVC in the extruder, preventing the occurrence of severe thermal degradation. The level of gelation of the PVC product is a measure for the degree to which the primary structure has

been destroyed in the final product and thus to which extent the entanglement network has developed between the fused PVC particles. The process conditions (temperature, pressure, velocity etc.) within the extruder should be kept within a tight range to realise an optimal degree of gelation. The variety of proposed techniques to characterise the level of gelation [12–18] indicates that there is still ambiguity in quantifying the level of gelation.

The difficulties in the processing of uPVC powder were not fully under control in the early stages of PVC pipe production, which has led to numerous studies on the influence of gelation on the mechanical properties of the uPVC pipes [19–22]. When the particulate structure is still partly intact (low level of gelation), it can act as a crack initiation site [23–25] and hence lead to a decrease in impact resistance [19, 20, 26], which makes the level of gelation a key parameter for the initial quality of the pipe. After processing the level of gelation remains constant [27] and consequently, it does not cause embrittlement of the PVC pipe during its service life. If the level of gelation was sufficiently high during installation, it does not limit the service lifetime of a uPVC gas pipe.

Other effects of the production on the mechanical properties of uPVC are the influence of molecular orientation [22, 28], residual stresses [29] and molecular weight of the uPVC powder used [30]. From the cited studies it can be concluded that the influence of molecular orientation and residual stresses on the impact behaviour is only marginal and can be neglected here. The molecular weight does have a significant influence on the impact performance. The molecular weight of most of the uPVC pipes produced from the mid-sixties up to the mid-seventies complied to a K-value of 65 or higher. For these K-values the impact resistance is almost constant and no changes in impact resistance are expected as long as chemical degradation does not take place in the polymer.

Installation

During the installation of the pipes, deterioration of the uPVC pipe is not limited to some scratches as a result of rough handling. The pipes can degrade under the influence of outdoor conditions [31–33] when stored prior to installation. This process is known as weathering and can cause chemical degradation, resulting in a decrease of the impact resistance of uPVC. It is important to note that, like the level of gelation, weathering does not cause a change in mechanical properties of uPVC during the service life: the ultraviolet rays, which contribute most to the change in mechanical properties, do not reach the surface of the buried pipe.

Service life

When deterioration by rodents, as discussed by Cocquyt [34], is neglected, four notable processes that influence the mechanical properties of uPVC during service remain: molecular degradation, slow crack growth, environmental stress cracking (ESC) and physical ageing. Each of these processes is briefly discussed below.

Not only heat and ultraviolet rays cause molecular degradation in uPVC. The presence of oxygen can, in time, also decrease the molecular weight and thus the impact resistance of uPVC. The existence of this degradation process was already known at the time of production of the uPVC gas pipes and the resistance against degradation increased with the improvement of stabilisation techniques [35]. Stabilisers such as lead salts, metallic stearates or organo-tin compounds, were added to prevent this process from occurring. Furthermore, the conditions of buried uPVC gas pipes are such (low temperature and low oxygen concentration) that the degradation can be expected to be very low. This process will therefore not be taken into account as a limiting factor for the service lifetime of uPVC gas pipes.

Slow crack growth occurs when the pipe is subjected to a tensile stress. The stress is concentrated around surface scratches or inherent flaws in the pipe. The latter can originate from, for example, alien particles or inhomogeneously dispersed additives with a size of typically about 50-250 µm in uPVC gas pipes [36, 37]. These flaws can evolve into a crack that slowly grows. The presence of cracks not only decreases the impact resistance of the pipes, but continuous growth can eventually result in a through-wall crack. These scenarios are, however, not likely to occur for a uPVC gas pipe during its service life as the stress exerted on the pipes is very low. The pipes are operated at a maximum of 100 mbar above atmospheric pressure and if installed correctly the surrounding soil supports external loads, such as those caused by (heavy) traffic.

The ESC process is similar to slow crack growth, but the presence of a chemical agent initiates and promotes the crack growth rate in this case. The physically induced acceleration can be such that crack growth becomes apparent even at low stresses. Several studies have been carried out on the influence of ESC on the mechanical properties of PVC, like those conducted by Wolf [38] and Breen *et al.* [39–42]. The cited studies showed that deterioration of the impact resistance hardly occurs in PVC pipes when subjected to aromatic components in concentrations that can be expected to occur in gas distribution mains. This does not hold for pipes in which gas condensate is present; the concentration of aromatic components in gas condensate can be such that ESC does occur. As gas condensate is hardly encountered in the Dutch gas network, ESC can only limit a very small part of the Dutch uPVC gas network.

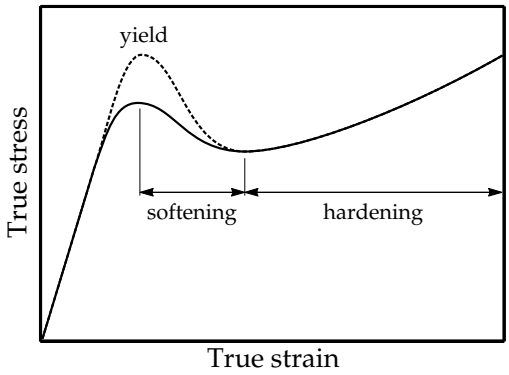

Figure 3 *Schematic representation of the influence of physical ageing on the intrinsic response of glassy polymers to an applied deformation at a constant rate. The solid line shows the response before physical ageing and the dashed line the response after physical ageing.*

The fourth mechanism that is known to influence the mechanical properties of amorphous polymers such as uPVC is physical ageing [43, 44]. Amorphous polymers are generally not in thermodynamic equilibrium below their glass transition temperature (T_g). The polymer tries to reach its thermodynamic equilibrium, but the low mobility of the polymer chains in the glassy state allows only small conformational changes. Physical ageing is directly related to these conformational changes. The mobility of the polymer chains increases with temperature, with the result that ageing effects become apparent at shorter timescales at elevated temperatures. Some of the consequences of physical ageing are (small) changes in density and the enthalpy of the polymer. An excellent review on the nature and consequences of physical ageing for amorphous polymers is given by Hutchinson [44].

In the present research project, the influence of physical ageing on the mechanical properties of uPVC is of importance. The intrinsic deformation behaviour of uPVC and the influence of physical ageing on this behaviour is schematically shown in Figure 3. The increase in resistance against plastic deformation is evident from the pronounced increase of the yield stress of the material. The amount of softening changes accordingly, whereas the strain hardening remains unchanged. The larger amount of strain softening, causes a more localised deformation response and thus a decrease in impact resistance as a result. This (physical) ageing induced embrittlement of polymers was first shown for polycarbonate [45–47]. Little is known, however, about the quantitative relation between the extent of physical ageing and the impact resistance of uPVC gas pipes. It is important to note that uPVC always ages physically at temperatures below its glass transition always and thus during its service life. The process

of physical ageing is therefore regarded as an important contributor to the embrittlement of uPVC and its consequences on the mechanical properties of uPVC gas pipes is studied in this thesis.

Outline of this thesis

It was already mentioned that the development of a framework for a method that can determine the residual lifetime of these pipes in a non-destructive way is the goal of this thesis. Such a method can potentially lead to not only huge economic savings, but also to an increase of the integrity of these parts of the gas distribution network. In the preceding sections it was argued that the residual lifetime of uPVC gas pipes is limited by their impact resistance.

In general, a lifetime assessment method of a product consists of four aspects, which are schematically shown in Figure 4. Each chapter in this thesis deals with one of these four aspects. Please note that as each chapter is written as an individual publication, some overlap is present. The first aspect of a lifetime assessment method is that a measure for the condition of the product should be defined. In the considerations presented above it was concluded that the impact resistance of the uPVC pipes is expected to limit the lifetime of these parts of the network and that physical ageing lowers this impact resistance. The property that is used as a measure for the condition should therefore be directly related to physical ageing and thus to the thermodynamic state of the material. It is shown in Figure 3 that the yield stress is strongly influenced by physical ageing. The yield stress is therefore used as a measure of the impact resistance of uPVC.

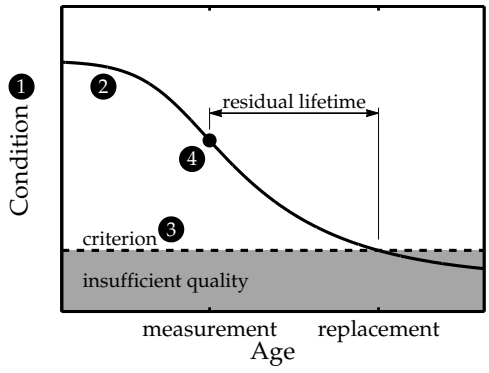

Figure 4 *Schematic representation of the lifetime assessment method of a product. The four aspects that can be distinguished (see text) are indicated in the figure and the numbers correspond to the chapter numbers in this thesis.*

The yield behaviour of uPVC is characterised and modelled in Chapter 1. This model is combined with a hypothesis for a critical plastic strain failure criterion and is applied to predict the failure times of pressurised pipes. The approach is therewith applied as an alternative for the conventional method to determine the long-term hydrostatic strength (LTHS) of plastic pipes. The model for the yield behaviour is verified by comparing the predictions with experimental data.

The second aspect of a lifetime assessment method is that the influence of the age of the product on the condition should be known. In this case, the influence of physical ageing on the yield stress is characterised and modelled in Chapter 2. Again the model is verified with experimental data. Long-term failure experiments, where physical ageing influences the time-to-failure, are both carried out and predicted.

Thirdly, a criterion should be determined that identifies when the quality of the product is insufficient for proper, or in this case, safe service. The relation between the yield stress and the increase in the ductile-to-brittle transition temperature (a measure for the impact resistance of the pipe) is studied in Chapter 3. Furthermore, a procedure to determine a criterion at which the impact resistance of uPVC becomes insufficient is presented.

For the last step in determining the residual lifetime of the product the condition of the product should be measured. Several contractors experienced that there is a large variation in the impact resistance of uPVC pipes: whereas a certain pipe segment might be ductile, its neighbouring pipe segment can be brittle. Therefore, a small number of checks at specially selected locations are insufficient to ensure the integrity of the network and non-destructive testing of all uPVC pipes in service is preferred. In Chapter 4 the application of micro-indentation experiments as a probe for the yield stress, and thus for the condition, of uPVC is studied.

The thesis concludes with a summary of the most important conclusions and some recommendations for future studies.

Bibliography

[1] J. Schenk. *Groningen-gasveld 50 jaar*. Boom Amsterdam, **2009**.

[2] A. Hendriks. Storingsrapportage gasdistributienetten 2008. Technical report, Netbeheer Nederland, **2009**. URL `http://www.energiened.nl/_upload/bestellingen/publicaties/186_315011-Storingsrap.g`

[3] *Data provided by the participating network operators: Cogas Infra en Beheer B.V., Enexis, Liander and Stedin in 2005.*

[4] A.C. Schouten. Een plastic buizennet te Ootmarsum. *Het Gas* 78:159–161, **1957**.

[5] J. Worp. Een en ander over hard p.v.c.-buis en haar toepassingsmogelijkheden. *Het Gas* 78:2–12, **1957**.

[6] S.W. Kercel, R.W. Tucker, and V.K. Varma. Pipeline flaw detection with wavelet packets and gas. In: *Proceedings of SPIE Vol. 5103*, **2003**.

[7] G. Vradis, D. Driscoll, H. Schempf, and R. Baker. Industry gains a new tool for long-range visual inspection of live gas pipe. *Pipeline and Gas Journal* 4:14–18, **2005**.

[8] M. Ezrin. *Plastics failure guide: cause and prevention*. Hanser publishers, **1996**.

[9] N. Piccinini, R. Tommasini, and E. Pons. Large N.G. explosion and fire involving several buried utility networks. *Process Safety and Environmental Protection* 87:73–80, **2009**.

[10] G. Butters. *Particulate nature of PVC: formation, structure and processing*. Applied Science Publishers LTD, **1982**.

[11] J.A. Juijn, J.H. Gisolf, and W.A. de Jong. Crystallinity in atactic poly (vinyl chloride). *Kolloid-Zeitschrift and Zeitschrift für Polymere* 251:456–473, **1973**.

[12] J.A. Covas. Hardness measurement as a technique for assessing gelation of rigid PVC compounds. *Plastics and Rubber Processing and Applications* 9:91–97, **1988**.

[13] J.W. Summers and E.B. Rabinovitch. Use of acetone in determining poly(vinyl chloride) processing morphology and product morphology. *Journal of Macromolecular Science Physics* B20:219–233, **1981**.

[14] S.J. Guerrero and A. Keller. The gelation of PVC: Characterization and control. *Journal of Macromolecular Science Physics* B20:167–184, **1981**.

[15] J.W. Summers, E.B. Rabinovitch, and P.C. Booth. Measurement of PVC fusion (gelation). *Journal of Vinyl Technology* 8:2–6, **1986**.

[16] H.S. Kim, B. Cotterell, and Y.W. Mai. Unnotched impact bend test assessment of the degree of gelation in unplasticized poly(vinyl chloride) pipe. *Polymer Engineering and Science* 27:277–281, **1987**.

[17] O.P. Obande and M. Gilbert. Effect of formulation and processing conditions on PVC fusion. *Plastics and Rubber Processing and Applications* 10:231–238, **1988**.

[18] J.W. Teh, A.A. Cooper, A. Rudin, and J.L.H. Batiste. Interpretation of DSC measurements of the degree of fusion of rigid PVC. *Journal of Vinyl Technology* 11:33–41, **1989**.

[19] P. Benjamin. The influence of the extrusion process on the quality of unplasticized Polyvinyl Chloride (uPVC) pressure pipe. *Journal of Vinyl Technology* 2:254–258, **1980**.

[20] B. Terselius, J.-F Jansson, and J. Bystedt. Gelation of PVC, Part 4: Impact strength. *Plastics and Rubber Processing and Applications* 5:1–7, **1985**.

[21] D.J. Calvert, B. Haworth, and D. Stephenson. The use of fracture mechanics to describe the impact strength of PVC window profiles. *Plastics and Rubber Processing and Applications* 15:229–242, **1991**.

[22] L.-A. Fillot, P. Hajji, C. Gauthier, and K. Masenelli-Varlot. Thermomechanical history effects on rigid PVC microstructure and impact properties. *Journal of Applied Polymer Science* 104:2009–2017, **2007**.

[23] K.V. Gotham and M.J. Hitch. Factors affecting fatigue resistance in rigid uPVC pipe compositions. *Britisch Polymer Journal* 10:47–52, **1978**.

[24] D.R. Moore, P.P. Benham, K.V. Gotham, M. Hitch, and M.J. Littlewood. Long-term fracture performance of uPVC pressure pipe as influenced by processing. *Plastics and Rubber: Materials and Applications* 5:146–150, **1980**.

[25] Y.W. Mai and P.R. Kerr. Effect of processing on fracture toughness and fatigue crack propagation in unplasticized polyvinyl chloride (uPVC). *Journal of Vinyl Technology* 7:130–139, **1985**.

[26] T. Kuriyama, I. Narisawa, R. Shiina, and M. Kotaki. Effects of morphology on the fracture toughness of PVC-U pipe. *Journal of Vinyl & Additive Technology* 4:164–168, **1998**.

[27] R.J.M. Hermkens, M. Wolters, J. Weller, and H.A. Visser. PVC pipes in gas distribution: still going strong! In: *Proceedings of Plastic Pipes XIV*. Budapest, **2008**.

[28] N. Walker, R.N. Haward, and J.N. Hay. Plastic fracture in poly(vinyl chloride). *Journal of Materials Science* 14:1085–1094, **1979**.

[29] J. Breen. Quality of PVC sewage pipes in the Netherlands. Technical report, TNO, **2008**.

[30] D.P. Jones, D.C. Leach, and D.R. Moore. The application of instrumented falling weight impact techniques to the study of toughness in thermoplastics. *Plastics and Rubber Processing and Applications* 6:67–79, **1986**.

[31] G. Roux and P. Eurin. Indentation test for predicting embrittlement of rigid PVC by weathering. *Journal of Macromolecular Science Physics* B20:505–517, **1981**.

[32] I. Hussain, S.H. Hamid, and J.H. Khan. Polyvinyl chloride pipe degradation studies in natural environments. *Journal of Vinyl & Additive Technology* 1:137–141, **1995**.

[33] C. Anton-Prinet, G. Mur, M. Gay, L. Audouin, and J. Verdu. Change of mechanical properties of rigid poly(vinylchloride) during photochemical ageing. *Journal of Materials Science* 34:379–384, **1999**.

[34] F. Cocquyt. Gasleidingen in polyvinylchloride en hoge-dichtheidspolyetyleen. *Het Ingenieursblad* 42:53–56, **1973**.

[35] K.S. Minsker and G.E. Zaikov. Achievements and research tasks for poly(vinyl chloride) aging and stabilization. *Journal of Vinyl & Additive Technology* 7:222–234, **2001**.

[36] H.J.M. Rijpkema and M. Wolters. Service life analysis of PVC gas pipes in practice: a predictable behaviour! In: *Proceedings of Plastics Pipes VIII*. Koningshof, **1992**.

[37] S. Burn, P. Davis, T. Schiller, B. Tiganis, G. Tjandraatmadja, M. Cardy, S. Gould, P. Sadler, and A.J. Whittle. Long-term performance prediction for PVC pipes. Technical report, Awwa research foundation, **2006**. URL `http://www.iwapublishing.com/template.cfm?name=isbn1843399504`.

[38] J. Wolf. Stres-cracking in hard PVC gasbuizen. *Gas* 87:433–442, **1967**.

[39] J. Breen and D.J. van Dijk. Environmental stress cracking of PVC: effects of natural gas with different amounts of benzene. *Journal of Materials Science* 26:5212–5120, **1991**.

[40] J. Breen. Environmental stress cracking of PVC and PVC-CPE Part 1: Crazing. *Journal of Materials Science* 28:3769–3776, **1993**.

[41] J. Breen. Environmental stress cracking of PVC and PVC-CPE Part 2: Failure mechanisms. *Journal of Materials Science* 29:39–46, **1994**.

[42] J. Breen. Environmental stress cracking of PVC and PVC-CPE Part 3: Crack growth. *Journal of Materials Science* 30:5833–5840, **1995**.

[43] L.C.E. Struik. *Physical aging in amorphous polymers and other materials*. Elsevier, **1978**.

[44] J.M. Hutchinson. Physical aging of polymers. *Progress in Polymer Science* 20:703–760, **1995**.

[45] G. Peilstöcker. Über das Temperaturverhalten von Polykarbonat. *Kunststoffe* 51:509–512, **1961**.

[46] G. Peilstöcker. The temperature behaviour of polycarbonate. *British Plastics* 35:365–369, **1962**.

[47] D.G. Legrand. Crazing, yielding, and fracture of polymers. I. Ductile brittle transition in polycarbonate. *Journal of Applied Polymer Science* 13:2129–2147, **1969**.

Lifetime assessment of load-bearing polymer glasses[1]

Chapter 1

Abstract

The most widespread application of polymers in structural applications is their use as pipe material for water, gas and sewer distribution systems. Pipes have a design lifetime of typically 50 years, which rules out real-time lifetime assessment methods. Instead, the lifetime is determined by extrapolating the results of pressurised pipe tests. During these tests three failure regions are observed. These regions are dominated by plastic deformation, slow crack growth and molecular degradation, respectively. Here, a new engineering approach is presented, which makes it possible to predict long-term ductile (region I) failure of loaded glassy polymers based on short-term tests. The approach is based upon the hypothesis that failure is governed by accumulation of plastic deformation up to a critical strain, where the polymer enters its softening region and fails. A pressure-modified Eyring relation is employed to calculate the accumulation of plastic strain for any given load case. The procedure to determine all relevant model parameters, which is based upon short-term tensile tests, is presented. Furthermore, it is shown that the approach can produce accurate quantitative time-to-failure predictions for both poly(carbonate) and unplasticised poly(vinyl chloride).

[1]Reproduced from: H.A. Visser, T.C. Bor, M. Wolters, T.A.P. Engels, L.E. Govaert, Lifetime assessment of load-bearing polymer glasses; An analytical framework for ductile failure, *Macromolecular Materials and Engineering*, submitted, **2010**

1.1 Introduction

The application of polymers in pressurised pipe systems was one of the first and is by far the most widespread application of polymers in load bearing structures since the 1950's. It is therefore not surprising that considerable research was directed to the service lifetime of polymer pipe systems. Most of this research focused on the pipe segments, other parts of the pipe system, e.g. joints, have not received as much attention. Although the service life of polymer pipes was recently found to exceed 50 years in a real time experimental setup [1], such real-time laboratory tests under service conditions are highly impractical. Therefore, the failure times are usually shortened by testing the pipe segments at internal pressures and/or temperatures well above service conditions. The stress that can be sustained for a period of 50 years at room temperature is referred to as the long-term hydrostatic strength (LTHS) and is determined by a standardised extrapolation procedure according to ISO 9080.

Typical results of pressurised pipe tests are shown schematically in Figure 1.1. The *logarithm* of the applied stress is plotted against the *logarithm* of the time-to-failure. In such plots, generally, three failure processes can be distinguished [2–4]:

region I: At relatively high stresses the pipe segments show large plastic deformations before failure. A large plastic zone forms ("bulging") that subsequently tears open as the tensile strength of the material is surpassed locally. This failure mode is referred to as ductile tearing in Figure 1.1 (right).

region II: At lower stresses the failure of the pipe segments follows different kinetics. A hairline crack is observed as a through-wall slit in axial direction. This kind of failure can be qualified as quasi-brittle behaviour. The knee that marks the transition between region I and region II is sometimes referred to as the "mechanical knee" [4].

region III: At relatively low stresses and long loading times, a third type of failure mode can be observed. Failures in this region can be ascribed to chemical/molecular degradation of the polymer leading to a reduction in molar mass and, ultimately, to brittle fracture or failure by a multitude of cracks. The failure time is nearly independent of the applied stress in this region. The transition from region II to region III failure is referred to as the "chemical knee" [4].

The position of the transitions between each of the three failure processes shown in Figure 1.1 (left) are influenced by parameters such as chemical structure,

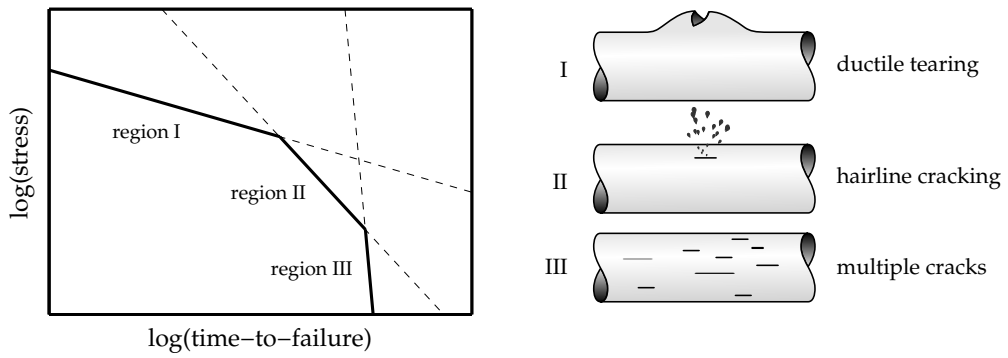

Figure 1.1 ***Left:*** *schematic representation of typical time-to-failure behaviour of plastic pipes subjected to a constant internal pressure.* ***Right:*** *three failure modes that can occur in pipes subjected to a constant internal pressure that are generally each associated to one of the three regions.*

molar mass distribution, processing and additives (stabilisers). Besides these parameters the environmental conditions of the pipe (temperature, internal pressure and internal/external medium) can influence the failure kinetics. As the individual failure processes can be influenced differently by each of these parameters, not all failure processes are always observed in the stress-failure time curve. For example, region III can, in some cases, occur after such a short time that it becomes critical before region II manifests itself.

In the past, each of the three failure processes has been studied separately to reveal the interdependence between the failure kinetics, the material properties and test conditions. These studies resulted in various models to predict the behaviour and location of each of the regimes. The models not only enabled extrapolation towards the lifetime at service conditions, but also increased the understanding of the failure processes themselves. The drive to use polymer pipes at higher service pressures [5] and to extend the service life towards 100 years [1], resulted in studies to improve the lifetime at higher stress levels.

An important issue is the improvement of the materials resistance to region III failure. Failure in this regime is attributed to molecular degradation (chain scission) resulting in the formation of multiple cracks in the pipe material. The molecular degradation rate depends on the type of polymer, its molecular weight and the amount and type of stabiliser [2, 6, 7]. Obviously, the service environment can cause the chemical knee to shift towards shorter failure times in case of, for example, an elevated service temperature, the loss of stabiliser to the surrounding media, and/or a high concentration of oxidiser [8]. As stabilisation techniques improved during the years, region III failures shifted towards such long failure

times [1] that region III is no longer regarded as a limiting factor for the LTHS of traditional pipe materials (polyolefins and PVC). It is therefore not surprising that most research on the lifetime prediction of polymer pipes has focused on region II.

The kinetics in regime II are believed to be dominated by slow crack growth [3], where existing imperfections in the polymer material are assumed to grow steadily until the resulting crack reaches a critical value. These imperfections can originate from processing (voids, impurities, local thermal degradation of the material, etc.) [3] and/or handling (scratches) [9]. The time to transform an initial imperfection to an actual crack, the initiation time (t_{ini}), is usually neglected. This implies that the approaches focus on situations where the initiation time is negligible compared to the time it takes for the crack to propagate to its critical value, the propagation time (t_{prop}), which is not always the case [10]. This makes the size of the initial flaw is a key parameter for the time scale at which slow crack growth failure occurs [11, 12]. Furthermore, the crack growth rate increases with an increasing applied load [13, 14], an increased temperature [13, 14], an increased residual stress [15–17], a decrease in molecular weight [18–21], a decrease in the level of gelation (for PVC) [21–23] and an increase in side-chain concentration (for PE) [24, 25].

Most lifetime prediction models developed for slow crack growth failure are based upon Linear Elastic Fracture Mechanics (LEFM). Starting point for these models is a relation between the crack growth rate ($\frac{\mathrm{d}a}{\mathrm{d}t}$) and the stress intensity factor (K), which is a function of the applied stress, the crack size (a) and the geometry of the specimen. Generally, this relation is described with a power law similar to the Paris law [26] that is normally used to describe fatigue crack growth:

$$\frac{\mathrm{d}a}{\mathrm{d}t} = AK^m, \tag{1.1}$$

where A and m are constants. The time-to-failure (t_f) can be calculated by integrating Equation (1.1) from the size of the initial imperfection up to a critical crack size. This can either be the wall thickness, or the flaw size belonging to the critical stress intensity factor (K_{Ic}) of the material considered. As already stated, the initiation time is generally neglected leading to t_f=t_{prop}. The strength of the fracture mechanics approaches is that failure predictions based on the size of inherent flaws in the polymer material, quantitatively agree with experimentally obtained failure data [27]. The size of these initial imperfections is typically in the range of 50-450 µm for polymer pipe material [7, 28, 29]. This approach has led to satisfying, quantitative predictions for a range of polymeric materials [13, 15, 30, 31].

As already stated, failure in region I is generally accompanied with relatively large plastic deformations. It is well known that the plastic deformation rate increases with an increase in temperature [32], applied stress [32] and concentration of plasticiser [33]. Moreover, the deformation kinetics of glassy polymers is influenced by an annealing treatment (defined as a heat treatment at a temperature below the glass transition temperature (T_g) of the polymer here) [34]. The underlying mechanism is referred to as *physical ageing* [34], which finds its origin in the fact that glassy polymers are generally not in a state of thermodynamic equilibrium below T_g. These polymers, however, display a continuous strive towards this equilibrium. As a consequence, the volume decreases [35], whereas relaxation times [36] and yield stress [37] increase, resulting in an increased resistance against plastic deformation.

In early approaches modelling of time-to-failure in region I was usually based on the assumption that the failure process is only activated by stress (σ) and temperature (T) [38–41]. Application of Eyring's theory of absolute reaction rates (Eyring flow) [42] leads to the following general expression:

$$t_f = A \cdot \exp\left(\frac{B}{T}\right) \cdot \sinh\left(\frac{C\sigma}{T}\right)^{-1}, \tag{1.2}$$

where A, B and C are constants. The relation consists of a pre-exponential term (which is in some cases dependent on T [41] or σ [38]), an Arrhenius type temperature activation term and a stress induced reaction rate term.[2] Remarkably, this relation proved satisfactory for predicting both brittle, chain scission dominated fracture [40] as well as yield dominated failure (failure of secondary bonds) [41]. All approaches produce satisfying results for *describing* the failure of *uniaxially* loaded polymers.

In the mid-seventies Bauwens-Crowet *et al.* [47] improved the previously mentioned approaches by using solid mechanics theories. Here, the time-to-failure follows from a relation describing plastic strain accumulation during continuous loading, and a critical strain value. This resulted in a relation similar to Equation (1.2), with the advantage that the stress dependence could be determined by short-term tensile tests. With this development the research on failure kinetics of glassy polymers evolved from *descriptive* towards *predictive*. Nonetheless, these models were still limited to *uniaxial* stress cases, making the lifetime predictions for pipes under a more complex loading geometry, e.g. as encountered in pressurised pipe tests, impossible.

[2] Besides this exponential relation between t_f and σ, other relations have been proposed that predict a linear relation between the logarithm of t_f and the logarithm of σ [43–45]. The ISO 9080 standard still uses log-log relations to extrapolate failure data of pipes subjected to an internal pressure. A discussion on the use of either of the two relations can be found in [46].

Recent developments in constitutive modelling of glassy polymers provided a new way to predict failure for polymers under complex loading [48]. Within the last twenty years major steps forward were achieved using three dimensional constitutive relations [48–56]. These models enabled accurate prediction of deformation and strain localisation phenomena in glassy polymers [57–59], revealing the crucial role of intrinsic post-yield characteristics in strain localisation behaviour. Application to long-term failure, by Klompen *et al.* [48], showed that ductile failure is governed by accumulation of plastic strain that eventually triggers the onset of strain softening, initiating strain localisation and failure. Despite the versatility of constitutive modelling, there is a serious drawback: quantitative application requires not only the characterisation of the yield behaviour, but of the *post*-yield strain softening and strain hardening regions too. This is especially complex if a description is required over a large temperature range.

In retrospect, one can state that model development for region I failure is not as mature as region II modelling. For region II quantitative predictions may be based on short-term measurements, whereas quantitative predictions of region I are only possible for either uniaxial loading cases, or after extensive material characterisation. There are, however, several reasons to develop a model that can predict region I failure:

- The location of the mechanical knee in Figure 1.1 can only be predicted when both region I and II are understood and modelled properly. Knowing only the slope of the region I failure kinetics is not sufficient as the location of this region is not only influenced by the type of polymer, but by the thermo-mechanical history of the material as well [48, 60, 61]. Two pipes of the same composition, but having received different cooling rates after processing (and thus having a different thermodynamic state as a result of physical ageing) will behave differently in region I. Consequently, the mechanical knee will be located at different time/stress levels.

- With the development of improved polymer grades, slow crack growth failure shifts towards longer times and may eventually not always be critical. The developments in PE pipe grades is an illustrative example. The slow crack growth resistance was improved considerably for HDPE pipe grades from the first to the third generation [1, 5].

- Changes in material properties can have different effects on the slow crack growth kinetics (region II) and the plastic deformation kinetics (region I). An improvement in slow crack growth kinetics might lead to an increase in plastic deformation rates, leading to a worse instead of a better LTHS.

The development of PE100+ multimodal pipe grades shows the importance of understanding the failure mechanisms of both region I and II. The low molecular weight fraction improves the creep rupture strength, whereas the high molecular weight fraction improves slow crack growth resistance, leading to a superior LTHS [1].

- The lifetime of polymer structures loaded in compression cannot be predicted with region II models as slow crack growth does not occur under compressive forces.

In the present study, therefore, a new engineering approach is developed to predict ductile (region I) failure of pressurised pipes based on short-term tensile experiments. The approach presented in this chapter is applicable to temperature dependent, region I failure for three dimensional load cases, such as encountered in the wall of a pipe subjected to an internal pressure. The main focus is on the application to unplasticised poly(vinyl chloride) (uPVC) pipe material, as this polymeric material is extensively used in the Dutch gas and water distribution systems. Additionally, the approach is applied to another glassy polymer:[3] polycarbonate (PC). PC is chosen as an additional material to validate the proposed approach, since a part of the characterisation and experimental data is available owing to the work of Klompen *et al.* [48, 63].

The outline of this chapter is as follows: in the theory section the hypothesis for the failure criterion used in the approach is discussed, followed by a (mathematical) description of the approach. After the experimental procedures have been specified, the experimental results for both PC and uPVC are presented. Subsequently, the approach is validated by the use of failure data of uPVC pipes subjected to an internal pressure as measured by Niklas and Kausch von Schmeling [64] and reproduced in Figure 1.2. Based upon the experimental observation that all failure modes showed similar circumferential strain behaviour up to failure, they stated that, unlike PE, all failure modes followed a common path up to failure. Their pipe failure data was, however, plotted on a semi-logarithmic scale. When the data is plotted in the more conventional double logarithmic plot, a mechanical knee appears at the transition from ductile rupture to hairline cracking. The approach presented in this chapter is applied to the prediction of the time-to-failure of ductile ruptures.

[3] Although PVC can have a crystallinity of up to 10% [62] its mechanical properties closely relate to that found for amorphous (glassy) polymers. Therefore uPVC is classified as a glassy polymer here.

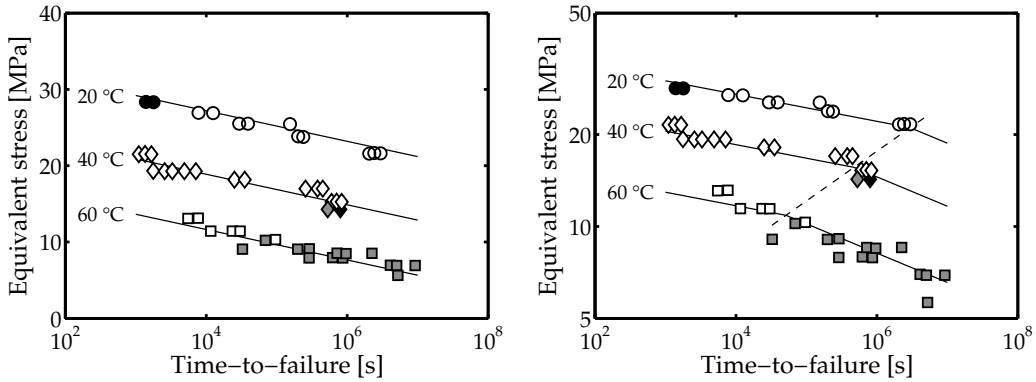

Figure 1.2 *Reproduction of the failure data of pressurised uPVC pipes as measured by Niklas and Kausch von Schmeling [64]. The three failure types (ductile tearing, hairline cracking and brittle fracture) are shown with unfilled, grey and black markers, respectively. The lines plotted to guide the eye.* ***Left:*** *data plotted on semi-logarithmic axes.* ***Right:*** *data plotted in the conventional way (double logarithmic axes).*

1.2 Theory

Consider a glassy polymer that is subjected to a constant load at a constant, specific temperature. The subsequent creep can be divided in three stages: primary creep, where linear viscoelastic behaviour prevails and the strain rate decreases in time; secondary creep, where the strain rate is constant for a constant applied stress, and tertiary creep, where the strain rate increases until failure occurs. The increase in strain rate is attributed to a decrease in the yield stress of the polymer glass as a result of strain softening [65]. The fact that tertiary creep also occurs in compressive experiments [66], where the applied true stress decreases for deadweight experiments, supports this statement. The three stages in a creep test can be visualised by plotting the strain rate versus the strain (a so-called Sherby-Dorn plot) as reproduced in Figure 1.3 for PC subjected to a compressive force [66]. Here, the primary creep shows a clear drop of the strain rate for strains up to about 8%. The plateau of constant strain rate corresponding to secondary creep stretches over just a small strain range here. Other polymers such as PE do show a plateau that persist over a broader strain range [67]. Subsequently, the strain rate increases as the material enters the tertiary creep stage until eventually failure occurs. Kramer *et al.* [68] and Crissman *et al.* [60] reported that the product of the strain rate at failure ($\dot{\epsilon}_f$) and the time-to-failure (t_f) is constant, or:

$$\frac{t_f(\sigma_1)}{t_f(\sigma_2)} = \frac{\dot{\epsilon}_f(\sigma_2)}{\dot{\epsilon}_f(\sigma_1)}. \tag{1.3}$$

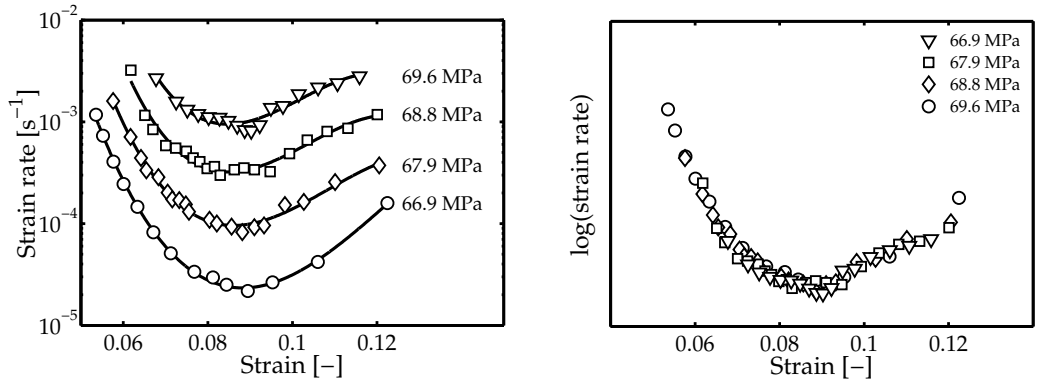

Figure 1.3 ***Left:*** *the compressive strain rate versus the strain for PC at four stress levels (reproduced from [66]).* ***Right:*** *the master curve resulting from vertical shifting.*

Sherby and Dorn [69] studied the strain rate during creep experiments for PMMA at several temperatures and creep stresses. They found that the strain rate versus strain curves could be shifted towards one mastercurve using Eyring's theory of absolute reaction rates [42]. The same observation was made by Mindel and Brown [66]. The results of their measurements on PC are reproduced in Figure 1.3. The Sherby-Dorn curves at four different stress levels were shifted towards one master curve, using an activation volume of $3.4 \cdot 10^{-3}$ m^3/mol. The consequence of their observation is that Equation (1.3) can be extended to:

$$\frac{t_f(\sigma_1)}{t_f(\sigma_2)} = \frac{\dot{\epsilon}_f(\sigma_2)}{\dot{\epsilon}_f(\sigma_1)} = \frac{\dot{\epsilon}_{min}(\sigma_2)}{\dot{\epsilon}_{min}(\sigma_1)}, \tag{1.4}$$

where $\dot{\epsilon}_{min}$ denotes the secondary creep strain rate (the minimum in a Sherby-Dorn plot), meaning that the relation also holds for the secondary creep rate. This is a very valuable result as it is well known that the state reached under constant strain rate conditions (yield in tensile experiments) and that reached under constant stress conditions (secondary creep in creep experiments) are equivalent [67, 70, 71]. Consequently, the stress and temperature dependency of the secondary strain rate can be characterised using tensile experiments, as demonstrated earlier by Bauwens-Crowet *et al.* [47]. They also showed that quantitative lifetime predictions can be obtained by introducing a critical plastic strain (ϵ_{cr}):[4]

$$\dot{\epsilon}_{min}(\sigma) \cdot t_f(\sigma) = \epsilon_{cr} \quad \Leftrightarrow \quad t_f(\sigma) = \frac{\epsilon_{cr}}{\dot{\epsilon}_{min}(\sigma)}. \tag{1.5}$$

[4]Bauwens-Crowet *et al.* denoted the critical plastic strain as $\Delta\epsilon_D$ in their study [47]

This relation can also be deduced from Equation (1.4). One should be careful not to interpret ϵ_{cr} as the total accumulated plastic strain[5] at failure, since the plastic strain rate is assumed to be constant in Equation (1.5) and the change in plastic strain rate in the tertiary creep stage is thus not taken into account. The use of Equation (1.5) is justified by the fact that the stress dependence of the minimum strain rate is equal to the stress dependence of the strain rate at failure.

Now that a suitable failure criterion is found, the approach only lacks a relation that describes both the deformation kinetics as measured in uniaxial tension and the deformation kinetics of the polymer under more complex loading geometries. A successful approach is the Eyring flow equation, which is able to describe the strain dependence of the yield stress over a wide temperature range (e.g. for PC [72, 73]). It is known that some glassy polymers, including PC and uPVC, show a secondary transition for deformation at higher rates or at lower temperatures, which can be successfully captured using a Ree-Eyring relation [72, 74]. Nevertheless, long-term creep failure is dominated by the contribution of the primary transition [63]. Therefore, in this study only the primary transition is taken into account for both PC and uPVC.

The models for the deformation kinetics discussed sofar are only capable of describing the deformation kinetics of uniaxially loaded polymers. To obtain a realistic description of the influence of an arbitrary 3D load on the deformation kinetics, it is essential that the influence of hydrostatic pressure on plastic deformation is taken into account. This was first recognised by Ward [32], who proposed a pressure-modified Eyring flow relation in which the influence of the hydrostatic pressure is quantified. Duckett *et al.* [73] were the first to show that this relation could successfully describe the yield behaviour of PC loaded in torsion with a super-imposed hydrostatic pressure. In the present study, the pressure-modified Eyring relation is given in equivalent terms, which enables the application to various loading geometries using a single set of material parameters:

$$\dot{\bar{\gamma}}\left(T,\bar{\tau},p\right)=\dot{\gamma}_0\cdot\exp\left(\frac{-\Delta U}{RT}\right)\cdot\sinh\left(\frac{\bar{\tau}v^*}{RT}\right)\cdot\exp\left(\frac{-\mu p v^*}{RT}\right). \tag{1.6}$$

The definitions for the equivalent strain rate ($\dot{\bar{\gamma}}$), hydrostatic pressure (p) and equivalent stress ($\bar{\tau}$) and their value for uniaxial tension and shear loads are given in Table 1.1. The right hand side of Equation (1.6) consists of four terms: a pre-exponential factor ($\dot{\gamma}_0$), an exponential term for the temperature dependence of the plastic deformation given by an Arrhenius type relation with activation

[5]For visco-elastic materials it is difficult to determine whether strain is anelastic or plastic. Here, the accumulation of strain associated to secondary creep is denoted as plastic strain.

energy (ΔU), an exponential term for the stress activation with activation volume (v^*) and an exponential term for the influence of the hydrostatic pressure with the pressure dependence μ. The symbol R denotes the universal gas constant and T the temperature.

The time-to-failure (t_f) for a geometry that is subjected to a constant stress at a constant temperature can be calculated using Equation (1.6) and a critical strain hypothesis similar to Equation (1.5):

$$t_f(\sigma) = \frac{\bar{\gamma}_{cr}}{\dot{\bar{\gamma}}\left(T, \bar{\tau}, p\right)}, \tag{1.7}$$

where, $\bar{\gamma}_{cr}$ is the critical equivalent strain. The time-to-failure relation for a specimen loaded in uniaxial tension can be expressed as:

$$t_f\left(T, \sigma\right) = \frac{2\bar{\gamma}_{cr}}{\dot{\gamma}_0} \cdot \exp\left(\frac{\Delta U}{RT} - \frac{\left(\mu + \sqrt{3}\right) v^*}{3RT}\sigma\right), \tag{1.8}$$

using the definitions of Table 1.1 and combining Equations (1.6) and (1.7). In the deduction of Equation (1.8) the approximation that $\sinh(x) \approx \frac{1}{2}\exp(x)$is used. This approximation is valid for x=$\frac{\bar{\tau}v^*}{RT} \gg 1$, which is true when $\bar{\tau} \gg$0.5 MPa for uPVC at room temperature and thus holds for the whole stress range applied in the present study.

As already stated, the deformation kinetics of PC depends on its thermal pre-treatment and thus its thermodynamic state [37]. The pre-exponential factor ($\dot{\gamma}_0$) captures the influence of the thermodynamic state on the deformation kinetics, since all other parameters are uninfluenced by a change in the thermodynamic state as shown by Klompen *et al.* [56]. This implies that two samples of a glassy polymer with different thermal and/or mechanical histories (for example

Table 1.1 *Definition of equivalent plastic strain rate ($\dot{\bar{\gamma}}$), equivalent stress ($\bar{\tau}$) and hydrostatic pressure (p) as expressed in the components of the deformation tensor and the driving stress tensor, respectively. For the case of uniaxial tension and simple shear explicit expressions have been derived.*

Definition	Tension	Shear
$\dot{\bar{\gamma}} = \sqrt{2 \cdot \left(\dot{\epsilon}_{11}^2 + \dot{\epsilon}_{22}^2 + \dot{\epsilon}_{33}^2 + 2\dot{\epsilon}_{12}^2 + 2\dot{\epsilon}_{23}^2 + 2\dot{\epsilon}_{31}^2\right)}$	$\sqrt{3}\dot{\epsilon}$	$\dot{\gamma}$
$\bar{\tau} = \sqrt{\frac{1}{6} \cdot \left[(\sigma_{11} - \sigma_{22})^2 + (\sigma_{22} - \sigma_{33})^2 + (\sigma_{33} - \sigma_{11})^2\right] + \sigma_{12}^2 + \sigma_{23}^2 + \sigma_{13}^2}$	$\frac{\sigma}{\sqrt{3}}$	τ
$p = -\frac{1}{3} \cdot \left(\sigma_{11} + \sigma_{22} + \sigma_{33}\right)$	$-\frac{1}{3}\sigma$	0

as a result of different processing conditions), can be described with different values for $\dot{\gamma}_0$, but with identical material dependent parameters ΔU, v^* and μ. Furthermore, it is possible that the thermodynamic state changes during a (long-term) test as a result of physical aging. The influence of this so-called progressive physical aging is neglected in the current study, i.e. $\dot{\gamma}_0$ is assumed to be constant for a given initial thermodynamic state. In Section 1.6 the consequences of this assumption are discussed in more detail.

Experimental data was used to characterise the deformation kinetics of PC and uPVC. With the obtained parameters the failure times for various loading geometries and thermodynamic states were predicted and compared with experimental data. Finally, the prediction of region I failure for uPVC pipe segments subjected to an internal pressure was studied. The results of these three steps are described in the Section 1.4

1.3 Experimental

1.3.1 Material and specimen preparation

Two materials were selected for the experimental work: PC and uPVC. Using results of previous studies of Klompen *et al.* [48, 56], PC acts as model material, whereas uPVC is used to test whether the approach is able to predict failure times of pipes subjected to a constant internal pressure.

The (bisphenol-A) PC grade used in this study is Lexan 101R from Sabic Innovative Plastics. This material was injection moulded into tensile bars with a geometry according to ASTM D638 (type III). Two sets of specimens with a different thermal treatment are used. The first set did not receive any heat treatment after injection moulding and is referred to as *as-manufactured*. The second set was annealed in a convection oven at a temperature of 100 °C for $4 \cdot 10^5$ s ($\sim$4.5 days) and is referred to as *annealed*.

The uPVC specimens were taken out of an excavated uPVC gas distribution pipe (∅ 160 mm) and a wall thickness of 4.1 mm) that had been in service for several decades. Pipe segments of 70 mm long were cut in half in axial direction. The two parts were then pressed into flat plates in a press at 100 °C,[6] thus at about 20 °C above the glass transition temperature of uPVC, in 25 minutes at a pressure of approximately 1 MPa. This procedure erases all prior effects of

[6] Although it is known that the treatment at 100 °C can influence the crystallinity of the uPVC [75], its consequences for the mechanical behaviour are expected to be insignificant and are not taken into account in the current study.

physical ageing, thus $\dot{\gamma}_0$ of the specimen is only dependent on the cooling rate in the cold press and subsequent heat treatments. Tensile bars with a gauge section of approximately $30\times5\times4.1$ mm^3 were milled from the plate material in the axial direction of the original pipe. Three sets of specimens were used, differing in the heat treatment they received after manufacturing. The first received no heat treatment, the second set was annealed for $5\cdot10^5$ s ($\approx$1 week) at 60 °C and the third set was aged for $3\cdot10^6$ s ($\approx$1 month) at 60 °C. These sets are referred to as as-manufactured, annealed and severely annealed, respectively, and their heat treatments are summarised in Table 1.2. The annealed set was used for the characterisation of the deformation kinetics of uPVC, to prevent a significant contribution of physical ageing during the experiments performed at elevated temperatures.

Table 1.2 *Thermal treatment of the specimens used for experiments during this study.*

Set	Thermal treatment	
PC 1	-	(as-manufactured)
PC 2	$4\cdot10^5$ s @ 100 °C	(annealed)
uPVC 1	-	(as-manufactured)
uPVC 2	$5\cdot10^5$ s @ 60 °C	(annealed)
uPVC 3	$3\cdot10^6$ s @ 60 °C	(severely annealed)

1.3.2 Experimental setup

All uniaxial tensile and creep measurements were carried out on an MTS Elastomer Testing System 810 equipped with a 25 kN force cell and a thermostatically controlled chamber. The tests were conducted at three different temperatures (20 °C, 40 °C and 60 °C). Engineering stresses were calculated using the average of the cross-sectional surface areas as measured at three locations in the gauge section. Tensile experiments were carried out at a constant crosshead speed, resulting in constant *engineering* strain rates ranging from $3\cdot10^{-5}$ s^{-1} to $1\cdot10^{-1}$ s^{-1}. The creep tests were conducted with a constant load, thus at constant *engineering* stress. To avoid dynamic effects the load is slowly applied in 3 seconds. All stresses and strains reported in this paper are engineering values.

1.4 Experimental results

In this work an engineering approach, represented by Equations (1.6) and (1.7), is applied to predict ductile, long-term failure of glassy polymers. The deformation

kinetics of the selected materials (PC and uPVC) are characterised first. The deformation kinetics are determined by material parameters μ, v^* and ΔU and the thermodynamic state of the material, which is represented by $\dot{\gamma}_0$. The pressure dependence was determined using yield data for tensile bars under a superimposed hydrostatic pressure as found in literature [76, 77] and reproduced in Figures 1.4 and 1.8. Tensile tests at a constant strain rate were carried out to determine the other parameters. Next, the critical equivalent plastic strain was derived from tensile creep test results. Once all the parameters required for the approach had been determined, the approach was validated by comparing the predictions and the experimental results for specimens that received different heat treatments and specimens that were subjected to two different loading geometries.

1.4.1 Deformation kinetics of PC

The activation volume (v^*) for PC was found to be $3.52 \cdot 10^{-3}$ m^3/mol by Klompen *et al.* [56] using tensile measurements on the same experimental setup as used in the present study. This value is in very close agreement with the activation volume found by Mindel and Brown [66] for creep measurements reproduced in Figure 1.3 ($3.4 \cdot 10^{-3}$ m^3/mol), proving the interchangeability between constant strain rate and creep experiments. The activation volume found by Klompen *et al.* is adopted throughout this study. Furthermore, Klompen *et al.* found μ=0.08, for *true*, uniaxial, tensile yield stress data obtained under superimposed hydrostatic pressure as measured by Christiansen *et al.* [76]. In the current study only *engineering* yield stress data is used. Therefore, it is verified whether this value can also be applied to *engineering* yield stress data as reproduced in Figure 1.4. The pressure dependence can be derived from the slope of the yield stress versus the superimposed hydrostatic pressure (p) by rewriting Equation (1.6) for this specific stress state and solving the differential equation:

$$\frac{\mathrm{d}\sigma}{\mathrm{d}p} = \frac{3\mu}{\mu + \sqrt{3}}. \tag{1.9}$$

The solid line in Figure 1.4 is calculated with a pressure dependence equal to that found for true yield stress (μ=0.08) and holds for the engineering stress data for the pressure range that is of interest in this chapter.

The tensile yield stress was measured at several strain rates and at three different temperatures to determine the activation energy ΔU and the pre-exponential factor $\dot{\gamma}_0$. At each combination of strain rate and temperature three tests were carried out. The resulting values for the yield stress are shown in Figure 1.5 (left).

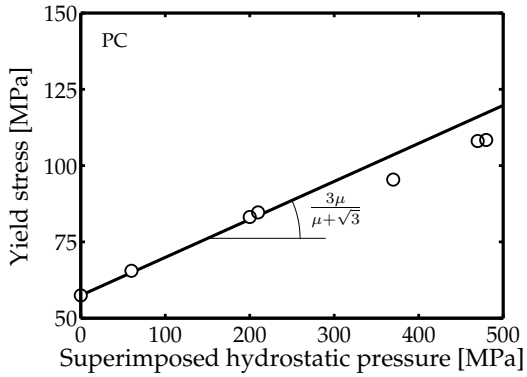

Figure 1.4 *The yield stress of PC as measured in tension with a superimposed hydrostatic pressure (reproduced from [76]). The solid line is a fit using Equation (1.9), resulting in μ=0.08.*

Very little scatter was found between the individual yield stress measurements and, as expected, an increase in yield stress was found for increasing strain rates and decreasing temperatures. The parameters ΔU and $\dot{\gamma}_0$ were determined by applying a least squares fit on all yield data, using Equation (1.6) and the adopted values for μ and ν^*. The resulting values are: ΔU=327 kJ/mol and $\dot{\gamma}_0$=$5.3 \cdot 10^{32}$ s^{-1}. It is emphasised that this value for $\dot{\gamma}_0$ is unique for this thermodynamic state, and will differ for sets of specimens with different thermo-mechanical histories. The solid lines in Figure 1.5 (left) represent the best fit using Equation (1.6) and show that the tensile yield behaviour of PC can be accurately described with the pressure-modified Eyring relation.

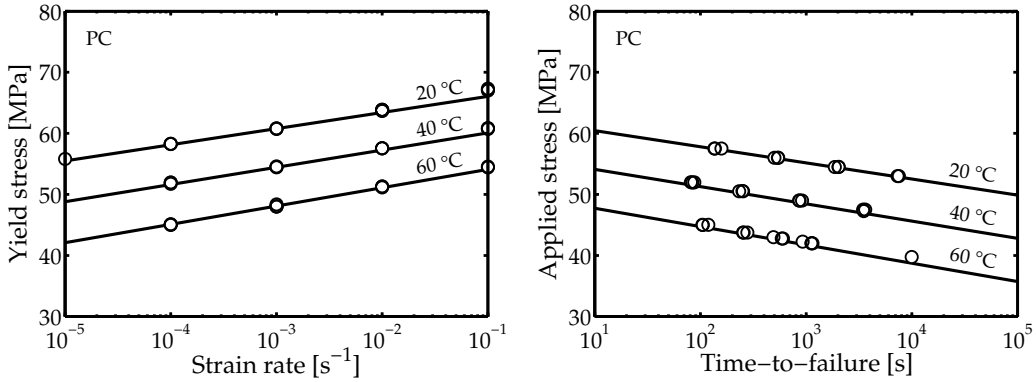

Figure 1.5 *Uniaxial tensile measurements on PC at 20 °C, 40 °C and 60 °C. **Left:** the yield stress for a range of strain rates. The solid lines represent the best **fit** using Equation (1.6). **Right:** the time-to-failure for specimen loaded at a range of constant stresses. The solid lines represent **predictions** using Equation (1.8) and the data at 20 °C to calculate the critical equivalent strain.*

1.4.2 Critical plastic strain of PC

The critical strain plastic strain ($\bar{\gamma}_{cr}$) of PC has been determined applying a series of creep tests. The time-to-failure for specimens subjected to different (constant) loads are shown in Figure 1.5 (right). Failure is defined as the occurrence of a sudden, steep increase of the strain rate: at the moment the PC tensile bars "fail" a neck is formed that grows rapidly over the whole gauge section. This neck initiates at the moment the material enters its softening region. This ductile behaviour is found for all experiments on PC specimens during this study. It is clear that at a constant temperature the time-to-failure increased in a logarithmic way for lower values of the applied engineering stress. The deformation process is strongly temperature dependent: the higher the temperature, the shorter the time-to-failure for a given applied stress. Moreover, in full agreement with the proposed hypothesis (i.e. Equation (1.7)), the slope of the experimental data points at each temperature in Figure 1.5 (left) and Figure 1.5 (right) is identical, but opposite in sign.

The data from Figure 1.5 (right) at 20 °C was used to calculate the critical equivalent plastic strain from Equation (1.8). A value of 1.3% was found and used to predict the failure times at 40 °C and 60 °C shown as solid lines in Figure 1.5 (right). These predictions quantitatively agree with the experimental data, proving that it is possible to describe the failure behaviour of PC for this specific experimental range with Equation (1.8). To investigate the predictive capacity of this approach with the parameters summarised in Table 1.3 for different situations, the approach was applied on specimens that differ in thermodynamic state, i.e. a different degree of physical ageing, and specimens that were subjected to a different loading geometry.

Table 1.3 *Parameters found for PC and uPVC in this study.*

	PC	uPVC	
μ	$0.08^{\dagger}$	0.14	[-]
ν^*	$3.52 \cdot 10^{-3}$ †	$2.06 \cdot 10^{-3}$	[m^3/mol]
ΔU	$3.27 \cdot 10^5$	$2.97 \cdot 10^5$	[J/mol]
$\bar{\gamma}_{cr}$	0.013	0.015	[-]
$\dot{\gamma}_0$ (set 1)	$5.3 \cdot 10^{32}$	$1.5 \cdot 10^{38}$	[s^{-1}]
$\dot{\gamma}_0$ (set 2)	$5.7 \cdot 10^{29}$	$3.7 \cdot 10^{36}$	[s^{-1}]
$\dot{\gamma}_0$ (set 3)	-	$1.1 \cdot 10^{36}$	[s^{-1}]

† value adopted from Klompen *et al.* [48]

1.4.3 Application to different thermodynamic states and loading cases for PC

The predictive capacity of the approach was tested in two ways. Firstly, a validation step is carried out using two sets of specimens with a different thermodynamic state. Here, the deformation kinetics and the time-to-failure of specimens that received an additional heat treatment (set 2: annealed) after manufacturing were compared with the results presented earlier for the "as-manufactured" specimens (set 1). The thermodynamic state of the annealed specimens will differ from that of the as-manufactured specimens, because of the process of physical aging taking place during the heat treatment of the annealed specimens. This results in a horizontal shift of the deformation kinetics, which is shown for both sets of specimens in Figure 1.6 (left). As expected, the resistance against plastic deformation increases after the heat treatment. The value for $\dot{\gamma}_0$ for the annealed specimens was calculated using one reference point (at a strain rate of 10^{-3} s^{-1}) and Equation (1.6), resulting in a value of $5.7 \cdot 10^{29}$ s^{-1}. Using this value and the parameters presented in Table 1.3, the deformation kinetics for a range of strain rates has been predicted and shown as a solid line in Figure 1.6 (left). These predictions agree very well with the experimentally obtained yield data. In Figure 1.6 (right) the failure times as measured in tensile creep tests with specimens from both the as-manufactured and the annealed set are shown. The increased resistance against plastic deformation of the annealed specimens causes the failure times to shift horizontally towards longer failure times. The solid lines

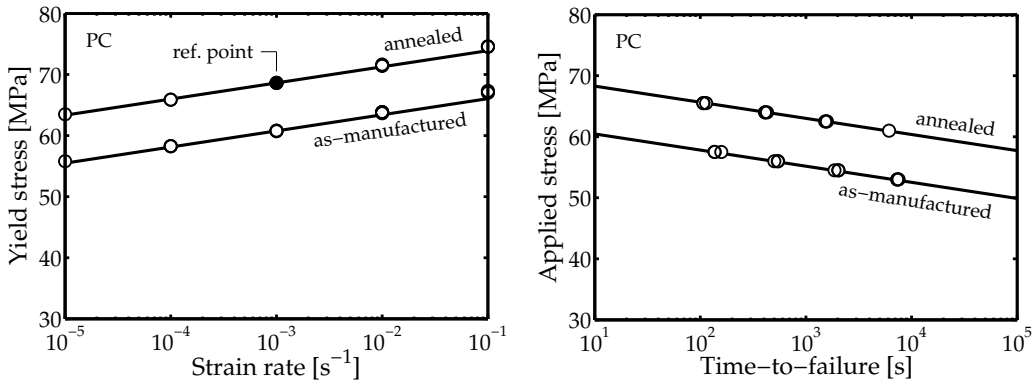

Figure 1.6 *Results of uniaxial tensile experiments at 20 °C on annealed PC specimens, compared with data adopted from Figure 1.5 (left) (as-manufactured).* ***Left:*** *the yield stress at various strain rates for both sets of specimens. The deformation kinetics of the annealed specimens is predicted using one reference point to determine $\dot{\gamma}_0$ and shown as solid line.* ***Right:*** *the time-to-failure at a range of constant stresses for both sets of specimens. The failure times for the annealed specimens are predicted using the calculated $\dot{\gamma}_0$ and Equation (1.8).*

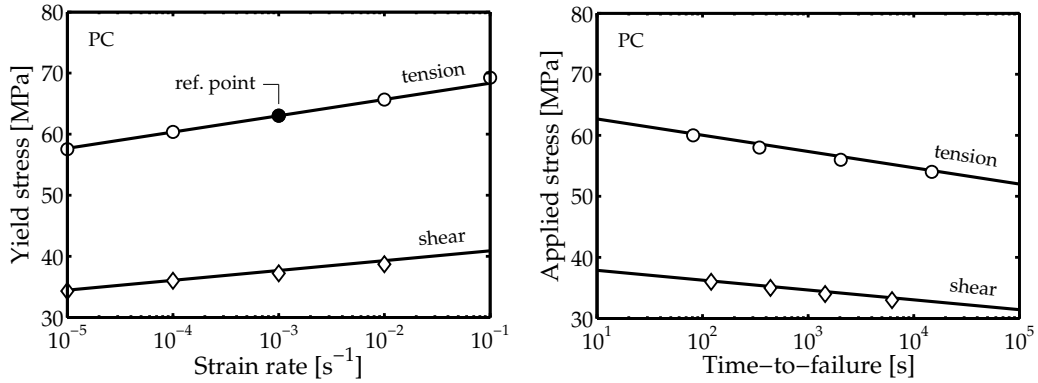

Figure 1.7 *Reproduction of the results of uniaxial tensile and shear experiments on PC at a temperature of 23 °C (adopted from [48]).* ***Left:*** *the solid lines are predictions for both loading cases using Equation (1.6) and one reference point.* ***Right:*** *the time-to-failure for both loading cases is predicted using this reference point.*

are predictions based on Equation (1.8) and the previously determined material parameters. The time-to-failure predictions prove to be very accurate in both the shift and the slope, showing that the approach is capable to anticipate to changes in the thermodynamic state.

The second way to test the predictive capacity of the approach focuses on the effect of different loading geometries. The creep and constant strain rate tests presented so far are all carried out in uniaxial tension, whereas in practice different loading geometries may be encountered, like for example shear or compressive loads. For this validation step experimental data from Klompen *et al.* [48] are used. They measured the deformation kinetics and failure times for PC in both uniaxial tensile and shear loading at room temperature (23 °C), using a different grade of PC (their specimens were milled from a 3 mm thick Makrolon extruded sheet). Although this material has a different molar mass distribution than the Lexan 101R used in this study, no differences in deformation kinetics are observed [56]. The thermodynamic state of the specimens is characterised by $\dot{\gamma}_0$=3.7 · 10^{31} s^{-1}, using the reference point as indicated. The other parameters that are used to predict both the deformation kinetics and the time-to-failure are identical to the values tabulated in Table 1.3. The experimental data is compared with the predictions in Figure 1.7. There is a clear difference between the yield stress versus strain rate data as measured in shear and that measured in tension. Not only is the yield stress significantly lower in shear, but its strain rate sensitivity is lower as well. The predictions using Equation (1.6) rewritten for the appropriate loading geometry, show that the pressure-modified Eyring relation is capable of accurately predicting these data quantitatively using the set of parameters obtained using tensile tests only. Apparently, deformation kinetics do

not change, and the influence of the loading geometry on the yield stress is taken into account correctly. The same holds for the predictions in Figure 1.7 (right), where again the time-to-failure is accurately predicted for both the specimens loaded in tension and the ones loaded in shear. These results clearly indicate that the presented approach can be successfully applied to PC. In the next sections the applicability to uPVC is tested to verify whether the approach can be employed for other glassy polymers.

1.4.4 Deformation kinetics of uPVC

The characterisation procedure for the deformation kinetics of uPVC is performed in the same way as for PC. The pressure dependence of uPVC is derived from data on yield stress measurements for tensile bars under superimposed hydrostatic stress as measured by Yuan *et al.* [77]. Their experimental data is reproduced in Figure 1.8. From the slope of the data points a value of μ=0.14 is derived using a least squares fit on Equation (1.9). The deformation of uPVC is somewhat more influenced by hydrostatic pressure than that of PC. The parameters ν^*, ΔU and $\dot{\gamma}_0$ were determined using tensile yield stress data as measured at various strain rates and temperatures for uPVC (see Figure 1.9 (left)). The experimental range was chosen such that no significant contribution of the secondary transition was expected, allowing the use of an Eyring instead of a Ree-Eyring relation for describing the deformation kinetics. The uPVC specimens show a steeper incline of the yield stress with increasing strain rates than found for PC. This reveals that the deformation of uPVC is more easily activated by an applied stress than that of PC, resulting in a lower activation volume. The

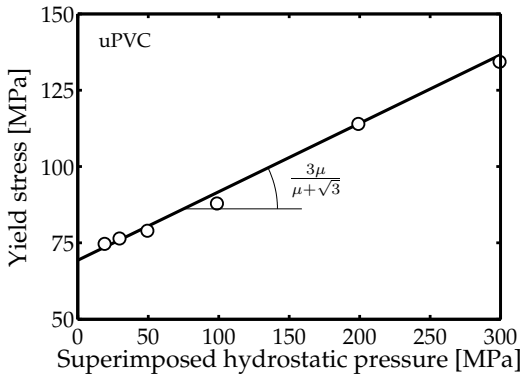

Figure 1.8 *The yield stress of uPVC as measured in tension with a superimposed hydrostatic pressure (data adopted from [77]). The solid line is a fit using Equation (1.9), resulting in μ=0.14.*

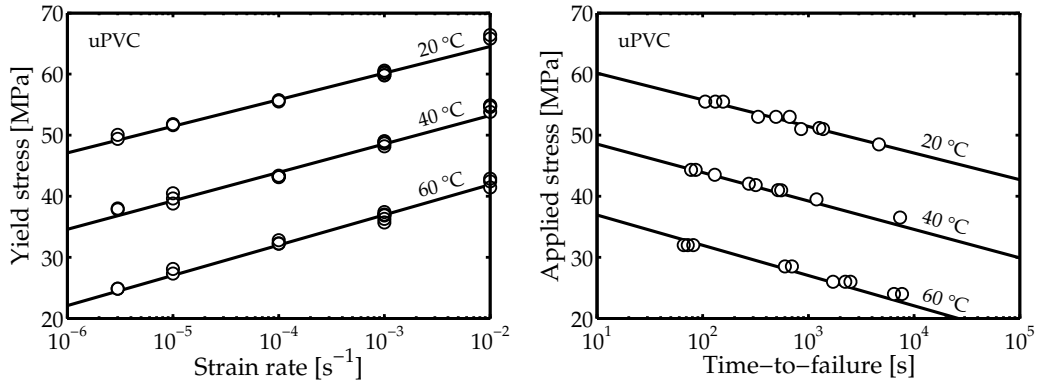

Figure 1.9 *Uniaxial tensile measurements performed on uPVC at 20 °C, 40 °C and 60 °C.* ***Left:*** *the yield stress for a range of strain rates. The solid lines represent the best fit using Equation (1.6).* ***Right:*** *the time-to-failure for specimen loaded at a range of constant stresses. The solid lines represent predictions using the data at 20 °C to calculate the critical equivalent strain and Equation (1.8).*

same can be observed for the influence of the temperature, although less distinct. Despite the differences in deformation kinetics the pressure-modified Eyring relation can be fitted accurately on the experimentally obtained yield data of uPVC. The least squares fit on all yield data resulted in the following values: ν^*=2.06 · 10^{-3} m^3/mol, ΔU=297 kJ/mol and $\dot{\gamma}_0$=3.7 · 10^{36} s^{-1}. The values for the activation volume and the activation energy are close to the values found by Bauwens-Crowet *et al.* [72] for uPVC (ν^*=1.9 · 10^{-3} m^3/mol and ΔU=295 kJ/mol respectively).

1.4.5 Critical plastic strain of uPVC

The critical equivalent plastic strain of uPVC was also determined using the failure times of uniaxial tensile creep experiments. Where the PC tensile bars failed in a ductile manner during the creep tests, the uPVC tensile bars mostly failed in a semi-ductile way. At the start of failure, a neck is formed, but the growth of this neck is limited and most bars break somewhere around the centre of the neck. Few tensile bars failed in a ductile way during experiments at 60 °C. As failure is defined here as the sudden steep increase of the strain rate, which starts at neck formation, this different behaviour can be regarded as post-failure behaviour and does not influence the failure kinetics considered here. The time-to-failure as measured for various applied stresses at three temperature levels is shown in Figure 1.9 (right). The solid lines represent the calculations using Equation (1.8), and applying the previously found material

parameters and a critical equivalent plastic strain of 1.5% as found using a fit on the 20 °C failure data. As for PC, the approach appears to take the influence of both temperature and stress appropriately into account, describing the experimental results accurately. Again the approach was validated for different thermodynamic states and finally for a practical application employing a different loading geometry.

1.4.6 Application to uPVC at different thermodynamic states

The deformation kinetics of three sets of uPVC specimens with a different thermal history (see Table 1.2) are compared here, to verify whether the approach can predict the failure kinetics for specimens that differ in thermodynamic state. The annealed specimens (set 2) were used to characterise uPVC. This set received an annealing treatment of $5 \cdot 10^5$ s at a temperature of 60 °C, whereas set 3 (severely annealed) was annealed for $3 \cdot 10^6$ s at 60 °C. These specimens differ in thermodynamic state from set 1 (as-manufactured), which did not receive an additional treatment. The difference in deformation kinetics between the three sets is shown in Figure 1.10 (left). The prediction of the deformation kinetics is based on one reference point for the as-manufactured and the severely annealed specimens, which is also used for the prediction of the time-to-failure of these specimens, shown in Figure 1.10 (right). Here, the quantitative prediction is

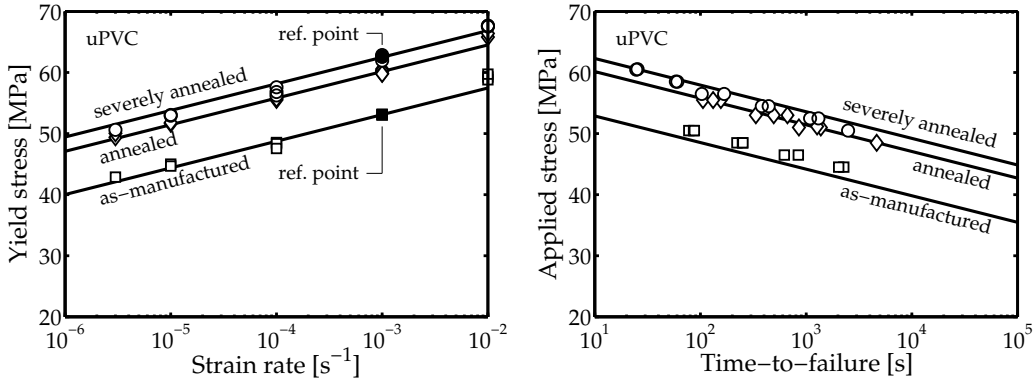

Figure 1.10 *Results of uniaxial tensile experiments at 20 °C on uPVC specimens from set 1 (as-manufactured) and set 3 (severely annealed), compared with data adopted from Figure 1.9 (left) (referred to as set 2 (annealed)).* ***Left:*** *the yield stress at various strain rates for the three sets of specimens. The deformation kinetics of set 1 and 3 are predicted using one reference point to determine $\dot{\gamma}_0$ and shown as solid lines.* ***Right:*** *the time-to-failure at a range of constant stress values for all three sets of specimens. The failure times for set 1 and 3 are predicted using the calculated $\dot{\gamma}_0$ and Equation (1.8), whereas the value of set 2 was obtained using the fitting procedure described in Section 1.4.4.*

good for the severely annealed specimens. For the as-manufactured specimens the slope is predicted well, but the absolute level is somewhat underestimated. The application of the approach results in a conservative prediction for the as-manufactured specimens. The origin of this effect might be the change in post-yield behaviour of uPVC upon ageing [78], an explanation that is addressed into more detail in Section 1.6.

1.5 Predicting time-to-failure of pressurised uPVC pipes

The predictive capacity of the presented approach for failure data of pipes subjected to an internal pressure is evaluated using data of Niklas and Kausch von Schmeling [64] on uPVC pipes. They applied various internal pressures on pipe segments in a thermal bath of 20 °C, 40 °C or 60 °C and measured the failure times. Their results have been reproduced in Figure 1.11. The stress state in the wall of a pressurised pipe is given by the stress in the circumferential (referred to as hoop stress, σ_h), longitudinal (σ_l), and the radial direction (σ_r). When a constant internal pressure (p_i) is applied these stresses can be calculated using Barlow's formula for thin-walled pressure vessels:

$$\begin{aligned} \sigma_h &= \frac{(D-2t_w)\cdot p_i}{2t_w}, \\ \sigma_l &= \frac{(D-2t_w)\cdot p_i}{4t_w}, \\ \sigma_r &= 0, \end{aligned} \tag{1.10}$$

with D, the outer diameter of the pipe and t_w, the wall thickness. Combining Equations (1.6), (1.7) and (1.10) and again using the approximation that $\sinh(x) \approx \frac{1}{2}\exp(x)$ for $x \gg 1$ results in the following relation for the time-to-failure of a pipe subjected to a constant internal pressure:

$$t_f\left(T, p_i\right) = \frac{2\bar{\gamma}_{cr}}{\dot{\gamma}_0} \cdot \exp\left(\frac{\Delta U}{RT} - \frac{(1+\mu)\cdot(D-2t_w)\cdot\nu^*}{4tRT}\cdot p_i\right). \tag{1.11}$$

Niklas and Kausch von Schmeling [64] presented their data in Von Mises stress (σ_{vm}) versus time-to-failure. The Von Mises stress for a pipe subjected to an internal pressure p_i is given by:

$$\sigma_{vm} = \sqrt{3}\frac{(D-2t_w)\cdot p_i}{4t_w}. \tag{1.12}$$

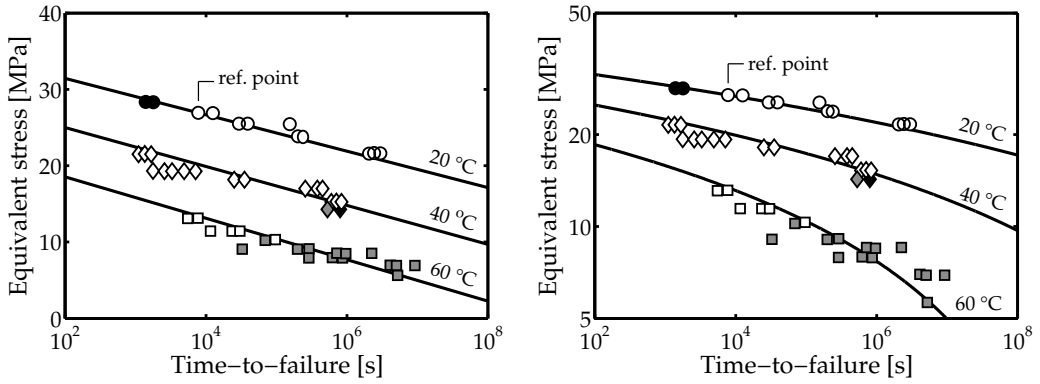

Figure 1.11 *Reproduction of the failure data of pressurised uPVC pipes as measured by Niklas and Kausch von Schmeling [64]. The three failure types (ductile tearing, hairline cracking and brittle fracture) are shown with unfilled, grey and black markers, respectively. The solid lines are predictions of the presented approach using Equation (1.11).* ***Left:*** *data and results plotted on semi-logarithmic axes.* ***Right:*** *data and results plotted on double logarithmic axes.*

The Von Mises stress is related to the equivalent stress according to: $\sigma_{vm}=\sqrt{3}\bar{\tau}$. The stress data of Niklas and Kausch von Schmeling can therefore be translated into equivalent stress values without actually knowing the diameter and wall thickness of the pipes used. The thermodynamic state of the specimens has to be known to compare the failure data of the pressurised pipes with the predictions of the approach presented in this paper. Therefore, $\dot{\gamma}_0$ is calculated using Equations (1.11) and (1.12) and one data point as a reference point. The resulting value, $\dot{\gamma}_0=1.8\cdot10^{36}$ s^{-1}, is between that of the annealed and the severely annealed specimens used in the current study. This indicates that the material has aged considerably caused by slow cooling after manufacturing or storage at an elevated temperature. The deformation kinetics in uniaxial tension of the pipe material can be predicted with the value of $\dot{\gamma}_0$. A comparison between the deformation kinetics of the pipe material (shown as dashed lines) with the as-manufactured and the annealed uPVC specimens used in this study is shown in Figure 1.12. The thermodynamic state of the pipe material used by Niklas and Kausch von Schmeling is comparable to that of the annealed specimens used in this study, resulting in nearly the same plastic deformation behaviour.

The lines in Figure 1.11 represent the predictions of the approach using the reference point indicated in the figure and the material parameters as derived for uPVC in the present study. Not only the stress dependence of the time-to-failure is predicted accurately, but also the temperature dependence agrees very well with the experimental values. This means that the stress and temperature dependence of the experimental data agrees with the plastic deformation kinetics of uPVC, leading to the conclusion that plasticity is the rate-determining step in

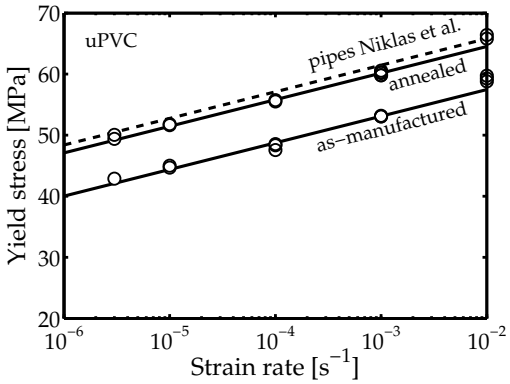

Figure 1.12 *Reproduction of Figure 1.10 (left) including the predicted yield stress of the pipe material of Niklas and Kausch von Schmeling [64] at various strain rates at 20 °C (dashed line).*

the failure process of these pipes. This is in line with observations of Castiglioni *et al.* [79], who showed that the deformation of pressurised pipe segments prior failure is comparable to the deformation of tensile bars subjected to a constant load.

Apparently, the influence of physical ageing during the experiments is low, as in the approach no changes in thermodynamic state during the experiments are taken into account. This is in line with statement that the pipes used by Niklas and Kausch von Schmeling were already aged considerably prior to testing. These results indicate that the presented approach is capable of predicting failure of a uPVC structure subjected to a 3D load. Remarkably, the approach gives accurate quantitative predictions of the time-to-failure for all three failure modes. This is in agreement with a statement of Niklas and Kausch von Schmeling [64]. Based on measurements of the circumferential strain they stated that all the failures modes they observed followed the same path up to failure. This remarkable result is discussed into more detail in the next section.

1.6 Discussion

As demonstrated in Figures 1.7 and 1.11, the approach gives quantitative predictions for the time at which ductile failure occurs for both PC and uPVC. Two observations could not be explained directly. Firstly, the failure time predictions for as-manufactured specimens slightly underestimated the experimental data. Secondly, the engineering approach seemed to be capable of predicting not only the time-to-failure for ductile failures, but also those for (semi-)brittle failures of

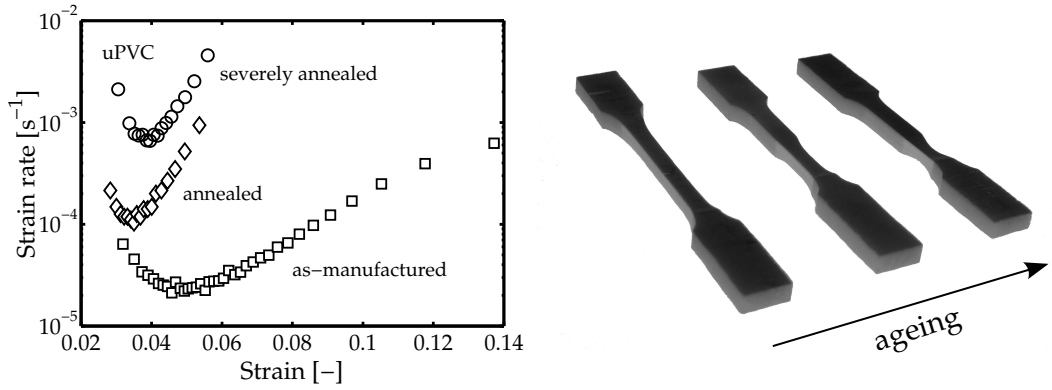

Figure 1.13 *The influence of physical ageing on the deformation behaviour of uPVC.* ***Left:*** *a Sherby-Dorn plot for set 1 (as-manufactured), set 2 (annealed) and set 3 (severely annealed) at a constant tensile load of 55.5 MPa, 44.5 MPa and 60.5 MPa respectively.* ***Right:*** *photo of tested tensile specimens with received different thermal treatments and, therefore, differ in age and strain localisation behaviour.*

uPVC pipes subjected to a constant pressure. Both observation seem to be related to the consequences of physical ageing and are discussed in this section.

The time-to-failure predictions for the uPVC as-manufactured specimens were found to slightly underestimate the experimentally obtained time-to-failure data, see Figure 1.10 (right). The predictions are based upon the hypothesis that the polymer fails when the accumulated plastic strain reaches a (constant) critical level at which strain softening sets in. Brady and Yeh [80] showed that glassy polymers that are cooled rapidly from the melt exhibit a more homogeneous deformation than glassy polymers that are annealed just below the glass transition temperature. These aged polymers show the tendency to localise the plastic deformation. This difference in deformation behaviour finds its origin in the post-yield behaviour of glassy polymers, which is influenced by the process of physical ageing [81]. Cross *et al.* [78] found that quenched PVC specimens showed uniform deformation in tensile experiments, whereas annealed specimens showed localised deformation behaviour (necking), as a result of an increased amount of strain softening. This difference in macroscopic plastic deformation is shown in Figure 1.13 (right) for uPVC specimens with an increasing age that were subjected to a tensile test. The influence of physical ageing on the amount of softening for the three sets of uPVC specimens used in this study is shown in a Sherby-Dorn plot in Figure 1.13 (left). With its reduced amount of strain softening in the as-manufactured specimens, the Sherby-Dorn plot of such a specimen does not superimpose on that of the two annealed specimens. This is the reason for the observed deviation. Assuming the approach can be applied for "young" specimens leads to predictions that deviate only

about 0.3 decade from experimentally obtained values. This difference decreases for older specimens and for the annealed and severely annealed specimens (for which the Sherby-Dorn plots *do* superimpose) the time-to-failure predictions are accurate.

A second point is that the presented approach proved to be capable of predicting not only the time-to-failure for pipe segments that failed in a ductile manner, but also the failure time of pipes with hairline cracks are accurately predicted. It seems counterintuitive that a quasi brittle failure mode can be predicted with an approach based on plastic deformation. Brittle failure is, however, usually preceded by a crazing mechanism [82], which in itself is initiated by (local) plastic deformation [83]. Physical ageing was already found to lead to a localisation of plastic strain of PVC by Cross *et al.* [78]. Let us now pose the hypothesis that upon ageing the polymer glass can reach a state in which the strain localises to such an extent that a craze forms. When this craze brakes down a crack is formed that is comparable to an extremely sharp notch. The subsequent crack grows at such a high rate that the time it takes the crack to grow to its critical value does not significantly contribute to the failure time [84]. The resulting failure time is approximately equal to the initiation time. Tervoort and Govaert [85] argued that the craze initiation kinetics for polystyrene are determined by nonlinear flow behaviour, which could be described with an Eyring flow relation. The initiation of strain localisation was found to depend only on the yield process. If the same holds for uPVC it supports the hypothesis in the sense that the initiation kinetics can be described with the plastic deformation kinetics of uPVC as found in this study. This implies that failures in region I do not necessarily have to be ductile. (Quasi) brittle failure can occur when strain localisation leads to a craze, which subsequently forms a crack that rapidly leads to failure. This failure path differs only slightly from region II failure where an *existing* imperfection grows up to failure. The significant contribution of the crack propagation time for failures that follow this mechanism (region II) explains the difference in failure kinetics.

Besides the two discussed consequences of physical ageing, a third consequence is reported in literature. From the mid-sixties onwards some authors noted to have found an endurance limit, i.e. a stress under which no failure seems to occur within experimentally acceptable timescales [86–89]. Such an endurance limit can be predicted by incorporating physical ageing kinetics in the plastic deformation behaviour as has been done by Klompen *et al.* [56] in a constitutive model for PC. The physical ageing kinetics of uPVC can be characterised in a similar way and is presented in the next chapter. The resulting aging kinetics are incorporated in the presented approach by making $\dot{\gamma}_0$ in Equation (1.6) a function of physical aging (thus time, temperature and stress dependent). The implementation and the implications for predictions of specimens that undergo a significant change in thermodynamic state during the test is the subject of the next chapter.

1.7 Conclusions

A new engineering approach for predicting the time-to-failure of loaded glassy polymers is presented, which has been applied to failure time prediction of ductile, region I, failure of uPVC pipes subjected to an internal pressure. The approach is founded on the hypothesis that plastic failure is governed by accumulation of plastic strain up to a critical value where the polymer enters its strain softening regime. A pressure-modified Eyring relation (Equation (1.6)) was employed to describe the deformation kinetics and to calculate the accumulation of plastic strain for a given load case. It has been shown, for both PC and uPVC, that this approach can predict the time-to-failure provided a single reference point is used to determine the thermodynamic state of the set of specimens. The approach has been validated and shown to hold quantitatively for specimens that received different heat treatments and for specimens subjected to different loading geometries. For rapidly cooled uPVC specimen the approach gives a somewhat conservative prediction, but for "older" specimens that do show strain softening behaviour the predicted failure times accurately agree with the experimental data. With the presented approach it is possible to determine the long-term hydrostatic strength (LTHS) with the engineering approach using only short-term tests, in some cases eliminating the necessity to carry out the conventionally used, expensive, long-term pressurised pipe tests.

References

[1] U. Schulte. A vision becomes true: 50 years of pipes made from High Density Polyethylene. In: *Proceedings of Plastic Pipes XIII*. Washington, **2006**.

[2] U.W. Gedde, J. Viebke, H. Leijström, and M. Ifwarson. Long-term properties of hot-water polyolefin pipes - A review. *Polymer Engineering and Science* 34:1773–1787, **1994**.

[3] R.W. Lang, A. Stern, and G. Doerner. Applicability and limitations of current lifetime prediction models for thermoplastics pipes under internal pressure. *Angewandte Makromolekulare Chemie* 247:131–145, **1997**.

[4] U. Andersson. Which factors control the lifetime of plastic pipes and how the lifetime can be extrapolated. In: *Proceedings of Plastic Pipe XI*. Munchen, **2001**.

[5] J.M. Greig. Polyethylene pipe in the British gas distribution system. *Plastics, Rubbers and Composites Processing and Applications* 21:133–140, **1994**.

[6] I. Hussain, S.H. Hamid, and J.H. Khan. Polyvinyl chloride pipe degradation studies in natural environments. *Journal of Vinyl & Additive Technology* 1:137–141, **1995**.

[7] S. Burn, P. Davis, T. Schiller, B. Tiganis, G. Tjandraatmadja, M. Cardy, S. Gould, P. Sadler, and A.J. Whittle. Long-term performance prediction for PVC pipes. Technical report, Awwa research foundation, **2006**. URL `http://www.iwapublishing.com/template.cfm?name=isbn1843399504`.

[8] H. Vogt, H.-F. Enderle, U. Schulte, and J. Hessel. Thermal ageing of PE 100 pipes for accelerated lifetime prediction under service conditions. In: *Proceedings of Plastic Pipes XIV*. Budapest, **2008**.

[9] L.S. Burn. Lifetime prediction of uPVC pipes - experimental and theoretical comparisons. *Plastics, Rubbers and Composites Processing and Applications* 21:99–108, **1994**.

[10] J.A. Sauer and C.C. Chen. Crazing and fatigue behavior in one- and two-phase glassy polymers. *Advances in Polymer Science* 52:169–224, **1983**.

[11] C. Jacob. Rupture fragile des produits en PVC rigide. *Pure and Applied Chemistry* 49:615–626, **1977**.

[12] G.J. Sandilands and J. Bowman. An examination of the role of flaw size and material toughness in the brittle fracture of polyethylene pipes. *Journal of Materials Science* 21:2881–2888, **1986**.

[13] R.W. Truss. Temperature derating of unplasticised polyvinyl chloride (uPVC) pressure pipes. *Plastics and Rubber Processing and Applications* 7:51–56, **1987**.

[14] Y. Hu, J. Summers, A. Hiltner, and E. Baer. Correlation of fatigue and creep crack growth in poly(vinyl chloride). *Journal of Materials Science* 38:633–642, **2003**.

[15] J.P. Lu, P. Davis, and L.S. Burn. Lifetime prediction for ABS pipes subjected to combined pressure and deflection loading. *Polymer Engineering and Science* 43:444–462, **2003**.

[16] R.K. Krishnaswamy. Analysis of ductile and brittle failures from creep rupture testing of high-density polyethylene (HDPE) pipes. *Polymer* 46:11664–11672, **2005**.

[17] N. Brown. Slow crack growth-notches-pressurized polyethylene pipes. *Polymer Engineering and Science* 47:1951–1955, **2007**.

[18] J.R. Martin and F.A. Johnson. Poly(vinyl chloride): Effect of molecular weight and vapor environment on viscoelastic and fatigue properties. *Journal of Applied Polymer Science* 18:3227–3236, **1974**.

[19] Y.-L. Huang and N. Brown. The effect of molecular weight on slow crack growth in linear polyethylene homopolymers. *Journal of Materials Science* 23:3648–3655, **1988**.

[20] K.V. Gotham and M.J. Hitch. Design considerations for fatigue in uPVC pressure pipes. *Pipes and Pipelines International* 20:10–17, **1975**.

[21] J. Robeyns and Ph. Vanspeybroeck. Molecular-oriented PVC (MOPVC) and PVC-U pipes for pressure applications in the water industry. *Plastics, Rubbers and Composites* 34:318–323, **2005**.

[22] P. Benjamin. Quality and quality control of unplasticised polyvinylchloride (uPVC) pressure pipes. *Plastics and Rubber: Materials and Applications* 5:151–160, **1980**.

[23] B. Terselius and J.-F Jansson. Gelation of PVC, Part 2: Effect on internal pressure resistance. *Plastics and Rubber Processing and Applications* 4:285–290, **1984**.

[24] Y.-L. Huang and N. Brown. Dependence of slow crack growth in polyethylene on butyl branch density: Morphology and theory. *Journal of Polymer Science Part B: Polymer Physics* 29:129–137, **1991**.

[25] D.B. Barry and O. Delatycki. The effect of molecular structure and polymer morphology on the fracture resistance of high-density polyethylene. *Polymer* 33:1261–1265, **1992**.

[26] P. Paris and F. Erdogan. A critical analysis of crack propagation laws. *Journal of Basic Engineering* 85:528–534, **1963**.

[27] E.H. Andrews and B.J. Walker. Fatigue fracture in polyethylene. *Proceedings of the Royal Society A* 325:57–79, **1971**.

[28] S.H. Joseph and P.S. Leevers. Failure mechanics of uPVC cyclically pressurized water pipelines. *Journal of Materials Science* 20:237–245, **1985**.

[29] L. Johansson and B. Törnell. Initiation of fractures in rigid PVC pipes by soft particles. *Journal of Vinyl Technology* 9:103–107, **1987**.

[30] A. Gray, J.N. Mallinson, and J.B. Price. Fracture behaviour of polyethylene pipes. *Plastics and Rubber Processing and Applications* 1:51–53, **1981**.

[31] N. Brown. Intrinsic lifetime of polyethylene pipelines. *Polymer Engineering and Science* 47:477–480, **2007**.

[32] I.M. Ward. Review: The yield behaviour of polymers. *Journal of Materials Science* 6:1397–1417, **1971**.

[33] J. Matthijs. Het gebruik van kunststoffen voor leidingen voor gasdistributie. *Ingenieursblad* 42:46–52, **1973**.

[34] J.M. Hutchinson. Physical aging of polymers. *Progress in Polymer Science* 20:703–760, **1995**.

[35] T. Alfrey, G. Goldfinger, and H. Mark. The apparent second-order transition point of polystyrene. *Journal of Applied Physics* 14:700–705, **1943**.

[36] J.R. McLoughlin and A.V. Tobolsky. Effect of rate of cooling on stress relaxation of polymethyl methacrylate. *Journal of Polymer Science* 7:658, **1951**.

[37] J.H. Golden, B.L. Hammant, and E.A. Hazell. The effect of thermal pretreatment on the strength of polycarbonate. *Journal of Applied Polymer Science* 11:1571–1579, **1967**.

[38] A. Tobolsky and H. Eyring. Mechanical properties of polymeric materials. *Journal of Chemical Physics* 11:125–134, **1943**.

[39] F. Bueche. Tensile strength of plastics below the glass temperature. *Journal of Applied Physics* 28:784–787, **1957**.

[40] S.N. Zhurkov. Kinetic concept of the strength of solids. *International Journal of Fracture* 1:311–323, **1965**.

[41] B.D. Coleman. Application of the theory of absolute reaction rates to the creep failure of polymeric filaments. *Journal of Polymer Science* 20:447–455, **1956**.

[42] H. Eyring. Viscosity, plasticity, and diffusion as examples of absolute reaction rates. *Journal of Chemical Physics* 4:283–291, **1936**.

[43] F.R. Larson and J. Miller. A time-temperature relationship for rupture and creep stresses. *Transactions of the American Society of Mechanical Engineers* 74:765–775, **1952**.

[44] K. Richard, G. Diedrich, and E. Gaube. Trinkwasserrohre aus Niederdruckpolyäthylen. *Kunststoffe* 49:516–525, **1959**.

[45] A.D. Whyman and E. Szpak. Pinpointing the hydrostatic design stress of HDPE pipe. *SPE Journal* 29:74–78, **1973**.

[46] S.J. Barton and B.W. Cherry. Predicting the creep rupture life of polyethylene pipe. *Polymer Engineering and Science* 19:590–595, **1979**.

[47] C. Bauwens-Crowet, J.-M. Ots, and J.C. Bauwens. The strain-rate and temperature dependence of yield of polycarbonate in tension, tensile creep and impact tests. *Journal of Materials Science Letters* 9:1197–1201, **1974**.

[48] E.T.J. Klompen, T.A.P. Engels, L.C.A. van Breemen, P.J.G. Schreurs, L.E. Govaert, and H.E.H. Meijer. Quantative prediction of long-term failure of polycarbonate. *Macromolecules* 38:7009–7017, **2005**.

[49] M.C. Boyce, D.M. Parks, and A.S. Argon. Large inelastic deformation of glassy polymers. Part I: rate dependent constitutive model. *Mechanics of Materials* 7:15–33, **1988**.

[50] E.M. Arruda and M.C. Boyce. A three dimensional constitutive model for the large stretch behavior of rubber elastic materials. *Journal of the Mechanics and Physics of Solids* 41:389–412, **1993**.

[51] O.A. Hasan, M.C. Boyce, X.S. Li, and S. Berko. An investigation of the yield and postyield behavior and corresponding structure of poly(methyl methacrylate). *Journal of Polymer Science Part B: Polymer Physics* 31:185–197, **1993**.

[52] C.P. Buckley and D.C. Jones. Glass-rubber constitutive model for amorphous polymers near the glass transition. *Polymer* 36:3301–3312, **1995**.

[53] C.P. Buckley, P.J. Dooling, J. Harding, and C. Ruiz. Deformation of thermosetting resins at impact rates of strain. Part 2: constitutive model with rejuvenation. *Journal of the Mechanics and Physics of Solids* 52:2355–2377, **2004**.

[54] J.J. Wu and C.P. Buckley. Plastic deformation of glassy polystyrene: A unified model of yield and the role of chain length. *Journal of Polymer Science Part B: Polymer Physics* 42:2027–2040, **2004**.

[55] T.A. Tervoort, E.T.J. Klompen, and L.E. Govaert. A multi-mode approach to finite, three-dimensional, nonlinear viscoelastic behavior of polymer glasses. *Journal of Rheology* 40:779–797, **1996**.

[56] E.T.J. Klompen, T.A.P. Engels, L.E. Govaert, and H.E.H. Meijer. Modelling of the postyield response of glassy polymers: influence of thermomechanical history. *Macromolecules* 38:6997–7008, **2005**.

[57] M.C. Boyce and E.M. Arruda. An experimental and anaiytical investigation of the large strain compressive and tensile response of glassy polymers. *Polymer Engineering and Science* 30:1288–1298, **1990**.

[58] P.D. Wu and E. van der Giessen. On neck propagation in amorphous glassy polymers under plane strain tension. *International Journal of Plasticity* 11:211–235, **1995**.

[59] L.E. Govaert, P.H.M. Timmermans, and W.A.M. Brekelmans. The influence of intrinsic strain softening on strain localization in polycarbonate: Modeling and experimental validation. *Journal of Engineering Materials and Technology* 122:177–185, **2000**.

[60] J.M. Crissman and G.B. McKenna. Relating creep and creep rupture in PMMA using a reduced variable approach. *Journal of Polymer Science Part B: Polymer Physics* 25:1667–1677, **1987**.

[61] R.K. Krishnaswamy and M.J. Lamborn. The influence of process history on the ductile failure of polyethylene pipes subject to continuous hydrostatic pressure. *Advances in Polymer Technology* 24:226–232, **2005**.

[62] G. Butters. *Particulate nature of PVC: formation, structure and processing*. Applied Science Publishers LTD, **1982**.

[63] E.T.J. Klompen and L.E. Govaert. Nonlinear viscoelastic behaviour of thermorheologically complex materials - A modelling approach. *Mechanics of Time-Dependent Materials* 3:49–69, **1999**.

[64] H. Niklas and H.H. Kausch von Schmeling. Molekularstruktur und mechanische Eigenschaften von Polyvinylchlorid III. Mitteilung: Ursachen zeitabhängiger Festigkeitseigenschaften von PVC-Rohren. *Kunststoffe* 53:886–891, **1963**.

[65] D.H. Ender. Stress softening and strain softening of poly(methyl methacrylate) in yielding under constant load. *Journal of Applied Physics* 39:4877–4882, **1968**.

[66] M.J. Mindel and N. Brown. Creep and recovery of polycarbonate. *Journal of Materials Science* 8:863–870, **1973**.

[67] I.M. Ward and M.A. Wilding. Creep behavior of ultrahigh-modulus polyethylene: Influence of draw ratio and polymer composition. *Journal of Polymer Science: Polymer Physics Edition* 22:561–575, **1984**.

[68] E.J. Kramer and E.W. Hart. Theory of slow, steady state crack growth in polymer glasses. *Polymer* 25:1667–1678, **1984**.

[69] O.D. Sherby and J.E. Dorn. Anelastic creep of polymethyl methacrylate. *Journal of the Mechanics and Physics of Solids* 6:145–162, **1958**.

[70] R.M. Ogorkiewicz and A.A.M. Sayigh. The strength of rigid PVC. *British Plastics* 40:126–128, **1967**.

[71] Y. Nanzai. Plastic deformation mechanism in PMMA under creep stress. *JSME International Journal Series A, Solid Mechanics and Material Engineering* 37:149–154, **1994**.

[72] C. Bauwens-Crowet, J.C. Bauwens, and G. Homès. Tensile yield-stress behavior of glassy polymers. *Journal of Polymer Science. Part A-2, Polymer Physics* 7:735–742, **1969**.

[73] R.A. Duckett, B.C. Goswami, L. Stewart, A. Smith, I.M. Ward, and A.M. Zihlif. The yielding and crazing behaviour of polycarbonate in torsion under superposed hydrostatic pressure. *Britisch Polymer Journal* 10:11–16, **1978**.

[74] T. Ree and H. Eyring. Theory of non-Newtonian flow. I. Solid plastic system. *Journal of Applied Physics* 26:794–800, **1955**.

[75] C. Tsitsilianis, M. Tsapatsis, and Ch. Economou. Effects of crystallinity on ageing phenomena in poly(vinyl chloride). *Polymer* 60:1861–1866, **1989**.

[76] A.W. Christiansen, E. Baer, and S.V. Radcliffe. The mechanical behaviour of polymers under high pressure. *Philosophical Magazine* 24:451–467, **1971**.

[77] J. Yuan, A. Hiltner, and E. Baer. The mechanical properties of PVC under high pressure. *Journal of Materials Science* 18:3063–3071, **1983**.

[78] A. Cross, R.N. Haward, and N.J. Mills. Post yield phenomena in tensile tests on poly(vinyl chloride). *Polymer* 20:288–294, **1979**.

[79] G. Castiglioni, D. Verzanini, and A. Pavan. Prediction of ductile failure in u-PVC pipes from creep tests on specimens. In: *Proceedings of Plastic Pipes XII*. Baveno, **2004**.

[80] T.E. Brady and G.S.Y. Yeh. Yielding behavior of glassy amorphous polymers. *Journal of Applied Physics* 42:4622–4630, **1971**.

[81] H.G.H. van Melick, L.E. Govaert, and H.E.H. Meijer. Localisation phenomena in glassy polymers: influence of thermal and mechanical history. *Polymer* 44:3579–3591, **2003**.

[82] R.P. Kambour. Mechanism of fracture in glassy polymers. II. Survey of crazing response during crack propagation in seval polymers. *Journal of Polymer Science. Part A-2, Polymer Physics* 4:17–24, **1966**.

[83] E.J. Kramer. Microscopic and molecular fundamentals of crazing. *Advances in Polymer Science* 52/53:1–56, **1983**.

[84] P.J.F. van den Heuvel. PVC pressure pipes: the importance of gelation to ensure pipe reliability. In: *Proceedings of Plastic Pipes V*. York, **1982**.

[85] T.A. Tervoort and L.E. Govaert. Craze-initiation kinetics in polystyrene. *Journal of Polymer Science Part B: Polymer Physics* 42:2066–2073, **2004**.

[86] J. Worp. Een en ander over hard p.v.c.-buis en haar toepassingsmogelijkheden. *Het Gas* 78:2–12, **1957**.

[87] D.H. Ender and R.D. Andrews. Cold drawing of glassy polystyrene under dead load. *Journal of Applied Physics* 36:3057–3062, **1965**.

[88] N.T. Smotrin. Limiting states of rigid polyvinyl chloride in creep. *Polymer Mechanics* 1:81–86, **1965**.

[89] D.J. Matz, W.G. Guldemond, and S.I. Cooper. Delayed yielding in glassy polymers. *Journal of Polymer Science: Polymer Physics Edition* 10:1917–1930, **1972**.

The influence of physical ageing on the yield behaviour of uPVC[1]

Chapter 2

Abstract

The timescale at which ductile failure occurs in loaded glassy polymers can be successfully predicted using the engineering approach presented in the previous chapter. This approach does not take progressive physical ageing into account. Physical ageing causes an increase resistance against plastic deformation, resulting in an increase in the failure time, which may eventually lead to an endurance limit. Such a limit is likely to occur in uPVC pipe networks used for gas distribution purposes, as these pipes are generally designed for very long service times (at least 50 years). In this chapter the influence of progressive physical ageing on the plastic deformation behaviour of uPVC is characterised and incorporated in the engineering approach. With this modification it is possible to make quantitative predictions, even for very long failure times where the influence of physical ageing becomes apparent. The predictions are compared with failure data of uPVC specimens which were subjected to constant or dynamic loads. In dynamic loading conditions a second type of failure mode was observed: fatigue crack growth. A brief study on the kinetics of this failure mechanism confirmed that slow crack growth failure is not expected to occur within the lifetime of uPVC gas pipes.

[1]Reproduced from: H.A. Visser, T.C. Bor, M. Wolters, J.G.F. Wismans, L.E. Govaert, Lifetime assessment of load-bearing polymer glasses; The influence of physical ageing, *Macromolecular Materials and Engineering*, submitted, **2010**

2.1 Introduction

Since the 1950's polymer pipes have been installed in water and gas distribution systems throughout the world. The same holds for the Dutch gas distribution network, in which a significant number of polymer pipes has been installed in the first decade after the discovery of the Slochteren gas field in 1959. The service life of these pipes was initially specified to be 50 years. This means that replacement based on the time a pipe has been in service will lead to the renewal of thousands of kilometres of pipelines in the near future. Since replacement of these distribution systems is labour intensive, its postponement will result in huge economic savings for society. On the other hand, the integrity of the network should not be compromised, especially in the case of gas distribution networks where failure can lead to life threatening situations [1, 2]. Consequently, the prediction of the residual lifetime of polymer pipes has received considerable attention, see for example [3–6]. As the lifetimes of the pipes can exceed 50 years, accelerating tests have been developed to determine the lifetime based on short-term tests. The most well known test used for this purpose are experiments where the failure time of a pipe segment that is subjected to a constant internal pressure is measured. The lifetime is estimated by extrapolating the time-to-failure measured at testing conditions (mostly at elevated temperatures) towards a reference condition according to a method described in ISO 9080. A typical result is shown schematically in Figure 2.1 (left). In general three regions can be observed with each having different failure mechanisms [3, 7, 8]. In the high stress region (region I) the pipe segment shows a considerable amount of

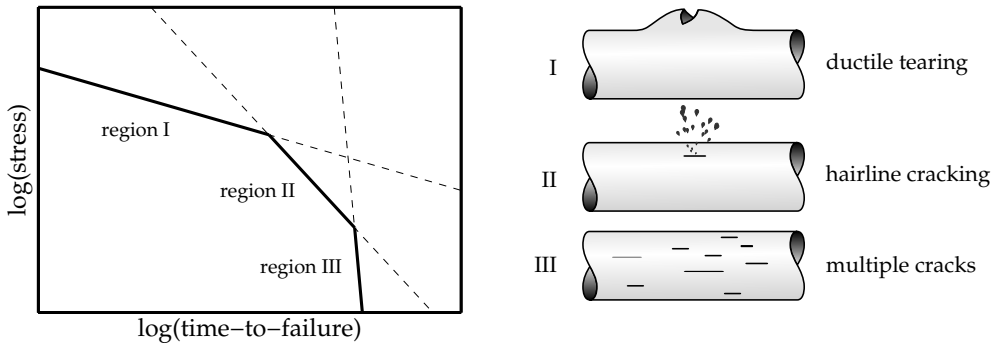

Figure 2.1 ***Left:*** *schematic representation of typical time-to-failure behaviour of plastic pipes subjected to a constant internal pressure.* ***Right:*** *three failure modes that can occur in pipes subjected to a constant internal pressure that are generally each associated to one of the three regions.*

plastic deformation before failure. The pipe bulges until the tensile strength is reached locally and rupture occurs. A model for the deformation kinetics can be employed to make quantitative predictions of the failure time of these ductile failures, as has been shown in the previous chapter. At lower stresses a knee can be observed in the curve describing the failure kinetics, which is sometimes referred to as the "mechanical knee" [8]. The failure in region II is attributed to slow crack growth, leading to a hairline crack. The hairline crack is a slit in axial direction with a small plastic zone at the ends. Various models exist that can predict the failure kinetics in regime II quantitatively, most of which are based on a fracture mechanics approach to calculate the crack growth rate (e.g. [5, 9, 10]). Failure in the third region is related to progressive molecular degradation leading to the formation of multiple cracks [7, 11]. The subsequent time-to-failure is almost independent of the applied stress.

In this study the focus is on the long-term behaviour of unplasticised poly(vinyl chloride) (uPVC) pipes, which have been used extensively in the gas, water and sewer distribution networks in the Netherlands. Increased knowledge on the stabilisation of uPVC [14, 15] and the influence of processing conditions on the mechanical properties [13, 16], has led to prolonged region III and region II failure times. As a result, the long-term behaviour of the pipes is improved considerably and region I failure has become the limiting region for a wider range of failure times. The predictive approach for region I failure as presented in Chapter 1 is based on the hypothesis that the polymer fails when the accumulated plastic strain reaches a critical value and the polymer enters its softening regime. This approach proved successful to quantitatively predict long-term failure of pipes subjected to a constant internal pressure as shown in Figure 2.2 (left). Remarkably, the predictions not only hold for the ductile failures, but also

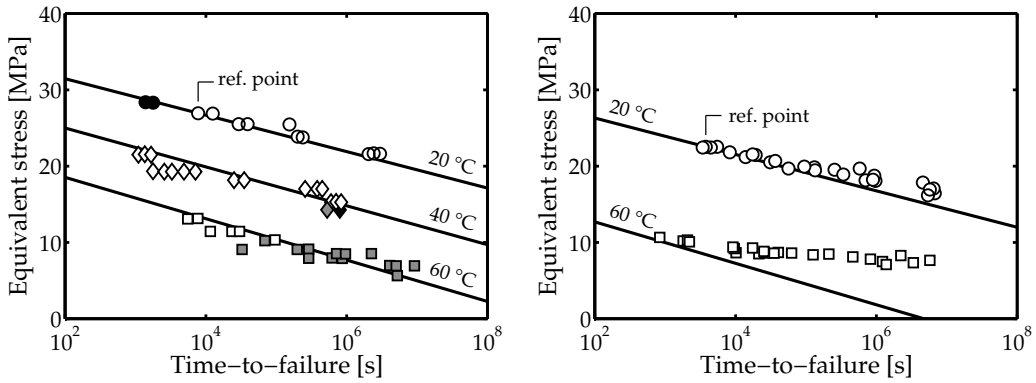

Figure 2.2 *Time-to-failure data for pipes subjected to an internal pressure. The three failure types (ductile tearing, hairline cracking and brittle fracture) are shown with white, grey and black filled markers, respectively. The solid lines represent predictions of the approach presented in Chapter 1.* ***Left:*** *Predictions for data from Niklas and Kausch von Schmeling [12].* ***Right:*** *Predictions for ductile failure data of Benjamin [13].*

for pipes which failed as a result of hairline cracks. This is in line with the statement of Niklas and Kausch von Schmeling [12] that slow crack growth did not significantly contribute to the failure time of the PVC pipes they subjected to an internal pressure. Based upon the experimental observation that all failure modes showed similar circumferential strain behaviour up to failure, they stated that all failure modes followed a common path up to failure. Where Niklas and Kausch von Schmeling modelled the complete visco-elastic creep behaviour to predict failure for pressurised pipes, the previous chapter showed that capturing the secondary creep alone is sufficient for quantitative failure predictions.

Here, the hypothesis is posed that the transition from ductile failure towards hairline cracking is caused by time-dependent changes in the mechanical properties of uPVC as a result of physical ageing. This phenomenon finds its origin in the fact that glassy polymers like uPVC[2] are not in a state of thermodynamic equilibrium, but display a continuous strive towards it [17]. As a consequence, the volume decreases, whereas the yield stress increases gradually in time [18]. The increase of the yield stress leads to increased strain softening, which has a strong influence on the failure mode of this type of materials. Increased strain softening leads to a stronger strain localisation [19–21]. Eventually, the plastic zone localises to such an extent that cavitation takes place and a craze is initiated [22]. When the craze breaks down, a crack is formed which acts as an extremely sharp notch. The subsequent crack growth occurs at such a high rate that the time it takes for the crack to grow to a critical level does not significantly contribute to the overall failure time [23]. This explains why a different failure mode is observed macroscopically, whereas the path up to failure (accumulation of plastic strain up to a critical value) is, in essence, the same.

Klompen *et al.* [24] observed a similar transition from ductile to a brittle failure mode for polycarbonate tensile bars subjected to a static load. They showed that the transition can indeed be attributed to an increase in yield stress resulting from progressive physical ageing, i.e. ageing occurring during the experiment itself, confirming the posed hypothesis. They also showed that the increase in yield stress not only influences the failure mode, but the progressive increase in resistance against plastic deformation also leads to the occurrence of a so-called endurance limit. Such a limit under which no failure is observed within experimentally acceptable timescales has been observed for several glassy polymers under deadweight load [25–28]. Despite the change in failure mode, such a change in kinetics is not apparent in the experimental data of Niklas and Kausch von Schmeling [12]. Comparable measurements by Benjamin [13], as reproduced in Figure 2.2 (right), do show an endurance limit. The solid lines represent

[2] Although PVC can have a crystallinity of up to 10% its mechanical properties closely relate to those found for other amorphous (glassy) polymers.

predictions of the current approach that do not take physical ageing into account. The predictions clearly underestimate the failure time observed experimentally, especially at 60 °C.

In the present study the physical ageing kinetics is incorporated in the existing engineering approach as presented in Chapter 1. The procedure employed in this work is similar to the procedure Klompen *et al.* [29] used to incorporate the kinetics of physical ageing into their constitutive model. In the resulting engineering approach the time-to-failure follows from a closed form expression. Moreover, it is shown that the more laborious characterisation and numerical calculations of the constitutive approach of Klompen *et al.* can be circumvented for simple structures subjected to 3D loads. In the next section this procedure for implementing the ageing kinetics is described and the relevant expressions are elucidated. Subsequently, the physical ageing kinetics including its dependence on temperature and stress, is characterised using short-term tensile experiments. To conclude, the approach is validated on experimentally obtained failure data for tensile specimens subjected to either constant or dynamic loads.

2.2 Theoretical background

The approach presented in Chapter 1 is based on the hypothesis that ductile failure occurs when the accumulated plastic strain reaches a critical value, where the polymer enters its softening regime. A pressure-modified Eyring relation [30] was employed to calculate the equivalent plastic strain rate ($\dot{\bar{\gamma}}$) for a given temperature (T), pressure (p) and equivalent stress ($\bar{\tau}$):

$$\dot{\bar{\gamma}}(T, p, \bar{\tau}) = \dot{\gamma}_0 \cdot \exp\left(\frac{-\Delta U}{RT}\right) \cdot \sinh\left(\frac{\bar{\tau} v^*}{RT}\right) \cdot \exp\left(\frac{-\mu p v^*}{RT}\right), \tag{2.1}$$

with R to denote the universal gas constant. The pre-exponential factor ($\dot{\gamma}_0$) in Equation (2.1) is related to the entropy of the system and thus the thermodynamic state of the polymer. The more the polymer has aged, the lower the value of $\dot{\gamma}_0$ will be, reflecting the increased resistance against plastic deformation of the aged glassy polymer. The first exponential term includes the influence of temperature on the plastic strain rate using activation energy (ΔU). In the second term the activation volume v^* determines the sensitivity of the plastic strain rate to the stress. The third term is included to take the influence of the hydrostatic pressure p into account via the pressure dependence parameter μ, making Equation (2.1) valid for any 3D loading geometry. Each of the parameters was determined using short-term tensile tests on the uPVC pipe material in Chapter 1. The definitions of

Table 2.1 *Definition of the equivalent plastic strain rate $\dot{\bar{\gamma}}$, the equivalent stress $\bar{\tau}$ and the hydrostatic pressure p as used in Equation (2.1) as a function of the strain and stress tensor.*

Definitions
$\dot{\bar{\gamma}} = \sqrt{2 \cdot \left(\dot{\epsilon}_{11}^2 + \dot{\epsilon}_{22}^2 + \dot{\epsilon}_{33}^2 + 2\dot{\epsilon}_{12}^2 + 2\dot{\epsilon}_{23}^2 + 2\dot{\epsilon}_{31}^2\right)}$
$\bar{\tau} = \sqrt{\frac{1}{6} \cdot \left[(\sigma_{11} - \sigma_{22})^2 + (\sigma_{22} - \sigma_{33})^2 + (\sigma_{33} - \sigma_{11})^2\right] + \sigma_{12}^2 + \sigma_{23}^2 + \sigma_{13}^2}$
$p = -\frac{1}{3} \cdot (\sigma_{11} + \sigma_{22} + \sigma_{33})$

the equivalent plastic strain rate ($\dot{\bar{\gamma}}$), the equivalent stress ($\bar{\tau}$) and the hydrostatic pressure (p) are given in Table 2.1.

Brady and Yeh [19] and Matz *et al.* [31] showed that the stress and temperature dependence (and hence the activation volume and energy) of polycarbonate are influenced by an annealing treatment. In other studies [32, 33] is was showed, however, that the deformation kinetics can still be described accurately using constant values for the activation volume and energy. Klompen *et al.* [29] proposed to make only $\dot{\gamma}_0$ in Equation (2.1) a function of time (t) to incorporate the influence of physical ageing. Here, a similar function is used to describe the behaviour of uPVC:

$$\dot{\gamma}_0(T, \bar{\tau}, t) = b_0 \cdot \left(\frac{t_{eff}\left(T, \bar{\tau}, t\right) + t_{ini}}{t_0} \right)^{b_1}, \tag{2.2}$$

where b_0 and b_1 are constants[3] and t_0=1 s. The initial age of the specimen is denoted as t_{ini}, which is related to the thermo-mechanical history of the material. As it is well known that the process of physical ageing is accelerated by temperature [18] and stress and strain [29, 34–38], the effective time (t_{eff}) is introduced. The effective time is a measure for the ageing time t at reference conditions (zero stress and T=T_{ref}) and is related to the ageing time at temperature T and stress $\bar{\tau}$ via the acceleration factors a_T and a_σ, respectively. The effective time is defined as:

$$t_{eff} = \int_0^t \frac{\mathrm{d}t'}{a_T(T) \cdot a_\sigma(T, \bar{\tau})}, \tag{2.3}$$

where a_T is the temperature-induced acceleration factor and a_σ the stress-induced acceleration factor. These acceleration factors are equal to unity for the reference condition. The relation for the plastic deformation rate including the influence

[3] The constants b_0 and b_1 presented here are directly related to some of the ageing parameters in the work of Klompen *et al.* [29]: b_0=$\dot{\gamma}_{0,rej} \cdot \exp(-c_0)$ and b_1=$\frac{-c_1}{\ln(10)}$.

of physical ageing can now be obtained by combining Equations (2.1), (2.2) and (2.3):

$$\dot{\bar{\gamma}}(T,p,\bar{\tau},t) = \frac{b_0}{t_0^{b_1}} \cdot \left(\int_0^t \frac{\mathrm{d}t'}{a_T(T) \cdot a_\sigma(T,\bar{\tau})} + t_{ini} \right)^{b_1} \cdots \\ \cdot \exp\left(\frac{-\Delta U - \mu p v^*}{RT} \right) \cdot \sinh\left(\frac{\bar{\tau} v^*}{RT} \right). \quad (2.4)$$

As failure occurs when the accumulated plastic strain reaches a critical level, the time-to-failure can be found by integrating the rate of plastic deformation (Equation (2.4)) up to the critical equivalent strain.

$$\bar{\gamma}_{acc} = \int_0^t \dot{\bar{\gamma}}(T,p,\bar{\tau},t)\,\mathrm{d}t, \qquad \text{failure occurs if:} \quad \bar{\gamma}_{acc} = \gamma_{cr} \quad (2.5)$$

This relation can be used to deduct analytical expressions for the time-to-failure for different load cases. In the validation procedure, which follows after the characterisation of the physical ageing kinetics of uPVC, the expressions for a constant and a dynamic (triangular) tensile load are given.

2.3 Experimental

2.3.1 Material and specimen preparation

The uPVC specimens were taken out of an excavated uPVC gas distribution pipe that was in service for several decades. The pipe has a diameter of 160 mm and a wall thickness of about 4.1 mm. A section of 70 mm was cut from the pipe with a bandsaw and subsequently sawed in half in axial direction. These parts were then pressed into flat plates in a press at 100 °C,[4] thus approximately 20 °C above the glass transition temperature of uPVC, in 25 minutes at a pressure of approximately 1 MPa. This procedure erased all prior effects of physical ageing, thus $\dot{\gamma}_0$ of the specimens that are manufactured in this way is only dependent on the cooling rate in the cold press and subsequent heat treatments. Tensile bars with a gauge section of approximately $30\times5\times4.1$ mm^3 were milled from the plate

[4] It is known that a heat treatment at 100 °C can influence the crystallinity of the uPVC [39]. A change in crystallinity can have marked effect on the physical ageing behaviour of uPVC [40]. As all specimens used throughout this study received the same preparation procedure, differences in ageing behaviour are not to be expected.

material with the length direction of the tensile bars parallel to the axial direction of the pipe.

The compact tension specimens were milled from plates that were produced in the same way as the ones used for producing the tensile specimens. The geometry of the compact tension specimens is in accordance with the ASTM E-647 standard, and have a characteristic width of 32 mm (from backside to center of holes). The notch was machined in the axial direction of the original pipe.

2.3.2 Experimental setup

All uniaxial tensile, creep and fatigue measurements were carried out on an MTS Elastomer Testing System 810 equipped with a 25 kN force cell or a Zwick Z010 equipped with a 2.5 kN force cell. Engineering stresses were calculated using the average of the cross-sectional surface areas as measured at three locations in the gauge section of the specimen. The tensile experiments were carried out at a constant crosshead speed, thus at a constant *engineering* strain rate. The creep tests were conducted at a constant load, thus at constant *engineering* stress. For all fatigue tests a triangular signal was used. Two sets of fatigue tests were conducted. For the first set of experiments the minimum stress was kept at a constant level of 2.5 MPa while varying the maximum stress level and frequency of the stress signal. The second set of fatigue experiments was conducted at three different levels of the stress ratio (minimum stress/maximum stress level) for a range of maximum stresses and a frequency of 1 Hz.

The fatigue crack growth measurements were carried out with a sinusoidal stress signal with a frequency of 1 Hz and at four different stress ratios. The crack growth was monitored with the use of a video camera.

2.4 Ageing kinetics of uPVC

At room temperature uPVC is about 60 °C below its glass transition temperature, T_g, and about 60 °C above its β-transition. Although the main chain segmental mobility is low at room temperature, it is sufficient to allow for small conformational changes towards their thermodynamically favoured positions [17]. With annealing, defined here as a heat treatment at a temperature below T_g, this process can be accelerated, which makes the ageing effect more apparent at shorter timescales.

The influence of annealing at four different temperatures on the yield stress of uPVC tensile specimens as measured at 25 °C and a strain rate of 10^{-3} s^{-1} is

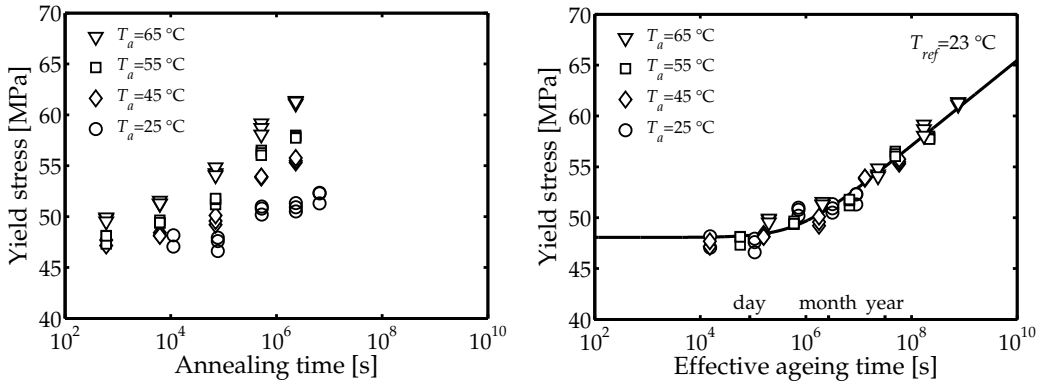

Figure 2.3 *Tensile yield stress data of uPVC measured at a strain rate of 10^{-3} s^{-1} and a temperature of 25 °C, after annealing at different temperatures.* ***Left:*** *plotted against the annealing time.* ***Right:*** *the same yield stress data plotted against the effective ageing time at a reference temperature of 23 °C, using an activation energy as calculated from the slope in Figure 2.4.*

shown in Figure 2.3. The yield stress increases about 20% after an annealing treatment of $2.3 \cdot 10^6$ s (corresponding to almost a month) at 65 °C. The data for the different annealing temperatures can be shifted towards one single curve, using only horizontal shift factors. The natural logarithm of the horizontal shift factors are plotted versus the inverse of the annealing temperatures in Figure 2.4. The data can be accurately described with a linear relation. This suggests that an Arrhenius type of time-temperature superposition can be employed to calculate

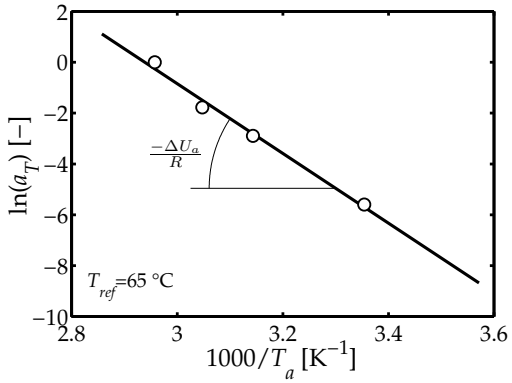

Figure 2.4 *The natural logarithm of the shift factor versus the annealing temperature. The factor a_T is defined in this figure as the factor required to shift the yield data for the different annealing times on top of the yield data for the specimens annealed at 65 °C. The activation energy (ΔU_a) in Equation (2.6) can be calculated from the slope of the solid line, resulting in a value of 115 kJ/mol.*

the shift factor a_T:

$$a_T(T_a) = \exp\left(\frac{\Delta U_a}{R} \cdot \left(\frac{1}{T_a} - \frac{1}{T_{ref}}\right)\right), \tag{2.6}$$

where the activation energy (ΔU_a) can be calculated from the slope of the best fit in Figure 2.4, resulting in a value of 115 kJ/mol. The temperature during annealing is denoted as T_a and T_{ref} is the reference temperature. A clear distinction should be made between T_a and T_{ref} in Equation (2.6) and the temperature T in Equation (2.1) at which the tensile test is carried out. T_a influences the ageing kinetics, T_{ref} the timescale of the mastercurve and T the plastic deformation rate. The mastercurve resulting from shifting the yield data in Figure 2.3 (left) to a reference temperature of 23 °C with Equation (2.6) is shown in Figure 2.3 (right). This mastercurve can be described with Equation (2.4), for which the initial age of the specimens t_{ini} and the constants b_0 and b_1 were obtained using a non-linear least squares fitting routine. The value for the initial age (t_{ini}) determines the length of the time-independent initial plateau and depends on the thermo-mechanical history of the material. The values of b_0 and b_1 determine the position and slope of the time-dependent yield behaviour. The value for b_0 depends on the choice of the reference temperature and b_1 is only material dependent. With the non-linear least squares fitting routine a best fit was found with b_0=$1.51 \cdot 10^{44}$ s^{-1} (at T_{ref}=23 °C), b_1=0.95 and t_{ini}=$7.1 \cdot 10^5$ s. The latter value implies that ageing will occur already after one week at T_a=T_{ref} and $\bar{\tau}_a$=0 MPa. The fit is shown as a solid line in Figure 2.3 (right) and accurately follows the experimental results.

As already stated, the segmental mobility of polymer chains in a glassy polymer is also known to increase by applying a mechanical load, resulting in mechanically enhanced ageing [29, 34–38] (also referred to as stress/strain induced ageing). The kinetics of stress-induced ageing are characterised by first subjecting specimens to a constant tensile stress of 25 MPa or 32.5 MPa for a range of ageing times. Subsequently, the cross-sectional area of the specimens is measured again and a tensile test is performed at a strain rate of 10^{-3} s^{-1} at 23 °C.[5] The resulting yield stress data are shown in Figure 2.5. The mastercurve at T=T_a=23 °C is

[5]The tensile measurements of the specimens aged at 25 MPa were carried out at a temperature lower than 23 °C. As the temperature during the tensile test has a marked influence on the yield stress (about 0.75 MPa/K around room temperature), the measured tensile yield stress is compensated to comply with a testing temperature of 23 °C with the use of Equation (2.1) and the parameters determined in Chapter 1.

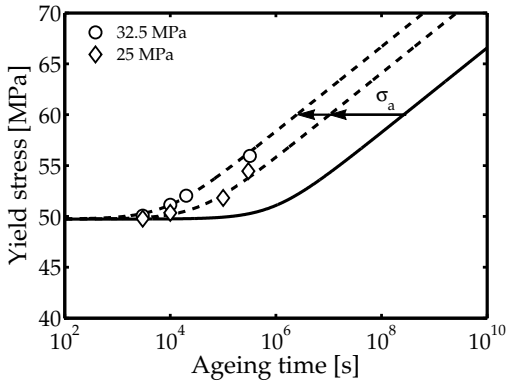

Figure 2.5 *Tensile yield stress of uPVC at a strain rate of 10^{-3} s^{-1} and a temperature of 23 °C, after ageing the specimens at a tensile stress of 25 MPa or 32.5 MPa for a range of ageing times. The solid line represents the mastercurve for uPVC at 23 °C. The dashed lines show the shifted mastercurve to the ageing condition of the respective specimens. For the shift as given by Equation (2.7) an activation volume (ν_a) of $9.65 \cdot 10^{-4}$ m^3/mol has been used.*

shown as a solid line in the same figure. This mastercurve can be shifted towards the yield stress data of the aged specimens using an Eyring type time-stress superposition as proposed by Tervoort *et al.* [41]:

$$a_\sigma(T_a, \bar{\tau}_a) = \frac{\bar{\tau}_a \nu_a}{RT_a} \cdot \sinh\left(\frac{\bar{\tau}_a \nu_a}{RT_a}\right)^{-1}. \tag{2.7}$$

The observed shift towards the dashed lines as a result of load application is well-predicted using ν_a=$9.65 \cdot 10^{-4}$ m^3/mol.

The parameters that followed from the characterisation of the temperature and stress-induced ageing kinetics of uPVC are summarised in Table 2.2. The next step is to verify whether the approach can successfully predict the influence of progressive physical ageing during creep and fatigue experiments.

Table 2.2 *The values for the parameters of uPVC as used in this work.*

μ=	0.14	[-]†	b_0=	$1.51 \cdot 10^{44}$	[s^{-1}]
ν^*=	$2.06 \cdot 10^{-3}$	[m^3/mol]†	b_1=	-0.95	[-]
ΔU=	$2.97 \cdot 10^5$	[J/mol]†	ΔU_a=	$1.15 \cdot 10^5$	[J/mol]
$\bar{\gamma}_{cr}$=	0.015	[-]†	ν_a=	$9.65 \cdot 10^{-4}$	[m^3/mol]

† Value determined in Chapter 1

2.4.1 Validation using uniaxial tensile creep failure data

The method is validated first with the use of creep failure data. In Chapter 1, it has been shown that the time-to-failure could be predicted employing Equation (2.1) to calculate the accumulation of the plastic strain up to a critical equivalent plastic strain ($\bar{\gamma}_{cr}$) for uPVC subjected to a constant tensile load. The predictions proved to agree quantitatively with experimental measurements as long as physical ageing did not have a significant influence. Beyond this point the influence of physical ageing emerges as the resistance against plastic deformation increases, leading to progressively longer failure times. With the use of Equations (2.4) and (2.5), this influence of physical ageing is into account for failure time predictions.

The deduction of the closed form solution of Equation (2.5) for isothermal, constant stress conditions (creep tests) can be found in Appendix 2.A. The equivalent stress and the hydrostatic pressure for specimens subjected to uniaxial tension can be calculated using the definitions given in Table 2.1 and are given in Table 2.3. During a creep test the ageing temperature is equal to the testing temperature and the ageing stress equal to the applied stress (σ), thus T_a=T and $\bar{\tau}_a$=$\frac{\sigma}{\sqrt{3}}$. For the time-to-failure this results in:

$$t_f(T,\sigma) = a_T(T)\cdot a_\sigma(T,\frac{\sigma}{\sqrt{3}})\cdots \\ \cdot\left(\left[\frac{\bar{\gamma}_{cr}\cdot t_0^{b_1}\cdot\,(b_1+1)\cdot\exp\left(\frac{\Delta U}{RT}-\frac{\mu\sigma\nu^*}{3RT}\right)}{a_T(T)\cdot a_\sigma(T,\frac{\sigma}{\sqrt{3}})\cdot b_0\cdot\sinh\left(\frac{\sigma\nu^*}{\sqrt{3}RT}\right)}+t_{ini}^{b_1+1}\right]^{\frac{1}{b_1+1}}-t_{ini}\right). \quad (2.8)$$

The only unknown parameter in this relation is the initial thermodynamic state represented by the initial age (t_{ini}). This parameter can be calculated from the yield stress of a specimen which has the same thermo-mechanical history as the specimens used in the creep tests. The relation between initial age and the yield

Table 2.3 *Relations for the equivalent stress and hydrostatic pressure as defined in Table 2.1 for uniaxial tension and a pipe with outer diameter D and wall thickness t subjected to an internal pressure (p_i).*

	Uniaxial tension	Internal pressure
$\bar{\tau}$	$\frac{\sigma}{\sqrt{3}}$	$\frac{(D-2t)\cdot p_i}{4t}$
p	$-\frac{\sigma}{3}$	$-\frac{(D-2t)\cdot p_i}{4t}$

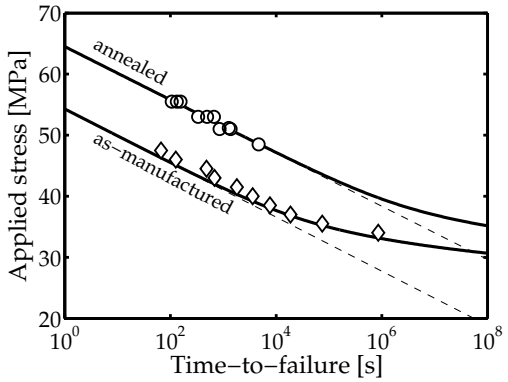

Figure 2.6 *The time-to-failure for uPVC under a constant uniaxial load for annealed (tested at 20 °C) and as-manufactured (tested at 24 °C) specimens. The predictions employing Equation (2.8) that includes the influence of physical ageing are shown as solid lines and the predictions excluding ageing are shown as dashed lines.*

stress as measured at a certain strain rate ($\dot{\epsilon}$) and temperature is obtained by rewriting Equation (2.4):

$$t_{ini} = \left(\frac{\sqrt{3}\dot{\epsilon} \cdot t_0^{b_1} \cdot \exp\left(\frac{3\Delta U - \mu\sigma_y v^*}{3RT}\right)}{b_0 \cdot \sinh\left(\frac{\sigma_y v^*}{\sqrt{3}RT}\right)} \right)^{\frac{1}{b_1}} . \tag{2.9}$$

The experimentally obtained time-to-failure data is shown for two different sets of specimens in Figure 2.6. The first set is referred to as "annealed" and was annealed for $5 \cdot 10^5$ s at 60 °C. The other set is referred to as "as-manufactured" and did not receive a heat treatment after the production procedure as described in Section 2.3.1. The annealed specimens were tested at a temperature of 20 °C, whereas the as-manufactured specimens were tested at 24 °C. Therefore, the difference between the failure times of the two sets of specimens cannot be attributed solely to the difference in thermal history, but is partly a testing temperature effect (for about 3 MPa).

The initial age as determined using the tensile yield stress of each set of specimens is found to be $1.2 \cdot 10^8$ s and $1.8 \cdot 10^6$ s for the annealed and as-manufactured specimens respectively (T_{ref}=23 °C). The time-to-failure predictions which follow from Equation (2.8) are shown as solid lines in Figure 2.6. The dashed lines in this figure represent failure predictions of the approach excluding the influence of physical ageing. Ageing does not influence the failure kinetics for short failure times. In this regime both predictions are in agreement with the experimental

data. At longer failure times the influence of ageing becomes apparent. For the as-manufactured specimens this occurs at failure times longer than about 10^3 s. At these timescales the resistance against plastic deformation of the specimen changes during the creep test, mainly owing to stress-induced ageing. The predicted endurance limit[6] is in quantitative agreement with the one observed experimentally. For the annealed specimens no endurance limit was observed experimentally, which is in agreement with the theoretical prediction that ageing effects appear for failure times longer than about 10^5 s. This marked difference with the as-manufactured specimens is a direct result of the difference in the initial age of the two sets of specimens caused by the ageing procedure of the annealed specimens.

Employing Equation (2.8) to predict the long-term failure data of PC as presented by Klompen *et al.* [24] results in a prediction that is comparable to their prediction. It is noteworthy that whereas Klompen *et al.* used a model incorporating the full constitutive behaviour of PC to calculate the failure times, here the predictions follow from a closed-form analytical relation (Equation (2.8)).

2.5 Validation using failure data for internally pressurised pipes

The engineering approach is validated by predicting the time-to-failure for two sets of failure data for pressurised pipes from different sources. The first set comprises failure data of pipes under an internal pressure as presented by Niklas and Kausch von Schmeling [12], that are reproduced in Figure 2.7 (left). Two types of predictions were calculated. The dashed lines represent the prediction for the approach in which physical ageing effects were not taken into account. The predictions represented as solid lines do include these effects. The initial age is calculated using one reference point and Equation (2.9), resulting in a value of $3.2 \cdot 10^8$ s which is relatively high when compared to the initial age values found for the tensile specimens used in this study (see Section 2.4). This explains why the prediction that neglects the influence of physical ageing, holds so well up to very long failure times. Furthermore, it is noteworthy that the transition from ductile failure to hairline cracking indeed occurs in the region where the solid lines start to deviate from the dashed lines; thus, where the approach predicts a change in yield behaviour as a result of physical ageing. This supports the

[6] Although no mathematical lower stress limit exists in Equation (2.8) where t_f becomes infinitive, such a limit is experienced within experimentally realistic timescales. As mentioned earlier, this "limit" is referred to as the endurance limit.

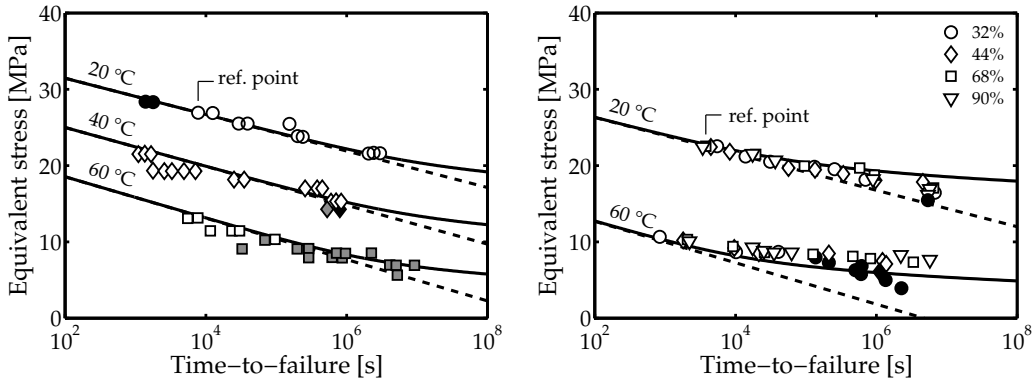

Figure 2.7 *Time-to-failure for uPVC pipes subjected to an internal pressure. Predictions with the approach including the influence of physical ageing on the resistance against plastic deformation are shown in solid lines and predictions excluding ageing effects in dashed lines.* ***Left:*** *as measured at three temperatures (reproduced from [12]). The white, grey and black filled markers represent the failure modes ductile rupture, hairline cracking and brittle fracture respectively.* ***Right:*** *failure data of pressurised uPVC pipes with different levels of gelation at two temperatures (reproduced from [13]). The white filled markers represent ductile failures and the black filled markers represent brittle failures.*

hypothesis that the transition to hairline cracking is governed by physical ageing, leading to a more localised deformation behaviour. The transition sets in when a certain thermodynamic state is reached, which, in this case, occurs directly when ageing becomes apparent. These two transitions do not necessarily have to be connected as can be seen in the other set of experimental pipe failure data that is predicted next.

The second set of failure data of pipes was presented by Benjamin in [42], who studied the influence of the level of gelation on the time-to-failure of pipes. As already stated in Section 2.1, the increased knowledge on stabilisation and processing has led to improved service lifetimes of uPVC pipes. Especially the processing conditions have a significant influence on the mechanical properties of the uPVC product. The degradation temperature of PVC is lower than the the melting temperature at which the primary particle structure[7] within the PVC grains is destroyed, thus uPVC, unlike most other polymers, cannot be processed from the melt. Destroying the primary particle structure is therefore difficult, and poor processing can result in a PVC product in which the primary particle structure is still partly intact. This primary particle grains can act as stress concentrators in the final product, influencing its mechanical properties. The level of gelation is related to the degree in which the primary PVC particle

[7] A comprehensive description of a working model of the particulate structure of PVC can be found in [43].

structure is destroyed during processing and thus a measure for the homogeneity of the molecular structure (e.g. [43, 44]). A significant part of the Dutch gas distribution network was installed in the period from the sixties up to the mid-seventies using uPVC pipes, when the developments in processing were still taking place. Evaluation of used pipe segments from this production period showed that the degree of gelation of these pipes varies from poor to "over-gelled" (thermally degraded) [45]. The failure data from Benjamin [13] (reproduced in Figure 2.7 (right)) are used to study the influence of the level of gelation on the ageing kinetics. Benjamin subjected four different sets of uPVC pipes to a constant internal pressure at two temperatures. Each set was processed under different extrusion conditions resulting in a range of gelation levels; from very poor gelation (32%), up to so-called over-gelation (90%). It is well known that the level of gelation has a marked influence on mechanical properties like impact strength and strain at break [13, 46–50]. The yield properties of uPVC, however, are insensitive for the level of gelation [13, 47–49]. This is also demonstrated in Figure 2.7 (right); the failure kinetics, including the development of an endurance limit, are equal for all four levels of gelation. The initial age is calculated using one reference point and is only $1.2 \cdot 10^6$ s. This supports the strong influence of physical ageing at relatively short failure times in the experimental data. The predicted influence of the ageing kinetics agrees reasonably well with the measurements at 20 °C, but is somewhat conservative for the measurements at 60 °C. Nonetheless, the approach gives quite an accurate prediction for the level of stress that can be sustained for a certain amount of time.

Like the data of Niklas and Kausch von Schmeling, the data of Benjamin show a transition towards a brittle failure mode. In the data of Benjamin, however, this transition in failure mode is accompanied by a transition in failure kinetics and a knee is observed. Only for the lowest level of gelation region II failure is observed. For low levels of gelation the primary particle structure is still partly present, which can act as a stress concentrator, leading to slow crack growth failure. For increased levels of gelation, the size of the initial flaws caused by the primary particle structure are expected to decrease, shifting region II failure towards longer failure times. Some remarks on region II (crack growth) failure are given in Section 2.7.

2.6 Validation using dynamic fatigue data

The predictions for the evolution of yield stress are shown to hold for constant loads. In water distribution networks oscillating pressures caused by opening and closing valves are common [51]. Oscillations in the applied stress are known

to accelerate the stress-induced ageing process, when compared to a constant mean stress [52]. Predictions of the proposed engineering approach are compared with data for uPVC tensile bars under a cyclic load in this section, to verify whether the proposed approach can adequately take dynamic stress effects into account.

2.6.1 Modelling dynamic fatigue failure

The triangular stress signal as applied on the tensile bars is shown schematically in Figure 2.8 (left). By calculating the equivalent plastic strain rate for small timesteps with Equation (2.1), the accumulation of the plastic strain can be determined. The accumulated plastic strain (excluding the influence of physical ageing) is plotted as a function of time in Figure 2.8 (right). The figure clearly shows that the plastic strain accumulates differently for a triangular stress signal than during a creep test at the mean stress level (σ_m) of the triangular signal. Therefore, the solution for the time-to-failure as found for constant loads (Equation (2.8)) cannot be employed directly for a dynamic load. An acceleration factor for the deformation kinetics ($a_{d,\dot{\tilde{\gamma}}}$) similar to the one proposed by Janssen *et al.* [53], is applied to circumvent a numerical procedure to find the failure time for dynamic stress signals. The acceleration factor is defined as the accumulated plastic strain after one triangular stress cycle (excluding physical ageing effects), divided by accumulated plastic strain for a constant stress with a value equal to

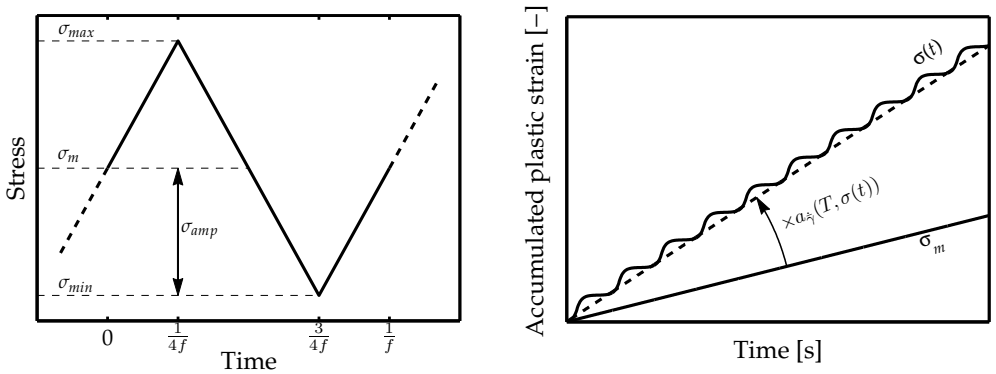

Figure 2.8 ***Left:*** *schematic representation of a triangular waveform of the stress as a function of time, including the definitions for the maximum (σ_{max}), mean (σ_m) and minimum stress (σ_{min}), the stress amplitude (σ_{amp}) and the frequency (f).* ***Right:*** *the accumulation of the plastic strain for a triangular waveform, $\sigma(t)$, and a constant load equal to the mean stress of the triangular waveform (σ_m), shown in solid black lines. The accumulation of the plastic strain for a triangular stress signal as calculated using the acceleration factor ($a_{d,\dot{\tilde{\gamma}}}$) is shown as a dashed line.*

σ_m during the time of one cycle (=$1/f$):

$$a_{d,\dot{\bar{\gamma}}}(T,\sigma(t')) = \frac{\int_0^{1/f} \left\{ \exp\left(\frac{\mu\,\sigma(t')\nu^*}{3RT}\right) \cdot \sinh\left(\frac{\sigma(t')\nu^*}{\sqrt{3}RT}\right) \right\} \mathrm{d}t'}{\frac{1}{f} \cdot \exp\left(\frac{\mu\sigma_m\nu^*}{3RT}\right) \cdot \sinh\left(\frac{\sigma_m\nu^*}{\sqrt{3}RT}\right)}. \tag{2.10}$$

The solution for a triangular and a square wave of this acceleration factor is deducted in the appendix of [53]. For a triangular waveform the solution is given by:

$$a_{d,\dot{\bar{\gamma}}} = \frac{\sinh\left(\frac{\sigma_{amp}}{\sigma_0}\right)}{\frac{\sigma_{amp}}{\sigma_0}}, \qquad \text{with:} \quad \sigma_0 = \frac{3RT}{(\mu+\sqrt{3})\cdot\nu^*}. \tag{2.11}$$

According to this result the acceleration factor for the triangular signal is independent of the frequency of the stress signal, which is consistent with the experimental data of Janssen *et al.* [53]. The equivalent plastic strain rate for a dynamic stress signal can be calculated by multiplying Equation (2.10) with Equation (2.1), resulting in the dashed line in Figure 2.8 (right). The dashed line deviates from the solid line during each cycle, but the accumulated plastic strains are equal after each whole cycle. The error in the predicted failure time is smaller than $(t_f f)^{-1}$ when using the acceleration factor. The accuracy of the predictions thus increases when the cycle time of the stress signal becomes much shorter than the time-to-failure.

Not only the plastic deformation kinetics, but also the ageing kinetics are influenced by a dynamic stress signal. The evolution of the effective time as defined in Equation (2.3) for a dynamic stress signal can also be calculated using an acceleration factor ($a_{d,age}$), which is defined in a similar way as $a_{d,\dot{\bar{\gamma}}}$:

$$a_{d,age}(T_a,\sigma(t')) = f \cdot a_\sigma\left(T_a, \frac{\sigma_m}{\sqrt{3}}\right) \cdot \int_0^{1/f} \frac{\mathrm{d}t'}{a_\sigma\left(T_a, \frac{\sigma(t')}{\sqrt{3}}\right)}. \tag{2.12}$$

The deduction of the analytical solution for a triangular wave form is given in Appendix 2.B. This acceleration factor is also found to be independent of the frequency. The effective time for a dynamic stress signal can be calculated by multiplying Equation (2.3) with Equation (2.12).

The closed form solution of the time-to-failure for a creep test can be rewritten to give the time-to-failure for a specimen under isothermal, uniaxial, dynamic

tensile stress conditions using the two acceleration factors $a_{d,\dot{\bar{\gamma}}}$ and $a_{d,age}$:

$$t_f(T,\sigma_m,\sigma_{amp}) = \frac{a_T(T)\cdot a_\sigma(T,\frac{\sigma_m}{\sqrt{3}})}{a_{d,age}(T,\sigma_m,\sigma_{amp})}\cdots$$
$$\cdot\left[\left(\frac{a_{d,age}(T,\sigma_m,\sigma_{amp})\cdot\bar{\gamma}_{cr}\cdot t_0^{b_1}\cdot(b_1+1)}{a_T(T)\cdot a_\sigma(T,\frac{\sigma_m}{\sqrt{3}})\cdot a_{d,\dot{\bar{\gamma}}}(T,\sigma_m,\sigma_{amp})\cdot b_0}\cdot\sinh\left(\frac{\sigma_m\nu^*}{\sqrt{3}RT}\right)^{-1}\right.\right.$$
$$\left.\left.\cdot\exp\left(\frac{\Delta U}{RT}-\frac{\mu\sigma_m\nu^*}{3RT}\right)+t_{ini}^{b_1+1}\right)^{\frac{1}{b_1+1}}-t_{ini}\right]. \quad (2.13)$$

Both $a_{d,\dot{\bar{\gamma}}}$ and $a_{d,age}$ are frequency independent, which makes the time-to-failure also frequency independent.

2.6.2 Frequency dependence

In this section the frequency independent failure behaviour as predicted by the relations presented in the previous sections is verified. Two different sets of uPVC tensile specimens were subjected to a triangular cyclic load at a range of maximum stresses and a constant minimum stress of 2.5 MPa, for various frequencies. One set was annealed for $2.2\cdot10^6$ s at a temperature of 60 °C ("annealed"), the other set of specimens did not receive any additional heat treatment ("as-manufactured"). The experimental results for the time-to-failure are shown in Figure 2.9. The most striking result is that two types of failure kinetics are observed. The failure kinetics in the high stress region (region I,

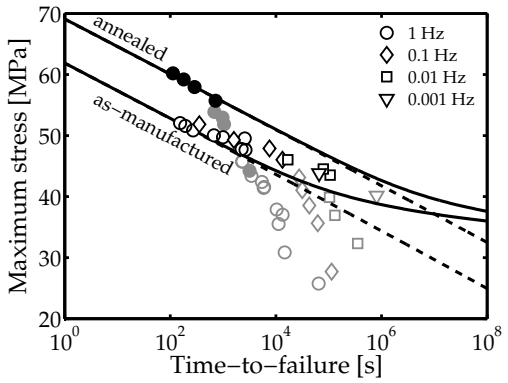

Figure 2.9 *Time-to-failure for uPVC tensile specimens subjected to a triangular stress signal at various frequencies. The minimum stress level is kept at a constant value of 2.5 MPa. The as-manufactured specimens (open markers) did not receive any additional heat treatment, whereas the annealed specimens (black filled markers) were annealed for $2.2\cdot10^6$ s at 60 °C. The specimens that failed as a result of fatigue crack growth are shown as grey markers.*

referred to as "yield line" in fatigue studies) is dominated by plastic deformation and has been the failure mode of interest in this chapter sofar. The region II failure mode observed at lower stresses (grey markers) is presumably related to fatigue crack growth failure. As anticipated, the yield line is frequency independent, whereas the fatigue crack growth failures shift towards longer failure times with a decrease in frequency. Furthermore, the yield line is clearly influenced by the annealing treatment; the line is shifted almost two decades towards longer failure times. On the other hand, the crack growth appears to be uninfluenced by the annealing treatment. More data for multiple sets of specimens at different thermodynamic states are required to confirm this observation. Only the yield line is of interest for validating the presented approach for plastic deformation and ageing kinetics. The region II failures are discussed in more detail in Section 2.7.

The predictions are again shown as solid and dashed lines for the approach including and excluding ageing kinetics. The initial age of each set of specimens is calculated from one reference point. The short failure times are predicted accurately, but the experimental data for the as-manufactured specimens level off at somewhat shorter failure times than the theoretical predictions. The ageing trend is captured reasonably well by the engineering approach, but is somewhat conservative. A similar but much more pronounced deviation was reported by Janssen *et al.* [52] for polycarbonate. This seems to suggest that the material ages somewhat faster for dynamic loading conditions than predicted. The subtle difference between the influence of a constant and dynamic stress signals on the ageing rate is not yet fully understood.

2.6.3 Stress ratio dependence

The experimental failure data presented in the previous section was measured for signals with a changing σ_{max}, but a constant σ_{min} (=2.5 MPa). In this section the influence of a change in stress ratio (R=$\sigma_{min}/\sigma_{max}$) is studied. The difference in stress signal for three levels of R and for a creep test (R=1) is shown in Figure 2.10 (left). The resulting (predicted) failure times are shown in Figure 2.10 (right) for these four stress signals. The failure times of ductile (yield) failures are shorter when the stress ratio increases towards unity; the time at high stress levels increases, increasing the rate at which the plastic deformation accumulates. Consequently, the critical level of plastic strain is reached in a shorter timeframe, and the failure time decreases. The failure time for creep tests shifts about 1.4 decade towards longer failure times for specimens subjected to a dynamic stress with a stress ratio of 0.1. The non-linear relation between the stress and the strain rate leads to the effect that the difference in failure time between

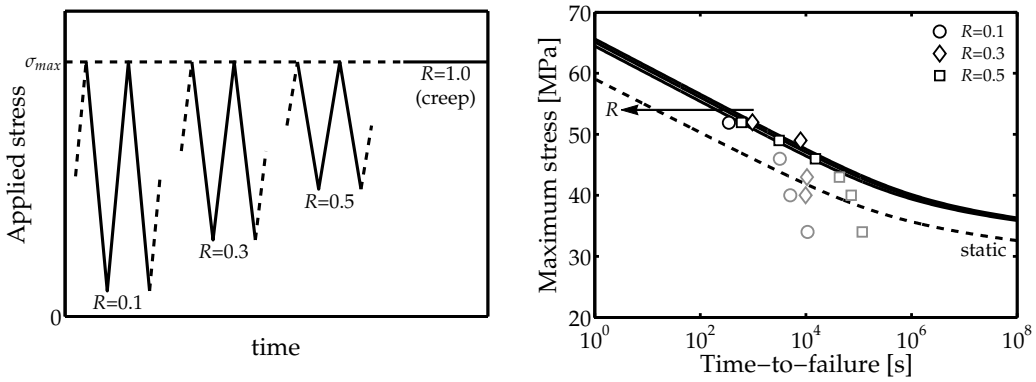

Figure 2.10 *Influence of variation of the stress ratio R on the time-to-failure.* ***Left:*** *schematic representation of the applied stress signal for three values of R, compared with a creep signal.* ***Right:*** *time-to-failure for uPVC tensile specimens subjected to a triangular stress load at a frequency of 1 Hz and for three R values: 0.1, 0.3, 0.5 at 23 °C. The solid lines represent model predictions for the three values of R. The dashed line is a prediction for the failure time of these specimens, subjected to a static load (creep, R=1).*

R=0.1 and R=0.5, is much less pronounced than the difference between R=0.5 and R=1. This behaviour is also observed experimentally: the failure times for the dynamic stresses at the three different stress ratios are within a tight range. Now it has been shown that the proposed engineering approach is capable of predicting the yield failure behaviour (including the influence of the frequency and the stress ratio of the applied stress signal), the behaviour of the other failure mechanism that is observed in the presented failure data is discussed.

2.7 Some preliminary remarks on crack growth

In Section 2.6 a knee was observed in the failure data of the fatigue measurements. The specimens that failed in the region after the knee are filled with surface cracks, which suggests the specimens have failed because of a fatigue crack growth mechanism. This mechanism is comparable to slow crack growth failure of a specimen subjected to a constant load in the sense that in both cases an inherent flaw grows as a result of a load and eventually causes the specimen to fail. Remarkably, the creep failure data of the tensile bars (Figure 2.6) and the data of Niklas and Kausch von Schmeling (Figure 2.7) did not show any transition towards slow crack growth failure. The question arises why this failure mechanism was not (yet) observed and at which timescale this second type of failure kinetics may become apparent. Therefore, a procedure to predict region II failure (slow crack growth) in creep tests, using region II failure data of

fatigue tests (fatigue crack growth), is discussed in this section. Such a procedure implicitly assumes that the underlying mechanism for slow crack growth failure and fatigue crack growth failure is similar and can be described with the similar relations. In the next sections it is shown that it is important to take the influence of both the frequency (f) and the stress ratio (R) of the dynamic stress signal into account. The influence of frequency is studied using a relation proposed by Kim *et al.* [54] to describe the dynamic fatigue failure data in Section 2.7.1. Subsequently, the influence of an increase of the stress ratio of the dynamic stress signal towards unity (=creep) on the fatigue crack growth is discussed in Section 2.7.2.

2.7.1 Influence of frequency on fatigue crack growth

Region II failure for tensile bars under dynamic loads is generally attributed to fatigue crack growth. Most fatigue crack growth models are based upon the Paris law [55], which relates the range of the stress intensity factor (ΔK_I) to the rate of crack propagation per cycle ($\frac{\mathrm{d}a}{\mathrm{d}N}$):

$$\frac{\mathrm{d}a}{\mathrm{d}N} = A\Delta K_I^m \,, \tag{2.14}$$

with A and m constants. Although these constants are sometimes assumed to be only material dependent, they are known to depend on the frequency (f) [54, 56–58], stress ratio (R) [59–61], temperature [54, 61, 62] and molecular weight (distribution) [63–65]. The dynamic fatigue experiments presented in Figure 2.9 are conducted at a wide range of frequencies, which rules out the use of Equation (2.14) to completely describe the measured data set with the use of only one parameter set.[8] Therefore, a modification to Equation (2.14) as proposed by Kim *et al.* [54] is employed here. Their empirical relation takes the influence of frequency and temperature into account and is shortly summarised in Appendix 2.C. The initial flaw size was used as a fit parameter, resulting in a value of 50 µm. This value is in agreement with the range of inherent defect sizes in uPVC pipes reported in other studies [66, 67].

The resulting calculated time-to-failure at different frequencies are shown in Figure 2.11 as solid lines. The good agreement between the experimental data (markers) and the model description supports the statement that the failure mechanism for failures after the knee is fatigue crack growth. The relation and

[8] The stress ratio R for the data in Figure 2.9 varies between 0.05 and 0.1. The experimental data of Kim *et al.* [59] suggests that the fatigue crack growth is only marginally influenced by the variation of R within this range. Therefore, this effect is neglected here.

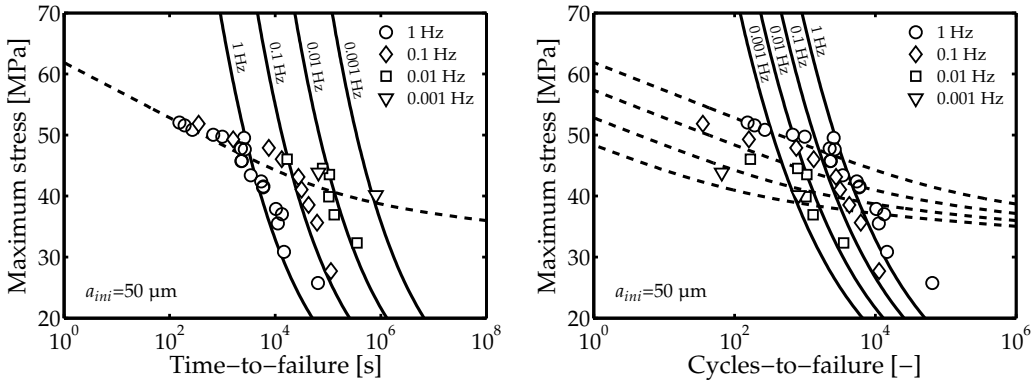

Figure 2.11 *Reproduction of the data for the as-manufactured specimens from Figure 2.9 including failure predictions for Region II failure (solid lines) using the fatigue crack growth model of Kim et al. [54] and an initial flaw size a_{ini} of 50 µm. The yield failure predictions are shown as dashed lines.* ***Left:*** *the maximum stress plotted versus the time-to-failure.* ***Right:*** *the maximum stress plotted versus the cycles-to-failure (N_f).*

parameters of Kim *et al.* accurately describe both the slope and the frequency dependence of the maximum stress versus time-to-failure. It is important to note that where failure in region I is insensitive for the frequency of the stress signal (as shown in Section 2.6.2 and Equation (2.13)), fatigue crack growth failures are influenced significantly by the frequency. A decrease in frequency results in an increase in the time-to-failure. The same data, plotted in Figure 2.11 (right) as a function of cycles-to-failure, shows a frequency dependent response for the failures in both region I and region II. The latter does not comply with the Paris law (Equation (2.14)), but is in agreement with the relation proposed by Kim *et al.*: the number of cycles-to-failure increases with an increase in frequency of the applied stress. These observations should be taken into account when estimating the slow crack growth rate from fatigue crack growth measurements, as discussed in the next section.

2.7.2 Influence of the stress ratio on fatigue crack growth

The stress ratio, R, of the dynamic signal influences the kinetics of Region II failures in uPVC [58, 68]. At the University of Leoben an approach has been developed that correlates the fatigue crack growth rate to the slow crack growth rate [6, 61]. They extrapolate fatigue crack growth kinetics for a range of stress ratios towards R=1 (creep). Here, a similar strategy is followed. Preliminary fatigue crack growth rate measurements were carried out on uPVC compact tension specimens. The crack growth rate was determined at four different

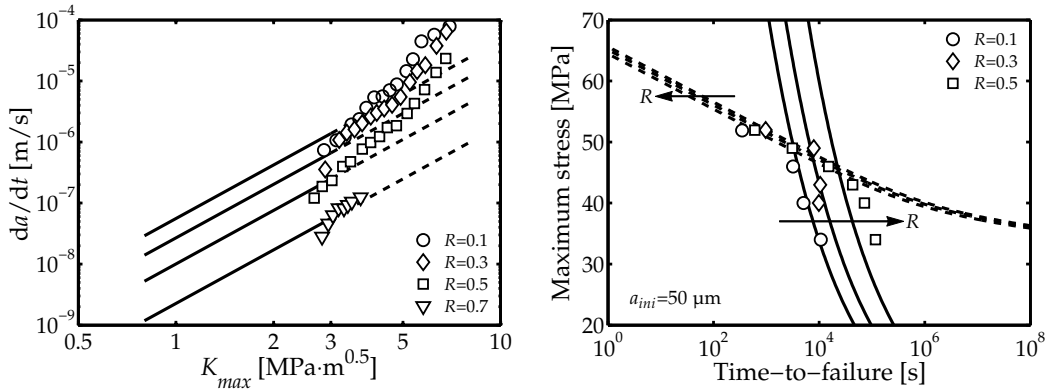

Figure 2.12 *Influence of variation of the stress ratio R on the fatigue crack growth in uPVC.* ***Left:*** *the crack growth rate of uPVC compact tension specimens versus the maximum stress intensity factor (K_{max}) on a double logarithmic scale for four different values for R (measured at a frequency of 1 Hz). The lines calculated using Equation (2C.1).* ***Right:*** *reproduction of Figure 2.10 (right) including failure predictions for Region II failure (solid lines) using the fatigue crack growth model of Kim et al. [54] and an initial flaw size of 50 µm. The yield failure predictions are shown as dashed lines.*

stress ratios (from 0.1 up to 0.7). The results of the measurements are shown as markers in Figure 2.12 (left), where the fatigue crack growth rate $\frac{da}{dt}$ is plotted versus the maximum stress intensity factor K_{max}. A clear decrease in the crack growth rate is observed for an increase in R. The slope of the crack growth rate versus maximum stress intensity factor in a double logarithmic plot remains more or less constant for the range of stress ratios investigated. The solid lines represent the fatigue crack growth rates as predicted using Equation (2C.1). The dashed lines represent the extrapolation of these results out of the range of K_{max} values in which Kim *et al.* [54] characterised their material. These extrapolated lines are in reasonable agreement with the experimental data for the range of maximum stress intensity factors lower than $5\,\mathrm{MPa}\cdot\mathrm{m}^{0.5}$: the influence of R on the crack growth rate is similar and the lines coincide with the markers at K_{max}=3 $\mathrm{MPa}\cdot\mathrm{m}^{0.5}$. Apparently, the molar mass of the material used by Kim *et al.* is comparable to that of the material used here.

The predictions of the time-to-failure at different (constant) values of R (again using an initial flaw size of 50 µm) are shown as solid lines in Figure 2.12 (right). The predictions are in good agreement with the experimental data (shown as markers). As already discussed in Section 2.6.3, both the predictions of the yield lines and the measured ductile failure times decrease with an increase in R. The failure time for crack growth failure (region II) is more sensitive to an increase in R and *increases*. For an increase in R from 0.1 to 0.5 the failure times increase about 1.2 decades (compared to a decrease of only about 0.3 decades for the yield failures).

The fatigue crack growth rate at a particular K_{max} (=3 MPa $\cdot$ m$^{0.5}$) is plotted against the stress ratio in Figure 2.13 (left). The experimental data (shown as markers) and the model predictions using Equation (2C.1) are in close agreement.[9] As Brown *et al.* [69] already noted, two regimes can be distinguished. At low stress ratios the crack growth rate is hardly influenced by a change in stress ratio, whereas at high stress ratio this influence on the crack growth ratio becomes much more pronounced. With the use of SAXS measurements they showed that at low R values the craze fibrils in polystyrene buckle during fatigue loading, as a result of compressive forces imposed by the material surrounding the crack tip on the fibrils. For ratios higher than about 0.6 the craze fibrils remain straight and the fibrils only contract in length and increase in diameter as the minimum stress level is approached. This difference in deformation behaviour of the fibrils can be the cause of a different failure mechanism, explaining the sharp decrease in crack growth rate as the stress ratio approaches unity.

The relation between R and $\frac{\mathrm{d}a}{\mathrm{d}t}$ is used to calculate the time-to-failure for uPVC subjected to a dynamic load with a stress ratio ranging from 0.1 up to 0.9. The resulting failure times are shown as solid lines in Figure 2.13 (right). These lines lead to the important observation that with an increase in R the time-to-failure *decreases* slightly for region I failures, whereas , in region II, failure times *dramatically increase*. In region I, failure is dependent of the level of the applied stress. Failure thus occurs on shorter timescales for high R-values as the polymer is subject to a high stress for a longer part of the cycle. In region II, failure mainly depends on the amplitude of the stress. Specimens can sustain a cyclic load with a high R-value for longer periods of time as the amplitude of the stress signal decreases with an increase in R.

The predicted fatigue crack growth failure at R=0.9 becomes apparent after $5 \cdot 10^6$ s; significantly longer than the longest failure time measured by Niklas and Kausch von Schmeling at 20 °C for pipes subjected to a constant load (see Figure 2.7). This explains why the second region of failure kinetics was not observed in their experimental data. This observation complies with predictions of Truss [70] who estimated that region II failure occurs after at least $3 \cdot 10^9$ s for a well processed uPVC pipe at 20 °C.

The model cannot be used to obtain a realistic value for the slow crack growth rate as extrapolation towards R=1 leads to a crack growth rate of 0 m/s. The uPVC pipes used in the gas network are operated at a pressure of only 100 mbar resulting in a very low wall stress during their service life. The prediction at R=0.9 rules out slow crack growth failure for these pipes within their service life.

[9] In this case the frequency is kept constant and the use of Equation (2.14) with corresponding values for A and m would therefore result in identical results.

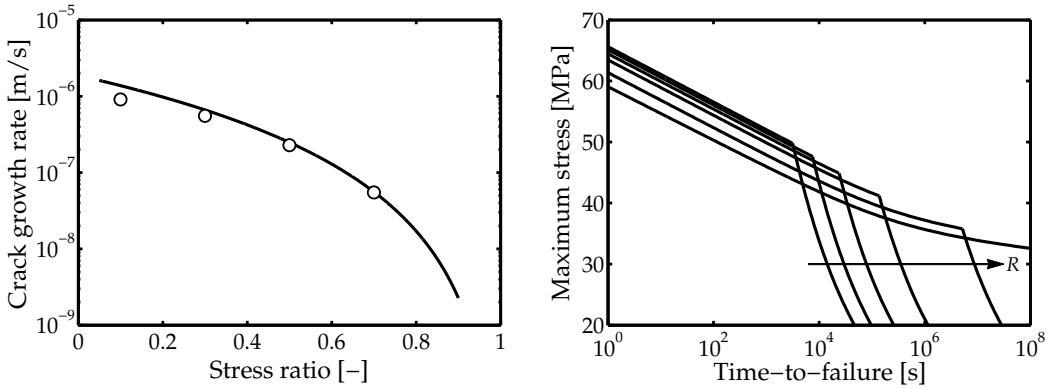

Figure 2.13 *Extrapolation of the fatigue crack growth rate towards the crack growth rate at R=1.* ***Left:*** *the crack growth rate at K_{max}=3 MPa · $m^{0.5}$ versus the stress ratio. The solid line represents the prediction of the model of Kim et al. [54] and the markers represent the measured crack growth rates at a frequency of 1 Hz.* ***Right:*** *the predicted time-to-failure for dynamic stress signals with stress ratios of 0.1, 0.3, 0.5, 0.7 and 0.9.*

The water and sewer networks are, however, operated at higher and sometimes oscillating pressures. As a consequence, it is of interest for the water and sewer network operators to characterise and model region II failure kinetics.

More research is required to obtain a more reliable estimate of the slow crack growth kinetics of uPVC. The research should focus on characterising the influence of the stress ratio up to R-values close to unity. In a previous section it was shown that the frequency also influences the fatigue crack growth rate. As the frequency is undefined for a static signal, one should be careful in extrapolating fatigue crack growth rates measured at one frequency only. It is therefore imperative that the influence of frequency is taken into account when extrapolating towards R=1. Furthermore, it should be verified whether compressive forces at the crack tip for fatigue loads with a low stress ratio indeed results in a different failure mechanism than that occurring for fatigue failure at higher stress ratios. More knowledge on the failure mechanisms is required to improve the extrapolation procedure. Other approaches such as the one proposed by Hu *et al.* [58] may also be viable. They proposed a model where the (fatigue) crack growth rate is the product of a creep contribution, that depends only on the maximum stress intensity factor, and a fatigue contribution, that depends on the local strain rate. The slow crack growth rate follows from the creep contribution. Another issue that should be addressed is the temperature dependence of the crack growth failure mechanism. This temperature dependent response should be characterised, as the service temperature of uPVC pipes is generally lower than room temperature at which most laboratory experiments are conducted.

2.8 Conclusions

The influence of physical ageing on the resistance against plastic deformation is successfully implemented in a pressure-modified Eyring relation by making the pre-exponential factor a function of time. The influence of temperature and stress on the physical ageing kinetics was characterised using tensile yield stress measurements on specimens that were aged under different conditions. With the resulting parameters it is possible to predict long-term ductile failure for not only tensile bars, but also pipe segments subjected to a constant load. The endurance limit, observed for specimens that age significantly during the measurement, is also predicted accurately. The predictions for specimens subjected to a dynamic load are in reasonable agreement. Both the predictions and the measurements of the time to ductile failure are shown to be frequency independent. The engineering approach presented in this chapter has the advantage that a less laborious characterisation procedure is required compared to the ones required for existing constitutive models that are also capable of producing long-term failure predictions.

During the dynamic fatigue tests fatigue crack growth failure was observed as a second type of failure kinetics in the maximum stress versus time-to-failure plots. This fatigue crack growth failure appeared to be highly dependent on both the frequency and the stress ratio of the applied stress signal. Preliminary fatigue crack growth experiments suggest that slow crack growth failure does not occur within the service life of uPVC gas pipes. Additional research to the fatigue and slow crack growth behaviour of uPVC is required to confirm this preliminary estimate.

References

[1] H. Montiel, J.A. Vílchez, J. Arnaldos, and J. Casal. Historical analysis of accidents in the transportation of natural gas. *Journal of Hazardous Materials* 51:77–92, **1996**.

[2] N. Piccinini, R. Tommasini, and E. Pons. Large N.G. explosion and fire involving several buried utility networks. *Process Safety and Environmental Protection* 87:73–80, **2009**.

[3] R.W. Lang, A. Stern, and G. Doerner. Applicability and limitations of current lifetime prediction models for thermoplastics pipes under internal pressure. *Angewandte Makromolekulare Chemie* 247:131–145, **1997**.

[4] G. Castiglioni, D. Verzanini, and A. Pavan. Prediction of ductile failure in u-PVC pipes from creep tests on specimens. In: *Proceedings of Plastic Pipes XII*. Baveno, **2004**.

[5] N. Brown. Intrinsic lifetime of polyethylene pipelines. *Polymer Engineering and Science* 47:477–480, **2007**.

[6] G. Pinter, R.W. Lang, and M. Haager. A test concept for lifetime prediction of polyethylene pressure pipes. *Monatshefte fur Chemie* 138:347–355, **2007**.

[7] U.W. Gedde, J. Viebke, H. Leijström, and M. Ifwarson. Long-term properties of hot-water polyolefin pipes - A review. *Polymer Engineering and Science* 34:1773–1787, **1994**.

[8] U. Andersson. Which factors control the lifetime of plastic pipes and how the lifetime can be extrapolated. In: *Proceedings of Plastic Pipe XI*. Munchen, **2001**.
[9] A. Gray, J.N. Mallinson, and J.B. Price. Fracture behaviour of polyethylene pipes. *Plastics and Rubber Processing and Applications* 1:51–53, **1981**.
[10] J.P. Lu, P. Davis, and L.S. Burn. Lifetime prediction for ABS pipes subjected to combined pressure and deflection loading. *Polymer Engineering and Science* 43:444–462, **2003**.
[11] H. Vogt, H.-F. Enderle, U. Schulte, and J. Hessel. Thermal ageing of PE 100 pipes for accelerated lifetime prediction under service conditions. In: *Proceedings of Plastic Pipes XIV*. Budapest, **2008**.
[12] H. Niklas and H.H. Kausch von Schmeling. Molekularstruktur und mechanische Eigenschaften von Polyvinylchlorid III. Mitteilung: Ursachen zeitabhängiger Festigkeitseigenschaften von PVC-Rohren. *Kunststoffe* 53:886–891, **1963**.
[13] P. Benjamin. Quality and quality control of unplasticised polyvinylchloride (uPVC) pressure pipes. *Plastics and Rubber: Materials and Applications* 5:151–160, **1980**.
[14] K.S. Minsker and G.E. Zaikov. Achievements and research tasks for poly(vinyl chloride) aging and stabilization. *Journal of Vinyl & Additive Technology* 7:222–234, **2001**.
[15] M. Schiller and W. Fischer. Stabilisers for PVC pipe systems - Quo Vadis? In: *Proceedings of Plastic Pipes XII*. Baveno, **2002**.
[16] B. Terselius and J.-F Jansson. Gelation of PVC, Part 2: Effect on internal pressure resistance. *Plastics and Rubber Processing and Applications* 4:285–290, **1984**.
[17] J.M. Hutchinson. Physical aging of polymers. *Progress in Polymer Science* 20:703–760, **1995**.
[18] J.H. Golden, B.L. Hammant, and E.A. Hazell. The effect of thermal pretreatment on the strength of polycarbonate. *Journal of Applied Polymer Science* 11:1571–1579, **1967**.
[19] T.E. Brady and G.S.Y. Yeh. Yielding behavior of glassy amorphous polymers. *Journal of Applied Physics* 42:4622–4630, **1971**.
[20] A. Cross, R.N. Haward, and N.J. Mills. Post yield phenomena in tensile tests on poly(vinyl chloride). *Polymer* 20:288–294, **1979**.
[21] H.G.H. van Melick, L.E. Govaert, and H.E.H. Meijer. Localisation phenomena in glassy polymers: influence of thermal and mechanical history. *Polymer* 44:3579–3591, **2003**.
[22] E.J. Kramer. Microscopic and molecular fundamentals of crazing. *Advances in Polymer Science* 52/53:1–56, **1983**.
[23] P.J.F. van den Heuvel. PVC pressure pipes: the importance of gelation to ensure pipe reliability. In: *Proceedings of Plastic Pipes V*. York, **1982**.
[24] E.T.J. Klompen, T.A.P. Engels, L.C.A. van Breemen, P.J.G. Schreurs, L.E. Govaert, and H.E.H. Meijer. Quantative prediction of long-term failure of polycarbonate. *Macromolecules* 38:7009–7017, **2005**.
[25] J. Worp. Een en ander over hard p.v.c.-buis en haar toepassingsmogelijkheden. *Het Gas* 78:2–12, **1957**.
[26] D.H. Ender and R.D. Andrews. Cold drawing of glassy polystyrene under dead load. *Journal of Applied Physics* 36:3057–3062, **1965**.
[27] D.J. Matz, W.G. Guldemond, and S.I. Cooper. Delayed yielding in glassy polymers. *Journal of Polymer Science: Polymer Physics Edition* 10:1917–1930, **1972**.
[28] K.V. Gotham and S. Turner. Procedures for the evaluation of the long term strength of plastics and some results for polyvinyl chloride. *Polymer Engineering and Science* 13:113–119, **1973**.
[29] E.T.J. Klompen, T.A.P. Engels, L.E. Govaert, and H.E.H. Meijer. Modelling of the postyield response of glassy polymers: influence of thermomechanical history. *Macromolecules* 38:6997–7008, **2005**.

[30] I.M. Ward. Review: The yield behaviour of polymers. *Journal of Materials Science* 6:1397–1417, **1971**.

[31] D.J. Matz, W.G. Guldemond, and S.I. Cooper. Yielding of polycarbonate and polysulfone in creep and stress-strain. *Polymer Engineering and Science* 13:300–307, **1973**.

[32] C. Bauwens-Crowet and J.C. Bauwens. Annealing of polycarbonate below the glass transition: quantitative interpretation of the effect on yield stress and differential scanning calorimetry measurements. *Polymer* 23:1599–1604, **1982**.

[33] C. Ho Huu and T. Vu-Khanh. Effects of physical aging on yielding kinetics of polycarbonate. *Theoretical and Applied Fracture Mechanics* 40:75–83, **2003**.

[34] P.I. Vincent. The necking and cold-drawing of rigid plastics. *Polymer* 1:7–19, **1960**.

[35] E.J. Kramer. Stress aging in anhydrous nylon 6-10. *Journal of Applied Physics* 41:7–19, **1970**.

[36] F.A. Myers, F.C. Cama, and S.S. Sternstein. Mechanically enhanced aging of glassy polymers. *Annals of the New York Academy of Sciences* 279:94–99, **1976**.

[37] E.R. Harrell, Jr. and R.P. Chartoff. Effects of thermal and mechanical history on the viscoelastic properties of rigid poly(vinyl chloride). *Journal of Macromolecular Science Physics* B14:277–305, **1977**.

[38] Y. Nanzai and A. Miwa. Mechanical and thermal analysis of aging in strained polymethyl methacrylate. *JJSME International Journal Series A* 42:479–484, **1999**.

[39] E.R. Harrell, Jr. and R.P. Chartoff. The influence of crystallinity on the beta-transition in poly(vinyl chloride). *Polymer Engineering and Science* 14:362–365, **1974**.

[40] C. Tsitsilianis, M. Tsapatsis, and Ch. Economou. Effects of crystallinity on ageing phenomena in poly(vinyl chloride). *Polymer* 60:1861–1866, **1989**.

[41] T.A. Tervoort, E.T.J. Klompen, and L.E. Govaert. A multi-mode approach to finite, three-dimensional, nonlinear viscoelastic behavior of polymer glasses. *Journal of Rheology* 40:779–797, **1996**.

[42] P. Benjamin. The influence of the extrusion process on the quality of unplasticized Polyvinyl Chloride (uPVC) pressure pipe. *Journal of Vinyl Technology* 2:254–258, **1980**.

[43] G. Butters. *Particulate nature of PVC: formation, structure and processing*. Applied Science Publishers LTD, **1982**.

[44] J. Parey and G. Menges. PVC-gelation model. *Journal of Vinyl Technology* 3:152–156, **1981**.

[45] R.J.M. Hermkens, M. Wolters, J. Weller, and H.A. Visser. PVC pipes in gas distribution: still going strong! In: *Proceedings of Plastic Pipes XIV*. Budapest, **2008**.

[46] B. Terselius, J.-F Jansson, and J. Bystedt. Gelation of PVC, Part 4: Impact strength. *Plastics and Rubber Processing and Applications* 5:1–7, **1985**.

[47] B. Terselius and J.-F Jansson. Gelation of PVC, Part 3: Effect on tensile properties. *Plastics and Rubber Processing and Applications* 4:291–299, **1984**.

[48] J.A. Covas, M. Gilbert, and D.E. Marshall. Twin screw extrusion of a rigid PVC compound - effect on fusion and properties. *Plastics and Rubber Processing and Applications* 9:107–116, **1988**.

[49] R.W. Truss. Understanding brittle failure of uPVC (unplasticised polyvinyl chloride) pipe. *Pure and Applied Chemistry* 57:993–1000, **1985**.

[50] J.W. Summers, E.B. Rabinovitch, and J.G. Quisenberry. Polyvinyl chloride processing morphology: Part III-Twin screw extrusion. *Journal of Vinyl Technology* 4:67–69, **1982**.

[51] G.P. Marshall, S. Brogden, and M.A. Shepherd. Evaluation of surge and fatigue resistance of poly(vinyl chloride) and polyethylene pipeline materials for use in the UK water industry. *Plastics, Rubbers and Composites Processing and Applications* 27:483–488, **1998**.

[52] R.P.M. Janssen, D. de Kanter, L.E. Govaert, and H.E.H. Meijer. Fatigue life predictions for glassy polymers: a constitutive approach. *Macromolecules* 41:2520–2530, **2008**.

[53] R.P.M. Janssen, L.E. Govaert, and H.E.H. Meijer. An analytical method to predict fatigue life of thermoplastics in uniaxial loading: sensitivity to wave type, frequency, and stress amplitude. *Macromolecules* 41:2531–2540, **2008**.

[54] H.S. Kim and X.M. Wang. Temperature and frequency effects on fatigue crack growth of uPVC. *Journal of Materials Science* 29:3209–3214, **1994**.

[55] P. Paris and F. Erdogan. A critical analysis of crack propagation laws. *Journal of Basic Engineering* 85:528–534, **1963**.

[56] R.W. Hertzberg, J.A. Manson, and M. Skibo. Frequency sensitivity of fatigue processes in polymeric solids. *Polymer Engineering and Science* 15:252–260, **1975**.

[57] J.C. Radon. Fatigue of polymers - Crack growth in PVC. *Journal of Macromolecular Science Physics* B14:511–523, **1977**.

[58] Y. Hu, J. Summers, A. Hiltner, and E. Baer. Correlation of fatigue and creep crack growth in poly(vinyl chloride). *Journal of Materials Science* 38:633–642, **2003**.

[59] H.S. Kim, R.W. Truss, Y.W. Mai, and B. Cotterell. Fatigue crack propagation in unplasticized poly(vinyl chloride): 1. Effect of mean stress. *Polymer* 28:268–276, **1988**.

[60] H.S. Kim, Y.W. Mai, and B. Cotterell. Effects of processing on fatigue crack growth and creep rupture in unplasticized polyvinyl chloride (uPVC). *Journal of Materials Science* 28:3367–3372, **1993**.

[61] W. Balika and R.W. Lang. Crack growth in a pipe grade PVC material under static and cyclic loading conditions. *Macromolecular Symposium* 181:341–352, **2002**.

[62] H.-S. Kim and Y.-W. Mai. Effect of temperature on fatigue crack growth in unplasticized polyvinyl chloride. *Journal of Materials Science* 28:5479–5485, **1993**.

[63] M. Skibo, J.A. Manson, R.W. Hertzberg, and E.A. Collins. Effects of molecular weight and plasticizer on fatigue crack propagation in PVC. *Journal of Macromolecular Science Physics* B14:525–543, **1977**.

[64] C.M. Rimnac, J.A. Manson, R.W. Hertzberg, S.M. Webler, and M.B. Skibo. Fatigue crack propagation in PVC: Effects of molecular weight and specimen history. *Journal of Macromolecular Science Physics* B19:351–375, **1981**.

[65] T.E. Bernal-Lara, Y. Hu, J. Summers, A. Hiltner, and E. Baer. Stepwise fatigue crack propagation in poly(vinyl chloride). *Journal of Vinyl & Additive Technology* 10:5–10, **2004**.

[66] H.J.M. Rijpkema and M. Wolters. Service life analysis of PVC gas pipes in practice: a predictable behaviour! In: *Proceedings of Plastics Pipes VIII*. Koningshof, **1992**.

[67] S. Burn, P. Davis, T. Schiller, B. Tiganis, G. Tjandraatmadja, M. Cardy, S. Gould, P. Sadler, and A.J. Whittle. Long-term performance prediction for PVC pipes. Technical report, Awwa research foundation, **2006**. URL `http://www.iwapublishing.com/template.cfm?name=isbn1843399504`.

[68] J.F. Mandell and J.-P.F. Chevaillier. Craze initiation, crack growth, and lifetime trends in fatigue of poly(vinylchloride). *Polymer Engineering and Science* 25:170–177, **1985**.

[69] H.R. Brown, E.J. Kramer, and R.A. Bubeck. Effect of deformation ratio on fibril deformation in fatigue of polystyrene. *Journal of Materials Science* 23:248–252, **1988**.

[70] R.W. Truss. Temperature derating of unplasticised polyvinyl chloride (uPVC) pressure pipes. *Plastics and Rubber Processing and Applications* 7:51–56, **1987**.

[71] L.R. Holloway and A.J. Naaktgeboren. Relationship between fracture toughness and other material properties of uPVC pressure pipes. *Pipes and Pipelines International* 35:32+34–36, **1990**.

2.A Appendix: Deduction of the time-to-failure under constant loads

The time-to-failure for a glassy polymer that is subjected to a constant load is calculated using the hypothesis that failure occurs after reaching a critical value of the equivalent plastic strain ($\bar{\gamma}_{cr}$), resulting in Equation (2.5). The rate of plastic strain accumulation including ageing kinetics is a function of time as given in Equation (2.4). Combining Equations (2.4) and (2.5) results in the following relation for the critical plastic strain, from which the time-to-failure for isothermal creep tests can be calculated:

$$\bar{\gamma}_{cr} = \frac{b_0}{t_0^{b_1}} \cdot \exp\left(\frac{-\Delta U - \mu p v^*}{RT}\right) \cdot \sinh\left(\frac{\bar{\tau} v^*}{RT}\right) \cdots \int_0^{t_f} \left(\frac{t'}{a_T(T) \cdot a_\sigma(T,\bar{\tau})} + t_{ini}\right)^{b_1} \mathrm{d}t'. \quad (2A.1)$$

An analytical solution can be found by substituting $x = \frac{t'}{a_T(T) \cdot a_\sigma(T,\bar{\tau})} + t_{ini}$ and $\frac{\mathrm{d}x}{\mathrm{d}t'} = \frac{1}{a_T(T) \cdot a_\sigma(T,\bar{\tau})}$:

$$\begin{aligned} \frac{\bar{\gamma}_{cr} \cdot \exp\left(\frac{\Delta U + \mu p v^*}{RT}\right)}{b_0 \cdot t_0^{-b_1} \cdot \sinh\left(\frac{\bar{\tau} v^*}{RT}\right)} &= a_T(T) \cdot a_\sigma(T,\bar{\tau}) \cdot \int_{t_{ini}}^{\frac{t_f}{a_T(T) \cdot a_\sigma(T,\bar{\tau})} + t_{ini}} x^{b_1} \, \mathrm{d}x \\ &= \frac{a_T(T) \cdot a_\sigma(T,\bar{\tau})}{b_1 + 1} \cdot \left[\left(\frac{t_f}{a_T(T) \cdot a_\sigma(T,\bar{\tau})} + t_{ini}\right)^{b_1+1} - t_{ini}^{b_1+1}\right]. \end{aligned}$$

Rewriting this equation gives the analytical solution for the time-to-failure:

$$t_f(T,\bar{\tau}) = a_T(T) \cdot a_\sigma(T,\bar{\tau}) \cdots \cdot \left(\left[\frac{\bar{\gamma}_{cr} \cdot t_0^{b_1} \cdot (b_1+1) \cdot \exp\left(\frac{\Delta U}{RT} + \frac{\mu p v^*}{RT}\right)}{a_T(T) \cdot a_\sigma(T,\bar{\tau}) \cdot b_0 \cdot \sinh\left(\frac{\bar{\tau} v^*}{RT}\right)} + t_{ini}^{b_1+1}\right]^{\frac{1}{b_1+1}} - t_{ini}\right). \quad (2A.2)$$

2.B Appendix: Analytical solution for a triangular waveform

A stress signal with a triangular waveform (see Figure 2.8 (left)), σ_{tria}, can be described with the continuous function:

$$\sigma_{tria}(t) = \sigma_m + \frac{2\sigma_{amp}}{\pi}\arcsin\Big(\sin(2\pi f t)\Big), \tag{2B.1}$$

where σ_m is the mean stress, σ_{amp} the stress amplitude and f is the frequency. To find an analytical solution for the deformation and ageing kinetics for this wave form, a more appropriate, discontinuous function for the triangular waveform was used.

$$\sigma_{tria}(t) = A + Bt, \tag{2B.2}$$

$$\text{with} \begin{cases} A = \sigma_m & \wedge \quad B = 4f\sigma_{amp} & \text{for} \quad 0 \le t < \frac{1}{4f} \\ A = \sigma_m + 2\sigma_{amp} & \wedge \quad B = -4f\sigma_{amp} & \text{for} \quad \frac{1}{4f} \le t < \frac{3}{4f} \\ A = \sigma_m - 4\sigma_{amp} & \wedge \quad B = 4f\sigma_{amp} & \text{for} \quad \frac{3}{4f} \le t < \frac{1}{f} \end{cases} .$$

Janssen *et al.* [53] already provided a solution for the acceleration factor of the deformation kinetics for a triangular wave (in tension) and with the approximation that $\sinh(x) \approx 0.5 \cdot \exp(x)$ for $x \ll 1$.

$$a_{\dot{\tilde{\gamma}},tria} = \frac{3RT}{\left(\sqrt{3}+\mu\right)\cdot \nu^* \sigma_{amp}} \cdot \sinh\left(\frac{\left(\sqrt{3}+\mu\right)\cdot \nu^* \sigma_{amp}}{3RT}\right) \tag{2B.3}$$

The acceleration factor for the aging kinetics can be calculated using Equation (2.12). Assuming isothermal conditions and combining the result with Equations (2B.2) and (2.12) the relation is as follows:

$$a_{d,age} = a_\sigma(T, \frac{\sigma_m}{\sqrt{3}}) \cdot f \cdot \int_0^{\frac{1}{f}} \frac{\sqrt{3}RT}{(A+Bt)\cdot \nu_a} \cdot \sinh\left(\frac{(A+Bt)\cdot \nu_a}{\sqrt{3}RT}\right) \mathrm{d}t. \tag{2B.4}$$

Using the substitutions σ_{tria}=$A + Bt$, $\mathrm{d}t$=$\frac{\mathrm{d}\sigma_{tria}}{B}$ and $\tau_{0,a}$=$\frac{RT}{\nu_a}$, in Equation (2B.4) results in:

$$a_{d,age} = \frac{\sqrt{3} f \tau_{0,a} a_\sigma(T, \frac{\sigma_m}{\sqrt{3}})}{B} \cdot \int_A^{A+\frac{B}{f}} \frac{\sinh\left(\frac{\sigma_{tria}}{\sqrt{3}\tau_{0,a}}\right)}{\sigma_{tria}} \mathrm{d}\sigma_{tria}. \tag{2B.5}$$

The following standard integral is used for the analytical solution:

$$\int \frac{\sinh(ax)}{x}\mathrm{d}x = \sum_{n=0}^{\infty} \frac{(ax)^{2n+1}}{(2n+1)(2n+1)!} = F(x). \tag{2B.6}$$

Applying this relation and solving it for each of the three sections of the wave results in:

$$a_{d,age} = \frac{\sqrt{3} f \tau_{0,a} a_\sigma(T, \frac{\sigma_m}{\sqrt{3}})}{4 f \sigma_{amp}} \cdot \left(\underbrace{F(\sigma_m + \sigma_{amp}) - F(\sigma_m)}_{0 \le t < \frac{1}{4f}} \cdots \right.$$
$$\left. - \underbrace{F(\sigma_m - \sigma_{amp}) - F(\sigma_m + \sigma_{amp})}_{\frac{1}{4f} \le t < \frac{3}{4f}} + \underbrace{F(\sigma_m) - F(\sigma_m - \sigma_{amp})}_{\frac{3}{4f} \le t < \frac{1}{f}} \right). \tag{2B.7}$$

This can be reduced to the final solution:

$$a_{d,age} = \frac{\sqrt{3} R T a_\sigma(T, \frac{\sigma_m}{\sqrt{3}})}{2 \nu_a \sigma_{amp}} \cdots$$
$$\cdot \left(\sum_{n=0}^{\infty} \frac{\left(\frac{\nu_a \sigma_{max}}{\sqrt{3} R T}\right)^{2n+1}}{(2n+1)(2n+1)!} - \sum_{n=0}^{\infty} \frac{\left(\frac{\nu_a \sigma_b}{\sqrt{3} R T}\right)^{2n+1}}{(2n+1)(2n+1)!} \right). \tag{2B.8}$$

2.C Appendix: Summary of fatigue crack growth model

Kim *et al.* [54] proposed a modified version of the Paris law to take the influence of frequency and temperature on the fatigue crack growth kinetics of uPVC into account:

$$\frac{\mathrm{d}a}{\mathrm{d}N} = \left(\frac{f}{f_{ref}}\right)^{-n} \cdot \left[B \cdot \exp\left(-\frac{\Delta H_{th} - \gamma \cdot \log\Delta K_I}{RT}\right)\right]_{ref}. \tag{2C.1}$$

The subscript "$_{ref}$" denotes an arbitrarily chosen reference point, ΔH_{th} the apparent activation energy and both n and γ (not to be confused with a strain) are constants. For a reference frequency of 1 Hz, the experimental data of Kim *et al.* [54] was best described with the values ΔH_{th}=43.6 kJ/mol, B=3.75 $\cdot 10^{12}$, γ=16.5 kJ/mol and n=0.295. These parameters were also used to describe the dynamic fatigue data as obtained in this study, although it is unknown whether the material used in the study of Kim *et al.* is comparable with the material used throughout the present study.

The stress intensity factor range is defined as:

$$\Delta K_I = K_{I,max} - K_{I,min} = (\sigma_{max} - \sigma_{min}) \cdot Y\sqrt{a}, \tag{2C.2}$$

where Y is a geometrical factor. The geometrical factor for the tensile bars as used in the current study can be calculated with the empirical solution for a Single End Notched Beam (SENB) specimen subjected to tensile loads:

$$Y = \frac{\sqrt{2w \cdot \tan\left(\frac{\pi a}{2w}\right)}}{\sqrt{a} \cdot \cos\left(\frac{\pi a}{2w}\right)} \cdot \left(0.752 + 2.02 \cdot \frac{a}{w} + 0.37 \cdot \left[1 - \sin\left(\frac{\pi a}{2w}\right)\right]^3\right), \tag{2C.3}$$

where w is the width of the specimen, which is chosen to be equal to the wall thickness of the original pipe (≈4.1 mm) as most cracks in the tensile bars grow in the radial direction of the original pipe geometry. The cycles to failure follow from solving differential Equation (2C.1) for the initial crack size up to the critical crack size. This critical crack size is taken as the crack size at which K_{max} is equal to the critical stress intensity factor ($K_{Ic} \approx 4$ MPa $\cdot \sqrt{\mathrm{m}}$ for PVC [71]). The initial crack size (a_{ini}) was used as a fit parameter and a best fit was found for a_{ini}=50 µm.

Influence of physical ageing on impact embrittlement of uPVC pipes[1]

Chapter 3

Abstract

Most failures of unplasticised poly(vinyl chloride) (uPVC) pipes used in the Dutch low pressure gas distribution network are a consequence of the occurrence of third-party damage. Brittle pipes should therefore be taken out of service. In this study, it is shown that physical ageing can result into embrittlement of uPVC gas pipes. The ductile-to-brittle transition temperature was measured for a water pipe grade uPVC at different stages of ageing using instrumented falling weight impact tests. As a hypothesis a critical stress criterion is proposed above which failure is brittle. This hypothesis is employed to relate ductile-to-brittle transition data with a model that describes the influence of physical ageing on the yield stress. The evolution of the ductile-to-brittle transition temperature that followed from this approach agrees qualitatively with the experimental data. Only a minor influence of physical ageing on the transition temperature was observed for the water pipe grade, both in the experimental data and the model predictions. Applying the same hypothesis to the yield evolution of a gas pipe grade of uPVC shows a more severe influence of physical ageing on the transition temperature. The yield stress can therefore be expected to be a key material property in monitoring the embrittlement process of uPVC gas pipes.

[1]Reproduced from: H.A. Visser, T.C. Bor, M. Wolters, L.L. Warnet, L.E. Govaert, Influence of physical ageing on impact embrittlement of uPVC pipes, in preparation for *Plastics, Rubber and Composites*

3.1 Introduction

One of the largest industrial applications for unplasticised poly(vinyl chloride) (uPVC) is its use in pipe systems. In the Netherlands uPVC is extensively used for water and sewer distribution systems. Moreover, uPVC pipes were also installed in the low pressure gas distribution network between the mid-fifties up to 1974. Currently, about 22,500 km of these uPVC pipes is still in service and reaches their initially specified 50 years of service life in near future. Replacing these pipes exactly after these years of service would result in an extremely labour intensive, and thus costly, project in the next decade. Consequently, postponing the replacement will result in huge economic savings. Postponement should, however, never compromise the safety of the distribution network, which emphasises the need for knowledge on the current status of the network.

Failure data on the existing gas distribution network show that spontaneous failure of uPVC gas pipes hardly occurs and most failures originate from third-party damage [1] and thus impact loads. Therefore, it is important in which way the uPVC behaves upon an impact load; more specifically, whether it fails in a ductile or a brittle way. A uPVC pipe that behaves in a ductile way upon impact can absorb significantly more energy before it fails. These pipes can therefore survive stronger impact events than brittle pipes. Furthermore, it is easier to stop the gas flowing from a pipe that failed in a ductile way, since it allows the instalment of a temporary stopper without a risk of further damage. If a pipe fails in a brittle manner a relatively large part of a pipe is usually destroyed instantly. The sharp, irregular fracture surface makes it more difficult to stop the gas flow. For these reasons, the probability of (fatal) incidents is higher for brittle pipes, making embrittlement a limiting factor for the service life of the pipe in a gas distribution network.

It is required that the uPVC pipes have a good impact performance during their entire service life and not just during installation, since third-party damage can occur at any moment in service. Therefore, the influence of physical ageing, which occurs during the service lifetime of a glassy polymer, on the impact behaviour of uPVC is studied in this chapter. Since the studies of Peilstöcker [2, 3] and LeGrand [4] it is known that physical ageing can have a significant influence on the impact behaviour of polycarbonate (PC, a glassy polymer like uPVC). Physical ageing is caused by the fact that glassy polymers are not in thermodynamic equilibrium, but continuously strive towards it. Although the mobility in the glassy state (below approximately 80 °C for uPVC) is low, the polymer chains are still capable of small conformational changes [5]. The mobility of the polymer chains increases at higher temperatures, shortening the timescales at which conformational changes occur. As a result of the conformational

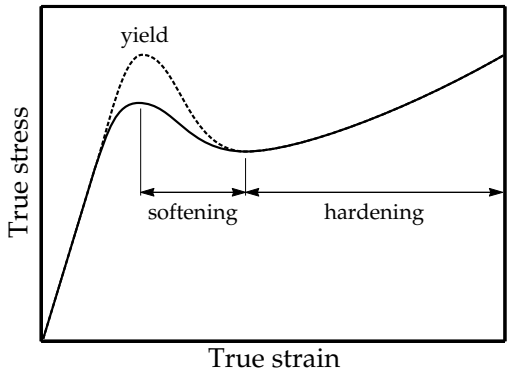

Figure 3.1 *Schematic representation of the intrinsic behaviour of a glassy polymer, such as uPVC, as measured in compression before (solid line) and after (dashed line) an annealing treatment.*

changes, the polymer density increases, the molecular mobility decreases and the resistance against plastic deformation increases. The latter is proven by a significant increase in the yield stress of glassy polymers during physical ageing [6], which was also demonstrated for uPVC in Chapter 2.

The influence of physical ageing on the intrinsic deformation behaviour of glassy polymers is schematically shown in Figure 3.1. The increase in yield stress and the unaffected strain hardening responds cause an increase in the yield drop, known as strain softening. The interplay between the amount of softening and the strain hardening modulus determines the degree of localisation of the plastic deformation when subjected to a tensile load [7–10]. Consequently, the increase in strain softening results in e.g. a decrease in elongation at break on a macroscopic scale [11–13]. An increase of strain softening will eventually lead to crazing and brittle fracture. Crazes are preceded by local plastic deformation according to the following mechanism [14]: plastic deformation in polymers starts locally (e.g. near an imperfection) in a plastic zone. Depending on the mechanical properties of the polymer this plastic zone is succeeded by global plastic deformation, or it grows further on a local scale. In the latter case the hydrostatic stress within the plastic zone is built up because its deformation is constrained by the surrounding material. Voiding occurs when the strain is localised to such an extent that the local hydrostatic tensile stress (near the edge of the yield zone) surpasses a critical value [15]. These voids grow and interconnect with the remaining highly oriented polymer ligaments between the voids: the craze fibrils. At this stage a craze is nucleated. The value of the critical hydrostatic stress at which crazing occurs is hardly influenced by physical ageing as was shown for PC [16, 17], poly(methyl methacrylate) (PMMA) [16] and polystyrene (PS) [18]. The change in failure behaviour can be related to the process of physical ageing by calculating

the thermodynamic state at which the deformation of the polymer localises to such an extend that the hydrostatic stress in the material can surpass the critical value.

The ageing induced changes in intrinsic behaviour can thus lead to a transition from ductile towards (macroscopically) brittle behaviour, which is indeed observed in studies on the influence of physical ageing on the Izod [12, 19, 20] and Charpy [21] impact performance of uPVC. It is known that the decrease in impact performance leads to a shift of the ductile-to-brittle transition temperature towards higher temperatures. Both Adam *et al.* [8] and Ryan [22] reported a marked increase of the ductile-to-brittle transition temperature of polycarbonate (PC) after an annealing treatment (which is defined here as a heat treatment at elevated temperatures, but below the glass transition temperature of the polymer). The goal of this chapter is to find out whether this ageing induced embrittlement can be related to physical ageing via the evolution of the yield stress resulting from an annealing treatment. In the next section the annealing embrittlement data of LeGrand [4] on PC are analysed to find that the ductile-to-brittle transition indeed occurred at a constant thermodynamic state and thus a constant yield stress. This observation is used in Section 3.3, where a hypothesis is posed which enables the prediction of the ductile-to-brittle transition temperature ($T_{d\rightarrow b}$) based on the influence of temperature and physical ageing on the yield stress. The experiments which are required to characterise the influence of physical ageing on the deformation and impact behaviour of uPVC are described in Sections 3.4, 3.5 and 3.6. The experimental data are compared to the predicted results in Section 3.7 using the posed hypothesis. This comparison is followed by a discussion where the results for the water pipe grade uPVC used in this chapter are translated to the behaviour which can be expected for the gas pipe grade uPVC used in the rest of this thesis.

3.2 Annealing embrittlement of polycarbonate

Following the path outlined in the introduction, one can expect the ductile-to-brittle transition to be related to the thermodynamic state and thus the yield behaviour of the polymer. As already stated, the value of the critical hydrostatic stress at which crazes initiate in PC remains constant after annealing [16, 17]. The ductile-to-brittle transition upon annealing can therefore be directly related to a critical amount of strain localisation, thus a critical thermodynamic state, with a corresponding yield stress (for a given strain rate and temperature) [17]. Consequently, the ductile-to-brittle data of PC as presented by LeGrand [4] can be coupled to the evolution of the yield stress upon an annealing treatment. Klompen *et al.* [23] proposed to describe the evolution of the yield stress (σ_y)

of PC as a function of annealing time t and annealing temperature T_a using the following relation:

$$\sigma_y = \sigma_{y,0}(\dot{\epsilon}, T) + c \cdot \log\left(t_{eff}(t, T_a) + t_{ini}\right) , \tag{3.1}$$

with c a constant equal to the slope of the yield stress versus the logarithm of the annealing time (t), t_{ini} the initial age and $\sigma_{y,0}$ the yield stress at the hypothetical case of $t_{eff} + t_{ini}$=1 s, which depends on the strain rate ($\dot{\epsilon}$) and temperature (T). Klompen *et al.* used $\sigma_{y,0}$=26.1 MPa, c=3.82 MPa per decade and t_{ini}=$7.3 \cdot 10^{10}$ s to describe the true tensile yield stress evolution of injection moulded PC tensile bars measured at a strain rate of 10^{-2} s^{-1} and a temperature of 23 °C. The effective time (t_{eff}) is a measure for the annealing time at the reference condition and is defined using an Arrhenius type time-temperature superposition:

$$t_{eff}(t, T_a) = t \cdot \exp\left[\frac{\Delta U_a}{R}\left(\frac{1}{T_{ref}} - \frac{1}{T_a}\right)\right] , \tag{3.2}$$

where ΔU_a is the activation energy that quantifies the difference in timescale of the influence of ageing at annealing temperature T_a compared to the timescale at which ageing becomes apparent at the reference temperature (T_{ref}=23 °C). Klompen *et al.* found a value of 205 kJ/mol for the activation energy of PC. With these values the evolution of the true tensile yield stress with the annealing time can be described for different annealing temperatures as shown in Figure 3.2 (bottom).

As mentioned before, not only yield, but also impact properties are influenced by physical ageing. The Izod impact data for notched PC specimens of LeGrand [4] are reproduced in Figure 3.2 (top). The data measured after annealing at 100 °C-125 °C are used for further analysis. The annealing times at 130 °C are shorter than the time to thermal equilibration within the specimens. The resulting data points are therefore not taken into account in the following analysis. The solid lines in Figure 3.2 (top) represent the best fit of the data to a fit function (an inverse tangent). These lines indicate the time frame in which the ductile-to-brittle transition occurs for each annealing temperature, which are marked as grey areas. The same time frames are also marked in the evolution of the yield stress shown in Figure 3.2 (bottom). Remarkably, the yield stresses corresponding to the ductile-to-brittle transitions at the four annealing temperatures fall within a range of only 2.5 MPa. This observation supports the existence of a critical thermodynamic state (and thus critical yield stress) at which the ductile-to-brittle transition occurs. This is in line with the results of Engels [17], who proposed the use of a critical yield stress to calculate the lifetime at service temperature. It should be noted, however, that the value found for the critical

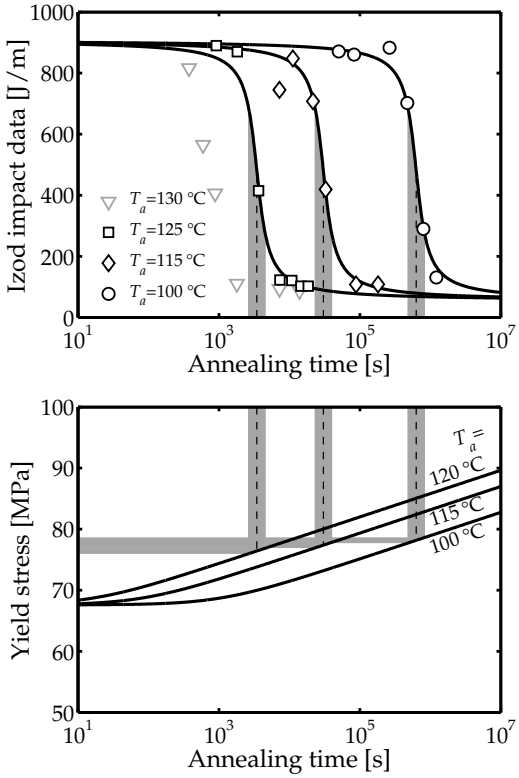

Figure 3.2 *The influence of annealing treatments at four different temperatures on the notched Izod impact strength and yield stress. Top: Izod impact data of notched PC specimens tested at room temperature. The specimens were annealed at 100 °C, 115 °C, 125 °C or 130 °C for different annealing times (reproduced from [4]). The data at 130 °C are not taken into account in the analysis and are shown in grey. Bottom: the evolution of the yield stress at 23 °C and 10^{-2} s^{-1} according to Equation (3.1) as proposed by Klompen et al. [23]. The vertical grey hatches indicate the annealing time at which the transition from ductile-to-brittle behaviour is observed in the data of LeGrand [4]. The horizontal grey hatches indicate the corresponding yield stress.*

yield stress cannot be applied to predict the transition towards brittle failure in other loading geometries. The critical yield stress value depends for example on the deformation field imposed by the impactor. It can merely be used as a tool to predict the ductile-to-brittle transition for these specific testing conditions.

3.3 Predicting $T_{d\rightarrow b}$ for uPVC

In the previous section a critical yield stress was found at which the ductile-to-brittle transition occurred for Izod tests performed on PC at a constant testing temperature. In the present study impact tests are performed on uPVC at a

range of temperatures and for various annealing treatments to find the influence of physical ageing on the ductile-to-brittle transition temperature $T_{d\rightarrow b}$. The evolution of $T_{d\rightarrow b}$ with physical ageing (a change in thermodynamic state) is related to the evolution of the yield stress by posing the following hypothesis: brittle fracture occurs when the yield stress (σ_y) of the uPVC specimens surpasses a critical tensile stress (σ_{cr}). This critical tensile stress is independent of the annealing treatment (defined by the annealing temperature T_a and time t) and temperature (T). In mathematical terms this means that the pipe behaves brittle when:

$$\sigma_y(T, t, T_a) \geq \sigma_{cr} \,. \tag{3.3}$$

This hypothesis is used to relate the impact behaviour with the yield behaviour of uPVC.

The proposed hypothesis can only be employed when the influence of strain rate, temperature and physical ageing on the yield behaviour of uPVC is characterised, such as done in Chapter 1 and 2. In these chapters the yield behaviour of uPVC was assumed to be thermorheologically simple: only one relaxation mechanism, the α-process related to the glass transition temperature, was considered to contribute to the yield behaviour. This assumption only holds for low strain rates and/or moderate temperatures. At high strain rates and/or low temperatures, such as encountered during the instrumented falling weight impact tests, the secondary, or β-transition, also contributes to the yield behaviour. Roetling [24–26] showed that the strain rate ($\dot{\epsilon}$) and temperature (T) dependence of thermorheologically complex yield behaviour of polymers can be described with a Ree-Eyring relation [27]. This is a modification of the Eyring reaction rate relation [28], in which the contribution of two (or more) relaxation mechanisms to the tensile yield stress (σ_y) are decomposed into two parallel contributions:

$$\sigma_y(T, \dot{\epsilon}) = \sum_{x=\alpha,\beta} \frac{RT}{\nu_x^*} \cdot \sinh^{-1}\left[\frac{\dot{\epsilon}}{\dot{\epsilon}_{0,x}} \cdot \exp\left(\frac{\Delta U_x}{RT}\right)\right] , \tag{3.4}$$

with R the universal gas constant, ν_x^* the activation volume, ΔU_x the activation energy and $\dot{\epsilon}_{0,x}$ the pre-exponential factor that is related to the entropy of the system. The subscript x in the parameters is substituted by α or β to refer to the parameter for the corresponding relaxation mechanism. In Chapter 2 it was shown that the influence of physical ageing on the yield stress of uPVC can be described by making the pre-exponential factor a function of time. In Section 3.5.2 it is shown that, in agreement with the behaviour of PC [29, 30], the pre-exponential factor for the β-process ($\dot{\epsilon}_{0,\beta}$) in uPVC does not change for the range of annealing temperatures investigated in this study (from 45 °C to 60 °C). The

local twisting mode around the main chain, to which the β-process is presumed to be related [31, 32], is in thermodynamic equilibrium in this temperature range, and therefore does not change upon annealing. As a result, the ageing kinetics can be incorporated in Equation (3.4) by making only $\dot{\epsilon}_{0,\alpha}$ a function of time in a similar way as presented in Chapter 2:

$$\dot{\epsilon}_{0,\alpha} = b_0 \cdot \left(\frac{t_{eff}(t, T_a) + t_{ini}}{t_0} \right)^{b_1}, \tag{3.5}$$

with b_0 and b_1 constants, t_0=1 s and t_{ini} the initial age of the material. The effective time (t_{eff}) accounts for the influence of temperature on the ageing rate and was already defined in Equation (3.2). Combining Equations (3.2), (3.4) and (3.5) gives the following expression that relates the yield stress with the strain rate and temperature and includes the influence of physical ageing:

$$\sigma_y(T, \dot{\epsilon}, t, T_a) = \frac{RT}{v_\alpha^*} \cdot \sinh^{-1} \left[\frac{\dot{\epsilon} \cdot \exp\left(\frac{\Delta U_\alpha}{RT}\right)}{b_0 \cdot \left(t \cdot \exp\left[\frac{\Delta U_{a,\alpha}}{R} \left(\frac{1}{T_{ref}} - \frac{1}{T_a} \right) \right] + t_{ini} \right)^{b_1}} \right] \cdots + \frac{RT}{v_\beta^*} \cdot \sinh^{-1} \left[\frac{\dot{\epsilon}}{\dot{\epsilon}_{0,\beta}} \cdot \exp\left(\frac{\Delta U_\beta}{RT}\right) \right]. \tag{3.6}$$

3.4 Experimental

3.4.1 Material and specimen preparation

A large amount of material is required for the type of instrumented falling weight tests used in this study. It is impossible to obtain this amount of material from uPVC gas pipes taken out of service, as multiple pipes are required and it is unknown whether these are all processed under the same conditions and have the same thermo-mechanical history. Therefore, all specimens were made from new, unused uPVC pipes all taken from a single processing batch. The pipes have a diameter of 110 mm, a wall thickness of 2.7 mm and are produced for water distribution purposes. Unfortunately, the uPVC used for these pipes has a different grade/formulation than the gas pipes produced between 1960 and the mid-seventies. Therefore, the characterisation presented in Chapter 1 and 2 cannot be used directly; the yield behaviour of the water grade pipes should be characterised for this type of uPVC as well.

The specimens for the instrumented falling weight tests were produced by cutting pipe segments with a length of 55 mm from the pipe with a lathe. These pipe segments were sawed in half (in the axial direction) to obtain two identical semi-cylindrical specimens. Five different sets of specimens were prepared that consisted of at least 180 specimens per set. Each set was given a different heat treatment (as summarised in Table 3.1) resulting in different thermodynamic states.

The characterisation of the yield stress behaviour was carried out with the use of tensile tests. The tensile specimens were produced by cutting a section of 70 mm from the pipe with a bandsaw. Subsequently, such a section was sawed in half in axial direction and then pressed into flat plates in a press at 100 °C, thus approximately 15-20 °C above the glass transition temperature of uPVC, in 25 minutes at a compressive stress of around 1 MPa. Tensile bars with a gauge section of approximately $30\times5\times2.7\,\mathrm{mm}^3$ were milled from the plate material (parallel to the axial direction of the pipe). The pressing procedure erased all prior effects of physical ageing. In some cases a heat treatment above the glass transition temperature can change the crystallinity of the uPVC, which in turn influences the β-relaxation as shown by Harrell and Chartoff [33]. They varied the crystallinity levels between 0% and 34% by selecting specimens with different amounts of stereoregularity and/or chain branching. Here, only one uPVC formulation was used. Consequently, the increase in crystallinity during the 25 minutes at 100 °C is expected to be only minor. The influence of the processing treatment on the β-relaxation and the associated physical ageing kinetics (as studied by Tsitsilianis *et al.* [34]) was therefore neglected.

Table 3.1 *Heat treatments of the five sets of specimens.*

#	Annealing time	Annealing temperature
1	as-received	
2	$2\cdot10^6$ s	45 °C
3	$1\cdot10^5$ s	60 °C
4	$1\cdot10^6$ s	60 °C
5	$3\cdot10^6$ s	60 °C

3.4.2 Test method

The experimental setup for the impact tests is similar to the one described by Meijering [35] and is (partly) schematically shown in Figure 3.3. All impact tests

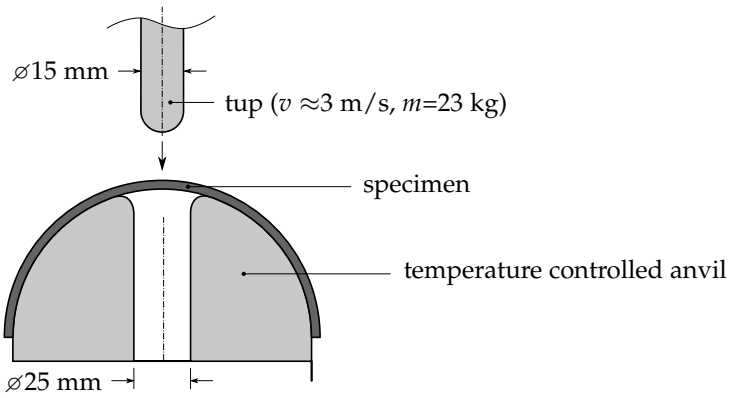

Figure 3.3 *Cross-sectional view of the setup (schematically) for the instrumented falling weight test.*

were carried out on a Dynatup 8250 impact machine. The specimens were placed on a temperature controlled anvil and impacted with a semi-spherical tup with a top radius of 7.5 mm. The tup was fixed on a falling weight of 23 kg at a height of 460 mm above the specimen prior to testing. The velocity at impact was around 3 $m \cdot s^{-1}$, resulting in a kinetic impact energy of 100 J. The force during impact was measured with a 15 kN Kistler force cell (9011A) and recorded with a Yokogawa DL 1540 digital oscilloscope. The displacement of the weight was measured using a Meter Drive ZAM 301 AAS linear encoder with a resolution of 0.1 mm.

The impact tests were carried out at various temperatures. Prior to testing the temperature of the specimens was controlled in a Sanyo MIR 583 Incubator. The temperature of the anvil was controlled by a ethylene glycol flow through a cooling circuit inside the anvil. The temperature of the ethylene glycol was controlled in a Haake F3 thermal bath. A thin layer of vaseline was applied on the anvil to ensure that any ice formed at the surface of the anvil could be easily removed prior to testing. In most cases 30 specimens were tested per temperature.

The uniaxial tensile tests were carried out on an MTS Elastomer Testing System 810 equipped with a 25 kN force cell and a thermostatically controlled chamber. These experiments were carried out at a constant crosshead speed, resulting in constant *engineering* strain rates. The tensile tests were carried out at strain rates ranging from 10^{-4} s^{-1} to 1 s^{-1} and temperatures ranging from -20 °C up to 40 °C. The value of the yield stress was calculated using the average of the cross-sectional surface areas as measured at three locations in the gauge section. All stresses and strains reported in this chapter are *engineering* values.

3.5 Characterisation

The uPVC pipe material used for the experiments presented in this chapter, differs from the grade used in Chapter 1 and 2. Moreover, the β-contribution to the yield behaviour has not been characterised in the previous chapters. The characterisation of the temperature and strain rate dependence of the yield stress and the influence of physical ageing is presented in the following two sections.

3.5.1 Characterising the deformation kinetics

The results of the tensile yield stress measurements plotted in Figure 3.4 clearly show a transition from α dominated yield towards α+β dominated yield; the influence of the β-relaxation becomes apparent at strain rates higher than 0.03 s^{-1} at room temperature. The solid lines represent the result of Equation (3.4) using the parameters summarised in Table 3.2. The parameters related to the α-relaxation were calculated from the parameters as determined in Chapter 1 for the different uPVC grade. The parameters that account for the contribution of the β-relaxation were adopted from a study of Bauwens-Crowet *et al.* [36]. The pre-exponential factors $\dot{\epsilon}_{0,\alpha}$ and $\dot{\epsilon}_{0,\beta}$ were obtained using a reference point in the α-regime and one in the α+β-regime, respectively. The excellent agreement of the solid lines compared to the experimental data shows that the deformation kinetics of the uPVC of the gas pipe grade that was characterised in Chapter 1 is equal to the uPVC grade used here, at least for the α-regime.

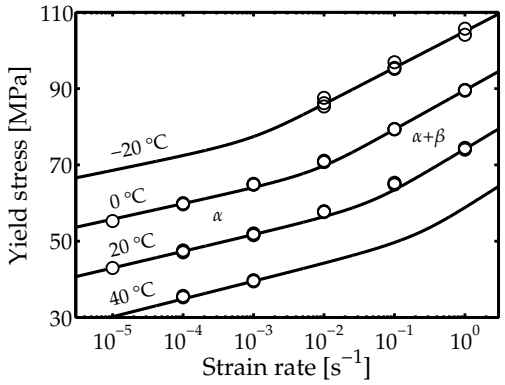

Figure 3.4 *The markers show the yield stress as measured in uniaxial tension at a range of strain rates and temperatures. Two regimes are indicated: the α-regime and the α+β-regime. The solid lines represent the description of Equation (3.4) using the material parameters given in Table 3.2.*

Table 3.2 *The values for the parameters in Equation (3.6) for the α and β relaxation mechanisms in uPVC.*

	α	β	
$\dot{\epsilon}_{0,x}$	$1.88 \cdot 10^{38}$	$2.21 \cdot 10^{0}$	[s^{-1}]
v_x^*	$1.29 \cdot 10^{-3}$ †	$8.39 \cdot 10^{-4}$ ‡	[m^3/mol]
ΔU_x	$2.97 \cdot 10^{5}$ †	$5.86 \cdot 10^{4}$ ‡	[J/mol]
$\Delta U_{a,x}$	$2.38 \cdot 10^{5}$		[J/mol]
b_0	$7.39 \cdot 10^{41}$		[s^{-1}]
b_1	-0.45		[-]

† value adopted from Chapter 1 (includes pressure dependence)

‡ value adopted from Bauwens-Crowet *et al.* [36]

3.5.2 Characterising the ageing kinetics

The physical ageing kinetics of the α-contribution to the tensile yield stress of (a different grade of) uPVC was characterised in Chapter 2. Both Bauwens-Crowet *et al.* [29] and Ho-Huu [30] showed that the β contribution to the yield stress of PC is not influenced by its thermal history. The same behaviour can be expected for uPVC; its β-transition temperature is about -40 °C and, therefore, the mobility that is related to the β-relaxation, is in thermodynamical equilibrium at the annealing temperature of 60 °C. To verify whether the β-contribution to the yield stress indeed remains constant during annealing treatments, the experimental data is compared with the predictions of the model taking only the ageing kinetics of the α-contribution to the yield stress into account.

The yield stress data at a strain rate of 10^{-4} s^{-1} and at 25 °C after different annealing treatments, are shown as unfilled markers in Figure 3.5 (left). From the shift between the data at the annealing temperature of 45 °C and 65 °C, the activation energy in Equation (3.2), $\Delta U_{a,\alpha}$, can be calculated and was found to be 238 kJ/mol. With this activation energy the location of the filled markers in Figure 3.5 (left) can be calculated. The filled markers represent the yield evolution of the uPVC aged at a reference temperature (chosen to be 25 °C here). The values of the constants b_0 and b_1 in Equation (3.6) were determined using a non-linear least square fitting routine on the shifted yield stress data, resulting in values of b_0=$7.34 \cdot 10^{41}$ s^{-1} and b_1=-0.45, respectively.

As shown in Section 3.5.1, the strain rate and temperature dependence of the yield stress of the water pipe grade used here is identical to that of the gas pipe grade used in Chapter 1 and 2. Remarkably, the ageing kinetics are significantly different. The activation energy for the gas pipe grade is about twice as low as

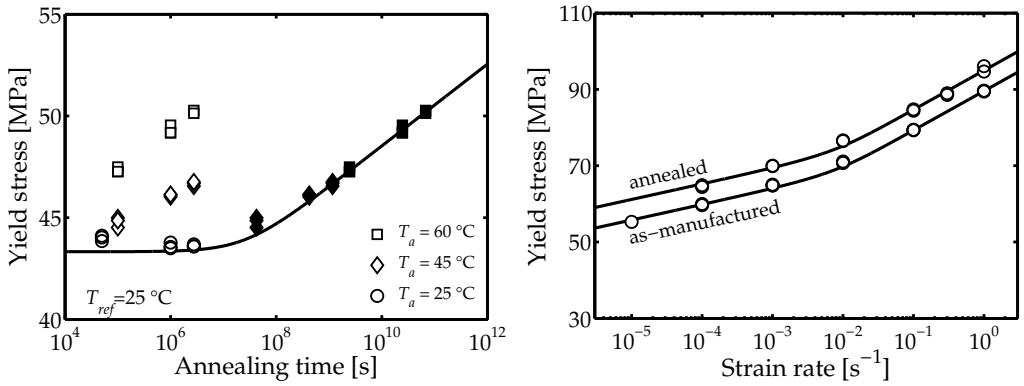

Figure 3.5 *Influence of physical ageing on the deformation kinetics of PVC.* ***Left:*** *yield stress at 10^{-4} s^{-1} and 25 °C versus the annealing time. The unfilled markers represent the yield stress versus the ageing time at the specific annealing temperature (T_a). The filled markers represent the same measurements where the annealing time is calculated for the reference temperature of 25 °C (the effective time in Equation (3.2)). The master curve that follows from Equation (3.6) is shown as solid black line.* ***Right:*** *the tensile yield stress versus strain rate at 0 °C for two sets of uPVC specimens. One set did not receive a heat treatment after production ("as-manufactured") and one set was annealed for $2.7 \cdot 10^6$ s at 60 °C ("annealed"). The solid lines are predictions using Equation (3.6).*

the value found for the material used in this chapter. Moreover, the constant b_1 is about twice as low for the gas pipe grade, resulting in a twice as steep slope of the mastercurve for the gas pipe grade. Apparently, the main chain segmental mobility that is related to yielding is identical for the two grades, whereas the mobility of the polymer chains to make small conformational changes, which are related to the ageing behaviour, is significantly lower for the water pipe grade. The physical background behind this difference is unknown at this stage, but it might be related to the different content and type of additives and filler. The glass transition temperature (T_g) as measured using differential scanning calorimetry (with a Mettler Toledo DSC823e) of the water pipe grade is about 3 °C higher than that of the gas pipe grade. This difference can be explained by a small content of plasticiser in the water pipe grade, causing an "anti-plasticisation" effect [37, 38]. The small amount of plasticiser inhibits segmental motion and increases the yield stress and also T_g. This difference in T_g only partly explains the difference in ageing kinetics, as it is too small to have such effects on the ageing kinetics. Another possible explanation might be a difference in the crystalline structure of the two grades. Differences in the conditions during polymerisation can result in a different crystalline structure [39], which can have an influence on the ageing behaviour [34]. Further research is required to reveal the physical background between the difference in ageing kinetics of the two pipe grades used in this study.

The influence of the strain rate on the yield stress at 0 °C was measured for specimens that were annealed for $2.7 \cdot 10^6$ s at 60 °C and specimens that did not receive a heat treatment. The results are shown in Figure 3.5 (right). The solid line for the annealed specimens is predicted using Equation (3.6) and the parameters listed in Table 3.2. Note that the β-contribution to the yield stress was considered to be independent of the thermodynamic state of the material. The quantitative agreement between the prediction and the experimental data supports the assumption that the β-contribution to the yield stress is not influenced by physical ageing. Consequently, the physical ageing kinetics of the α-contribution is taken into account only.

3.6 Impact results

3.6.1 Types of failure

The conditions during the instrumented falling weight tests were such that an excess kinetic impact energy was exerted to ensure all specimens failed. The behaviour of the specimens during impact can be divided in three categories: ductile, semi-ductile and brittle behaviour. A typical force-displacement diagram for each of these three types of failure is shown in Figure 3.6. At critical points in the force-displacement curves the corresponding image, obtained using a high speed camera, is shown.

The force-displacement diagram of a ductile failure, Figure 3.6 (topleft), shows a continuous increase of the force up to a force between 5 and 6 kN. A "shoulder"can be distinguished during the start of deformation, between the first two image stills (a and b). The deformation occurring before this shoulder can be ascribed mainly to elastic deformation, whereas the deformation occurring after the shoulder is mainly plastic. A considerable amount of stress whitening takes places in the material underneath the tup. At the moment the force reaches its maximum value the sides of the specimen have deflected upwards and lose contact with the anvil. Furthermore, the material underneath the tup is drawn into the anvil in a similar way as the ductile failures described in [40]. In the highly drawn regions the material starts to rupture locally. These ruptures grow and coalesce, followed by the formation of a crack that is large enough for the tup to penetrate the specimen. The material folds around the tup, between the tup and the hole in the anvil. The force does not decrease directly to zero after the puncture of the tup, because of frictional forces between the moving tup and the stationary specimen.

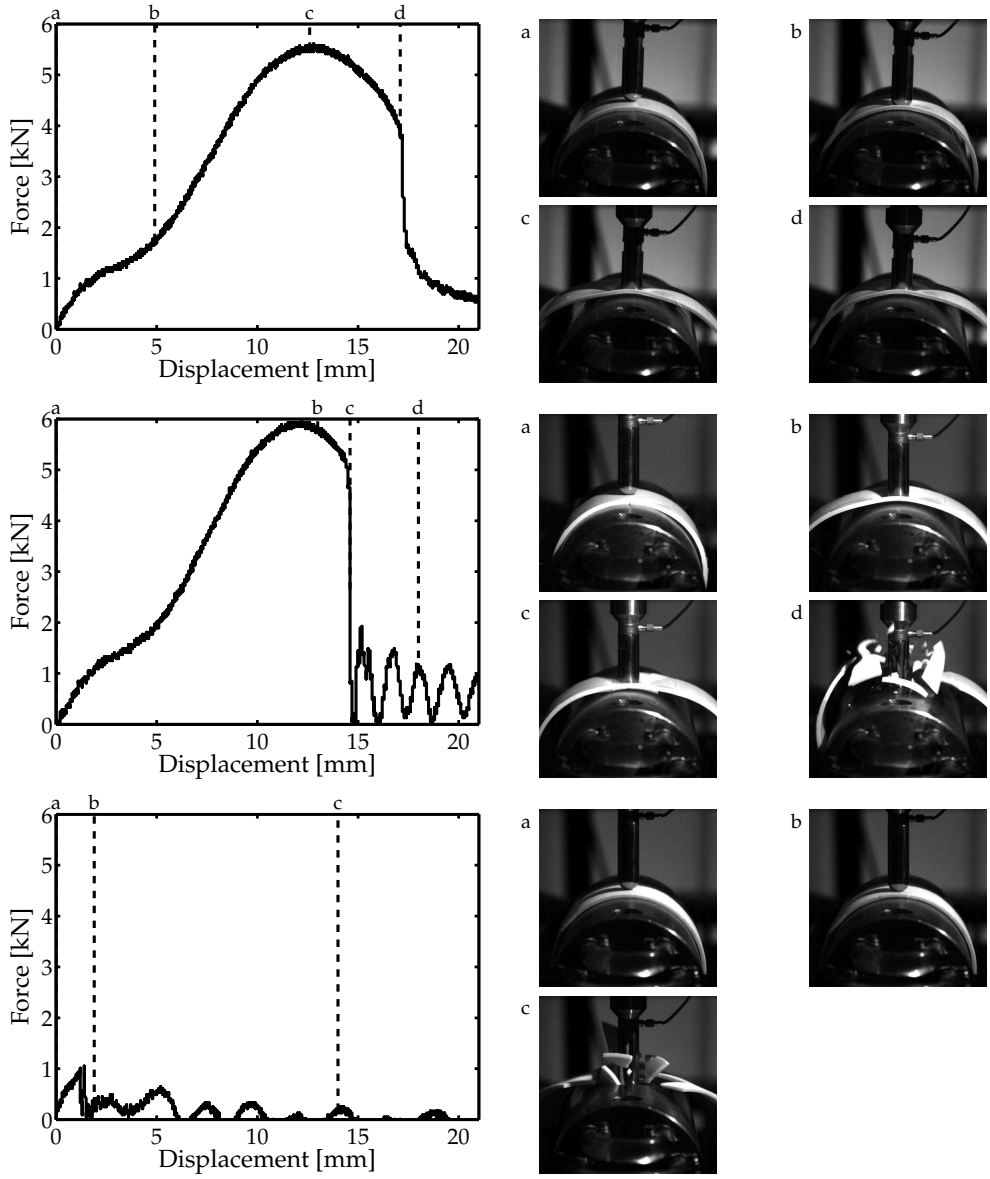

Figure 3.6 *Typical force versus displacement signals including video stills from a high speed camera for three failure types encountered during falling weight tests. The letters indicated on top of the figures on the left correspond to the video stills displayed on the right. Top: ductile failure. Middle: semi-ductile fracture. Bottom: brittle fracture.*

The semi-ductile specimens follow the same path as the ductile specimens up to the point where the force reaches its maximum. After the maximum in force, at still c, the tup punches out a piece of material that is roughly the size of the hole of the anvil. This part of the fracture is ductile, but the remaining part of the specimen fractures in a brittle way. As a result of the build-up of elastic energy, the fractured pieces scatter around at high velocity.

Brittle fracture occurs somewhere on the (left side of the) curve of the ductile specimens, far before the maximum force is reached. Most of the brittle fractures occur before the shoulder can be distinguished, thus before a significant amount of plastic deformation has been built up. After fracture, dynamic effects cause some oscillations in the force signal although no forces are exerted on the specimen anymore.

3.6.2 Impact energy analysis

During impact testing the kinetic energy of the impactor is partly stored as elastic energy and partly dissipated in the specimen as a result of plastic deformation and friction. The amount of energy absorbed by the specimen (E) is a measure for the ductility of the specimen upon impact, and can be calculated with:

$$E = \int_{s(t_{contact})}^{s(t_f)} F(s)\ \mathrm{d}s\,, \tag{3.7}$$

where F is the force, s the displacement, $t_{contact}$ the time at which the tup makes contact with the specimen and t_f the time when failure occurs. Two definitions of

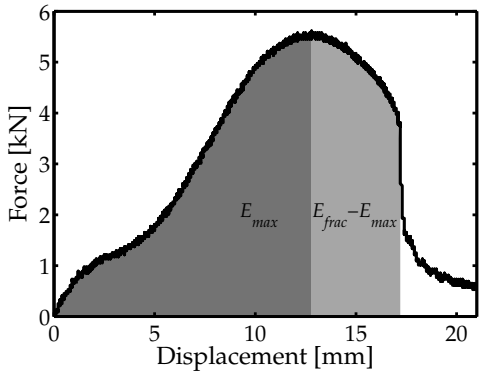

Figure 3.7 *Typical force versus displacement signal for a ductile failure. The energy up to the maximum force (E_{max}) and the energy up to fracture (E_{frac}) are defined as the filled, grey areas.*

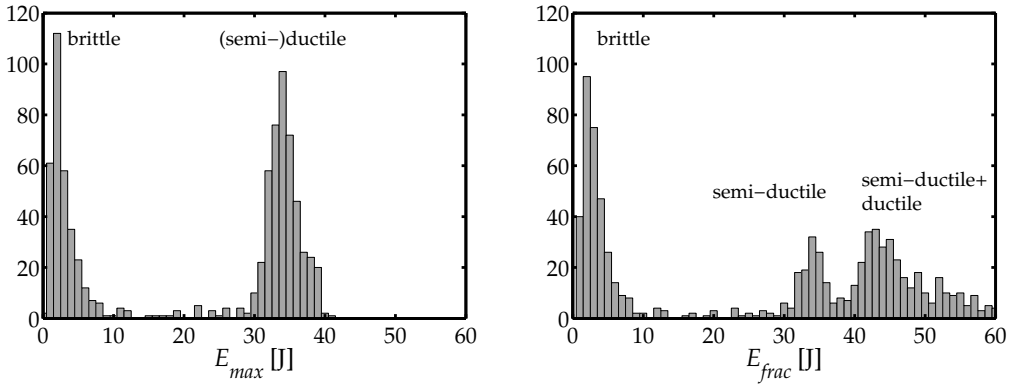

Figure 3.8 *Histogram of the surface area underneath the force-displacement plot (equal to the energy taken up by the specimen) of all tested specimens.* ***Left:*** *energy up to the maximum in the force signal.* ***Right:*** *energy up to fracture of the specimen.*

the failure time are compared here. The first, rather arbitrarily chosen, criterion is that failure occurs at the time at which the maximum force is reached. The amount of energy that follows from this criterion is referred to as the energy up to maximum force (E_{max}) throughout this chapter. The other definition of failure time is the time at which the force suddenly drops and the specimens actually fractures/ruptures. Using this time in Equation (3.7) gives the energy up to fracture (E_{frac}). An illustration of both definitions is shown in Figure 3.7.

The value of E_{max} was calculated for all experiments in this study and is presented in an histogram in Figure 3.8 (left). This figure clearly shows the existence of two distinct populations. The brittle fractures have a mean energy up to the maximum force of about 3 J. As the force-displacement behaviour during a semi-ductile failure is equal to that of a ductile failure up to the maximum force, these populations coincide and are brought together under the ductile population. The mean of the energy up to the maximum force of these failures is about 34 J.

A histogram of the energy up to fracture for all the experiments is shown in Figure 3.8 (right). As expected, the distribution of the brittle fractures is similar, whereas that of the semi-ductile and the ductile failures differ from the histogram of E_{max}. The distribution of the semi-ductile failures is very broad and coincides partly with the E_{frac} of the ductile failures, which makes it difficult to distinguish a semi-ductile failure from a ductile failure using E_{frac} only. E_{max} is used for the further analysis as E_{frac} does not give extra information. All semi-ductile and ductile failures are referred to as ductile failures for the remainder of this chapter.

The energy up to the maximum force (E_{max}) was determined for a range of test temperatures for each set of specimens listed in Table 3.1. All determined values are plotted versus the test temperature in Figure 3.9 for the as-received specimens

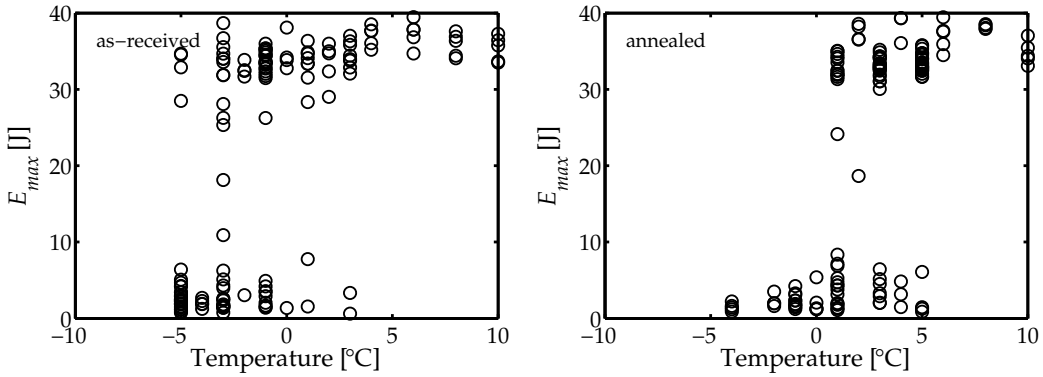

Figure 3.9 *Amount of energy taken up by the specimens during a falling weight test up to the maximum force versus the test temperature.* ***Left:*** *for the as-received specimens.* ***Right:*** *for specimens annealed for $3 \cdot 10^6$ s at 60 °C.*

(left) and the specimens that were annealed for $3 \cdot 10^6$ s at 60 °C (right). As already stated, the difference between ductile and brittle failure is very distinct, as can be seen in Figure 3.9 as well. The transition from ductile failures at higher temperatures towards brittle fractures at lower temperatures is, however, not very distinct. In the transition range both brittle and ductile failures occur, causing large standard deviations around the average of E_{max} at temperatures in this transition region (even for the temperatures at which a large number of experiments were carried out). Nonetheless, it is clear from the experimental data that the as-received specimens do show a transition towards brittle fracture at a lower temperature than the annealed specimens. An attempt to quantify this shift of the ductile-to-brittle transition temperature as a result of physical ageing is presented in the following section.

3.7 Ductile-to-brittle transition analysis

A failure is categorised here as "brittle" when E_{max} is lower than 25 J. The choice for this value is rather arbitrary as the analysis that follows is not sensitive for values between 10 J and 30 J. The percentage of ductile failures at each test temperature is shown in Figure 3.10 for the as-received specimens (left) and the specimens that were annealed for $3 \cdot 10^6$ s at 60 °C (right). The transition temperature is obtained by fitting an error-function (erf) to the percentage of ductile failure at each temperature:

$$\text{Percentage of ductile failures} = 50 + 50 \cdot \text{erf}\left(d_0 + d_1 \cdot T\right) , \tag{3.8}$$

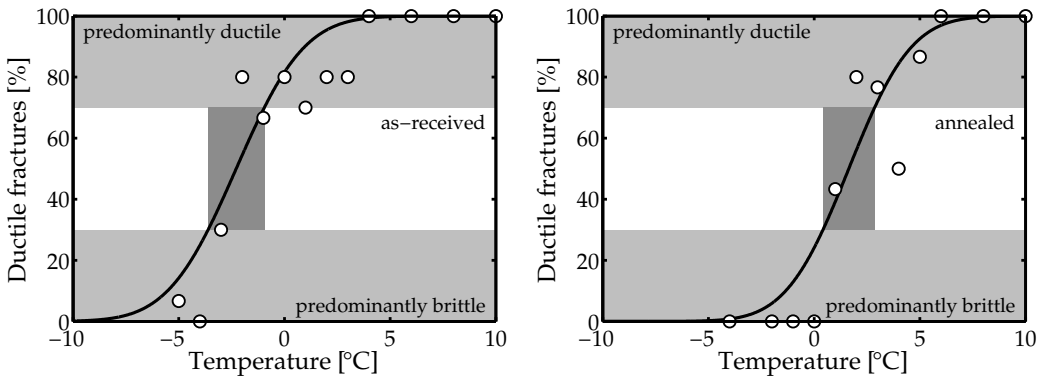

Figure 3.10 *Percentage of (semi-)ductile failures versus the test temperature. At the even temperature values, five measurements were conducted. At the uneven temperature values 30 measurements were carried out. The solid lines are the best fit to Equation (3.8).* ***Left:*** *for the as-received specimens.* ***Right:*** *for specimens that were annealed for* $3 \cdot 10^6$ *s at 60 °C.*

using d_0 and d_1 as fit parameters that determine the temperature at which the transition occurs and the width of the transition range, respectively. The number of experiments differs per testing temperature, as can be seen in Figure 3.9. The non-linear fitting routine was carried out on all individual experimental data points to account for this difference in number of data points per temperature. The resulting best fits are shown as a solid line for the as-received (left) and the annealed specimens (right) in Figure 3.10.

The ductile-to-brittle transition is defined here as the temperature region in which the percentage of ductile failure is between 30% and 70%. This transition temperature region can be calculated with the fitted function and is shown as the darker grey area in Figure 3.10. The transition temperature is found to be between -3.5 °C and -1 °C for the as-received specimens and between 0.4 °C and 2.8 °C for the annealed specimens. The transition regions for the specimens that received intermediate annealing treatments (set 2, 3 and 4 in Table 3.1) were calculated using the same procedure and shown as grey areas in Figure 3.11. On the abscissa of this figure the ageing time at 10 °C (the average service temperature of uPVC gas pipes) is given. This ageing time at 10 °C was calculated from the annealing treatment of each set, Equation (3.2) and the activation energy $\Delta U_{a,\alpha}$ as determined in Section 3.5.2. The transition temperature region for the as-received specimens is shown as a light grey area as its ageing time at 10 °C is 0 seconds which cannot be shown on a logarithmic scale. The experimental data did not show a significant increasing trend of the transition temperature with an increase in ageing time.

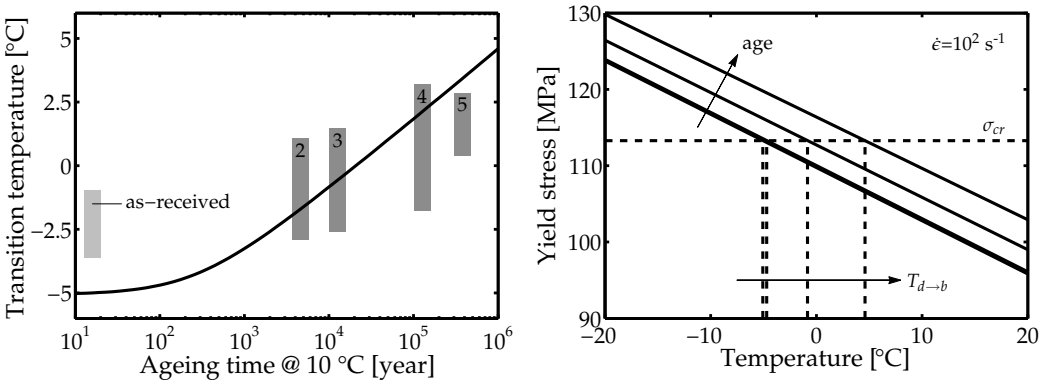

Figure 3.11 *Left: the ductile-to-brittle transition temperature range (grey patches) versus the calculated age at 10 °C in years (using Equation (3.2)). The solid line represents a prediction using Equation (3.6) and the hypothesis given by Equation (3.3).* ***Right:*** *the tensile yield stress of uPVC at four ages (1, 100, 10,000 and 1,000,000 years at 10 °C) and a strain rate of 10^2 s^{-1} versus the test temperature are shown in solid black lines. The critical stress, σ_{cr}, is shown as a dashed black line and the resulting $T_{d\rightarrow b}$ for each age is shown as a grey dashed line.*

The evolution of $T_{d\rightarrow b}$ resulting from an annealing treatment can be predicted assuming that the ductile-to-brittle transition occurs when a critical, temperature independent, tensile stress is reached (Equation (3.3)). As a first step, the value for this critical stress (σ_{cr}) was determined, which applies to the conditions during the impact experiments conducted in this study. From Equation (3.6) and the parameters listed in Table 3.2 the tensile yield stress at any given strain rate and temperature can be calculated as a function of the thermal treatment. The yield stress for the specimens of set 3 at its $T_{d\rightarrow b}$ was calculated to be 113 MPa for a strain rate of 10^2 s^{-1}, which is a rough estimate of the overall strain rate of the material during impact (neglecting local differences).[2] This yield stress value is assigned as the critical stress σ_{cr}. Once again, it should be emphasised that σ_{cr} is not a material parameter, but is merely a tool to calculate the evolution of $T_{d\rightarrow b}$ for these specific experimental conditions.

The procedure to obtain the evolution of $T_{d\rightarrow b}$ with the age of the material is outlined in Figure 3.11 (right). The $T_{d\rightarrow b}$ for specimens with a different annealing treatment was determined by calculating at which temperature the yield stress of these specimens is equal to the critical stress. The initial age (t_{ini}) was estimated from the age of the pipe material; at the time of testing the pipe material was 3 years old. Assuming a storage temperature of 23 °C the initial age was estimated to be equivalent to about 225 years at the service temperature

[2]The value of the strain rate has an influence (albeit small) on the resulting evolution of $T_{d\rightarrow b}$, as the lines in Figure 3.4 are not exactly parallel in both the α and the α+β-region.

of 10 °C using Equation (3.2). The solid line shown in Figure 3.11 (left) is the result of employing the hypothesis on the yield evolution and qualitatively agrees with the experimentally obtained $T_{d\to b}$ in the sense that the increase with age is marginal. The predicted gradient of $T_{d\to b}$ versus the logarithm of age is somewhat higher than the gradient found experimentally, but is still a good estimate. Furthermore, the predicted transition temperature of the as-received specimens (the level of the initial plateau of the solid line) is lower than the measured value. A possible explanation for this difference is that the initial age of the pipe material was actually higher than expected because of a higher storage temperature or a slow cooling rate after processing. Another explanation is that the hypothesis is not valid. Ishikawa *et al.* [41] showed that the critical hydrostatic stress at which crazes nucleate decreases with temperature, which contradicts the hypothesis posed in this chapter. Employing a decreasing critical stress with temperature would, however, result in an even more pronounced increase of $T_{d\to b}$ with annealing. The posed hypothesis thus results in a better description of the evolution of $T_{d\to b}$ and is therefore used to describe this evolution throughout the rest of this chapter.

The practical implication of these results is that physical ageing does not lead to embrittlement during 50 years of service life for *this water pipe grade* of uPVC for unloaded pipe conditions. The 50 years of service at 10 °C only adds about 0.2 °C to $T_{d\to b}$ for the prediction based on the estimated initial age of 225 years. As already stated, the yield behaviour of the uPVC grade that was used for gas distribution pipes is much more influenced by physical ageing. In the next section the consequences of this difference are discussed.

3.8 Discussion

In both the experimental and the model the influence of physical ageing results in a small effect on the $T_{d\to b}$ of uPVC water pipe grade: 50 years of ageing at 10 °C hardly changes the $T_{d\to b}$. In Section 3.5.2 the ageing kinetics of this water pipe grade was found to differ significantly from a pipe grade used for gas distribution pipes, which was characterised in Chapter 2. For the operators of the gas distribution network the influence of this difference on the prediction of the ductile-to-brittle transition is of interest. As a first approximation the same critical yield stress was used to calculate the evolution of the transition temperature. This choice for the critical yield stress determines the temperature at which the transition occurs at a given state of ageing, but not the rate at which $T_{d\to b}$ changes with the age of the pipe. The initial age of the uPVC gas pipe material was chosen to correspond to a yield stress of 50 MPa (at 10^{-3} s^{-1} and 23 °C) and a moderate

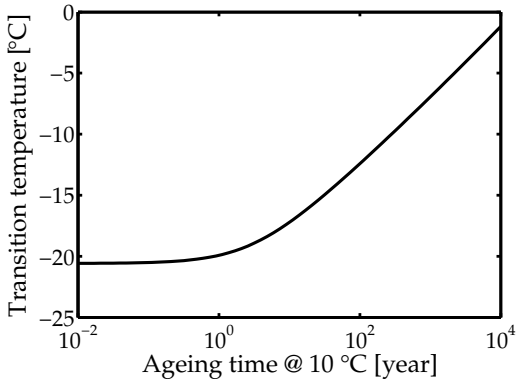

Figure 3.12 *Prediction of the ductile-to-brittle transition temperature of uPVC gas pipes using the ageing parameters as determined in Chapter 2, assuming an initial age that corresponds to a tensile yield stress of 50 MPa (at 10^{-3} s^{-1} and 23 °C) and the same critical yield stress as used in Figure 3.11.*

cooling rate after processing. The resulting relation between the age and $T_{d\to b}$ for the gas pipe grade is shown in Figure 3.12. Note that both the time and the temperature range along the axes in Figure 3.12 are different from those in Figure 3.11 (left).

The model predicts that the transition temperature for the gas pipe grade is much more sensitive to physical ageing than the water pipe grade; the $T_{d\to b}$ increases 5.7 °C per decade for the gas pipe grade and 2.5 °C per decade for the water grade pipe. Within a service life of 50 years at 10 °C the ductile-to-brittle transition temperature can be expected to increase about 7 °C;[3] depending on the initial age of the pipe at the moment it is installed. In this case the initial age was chosen such that it complies with cooling rates encountered during the extrusion process of PVC pipes. Storing the pipe for 3 years at 23 °C (as assumed for the water pipe grade) results in an increase of 5 °C of the $T_{d\to b}$. Subsequent ageing in the ground (at 10 °C), only results in minor changes as the changes in $T_{d\to b}$ occur on a logarithmic timescale. The storage time *and* temperature prior to installation of the pipes therefore have an important influence on the quality of the pipe at the moment it is installed.

For the operators of the gas distribution network it is important to determine a criterion for the uPVC pipes at which the pipes become too brittle. In this study it is shown that this criterion can be related to the age, and thus to the thermodynamic state, of the material. A procedure comparable to the procedure used by LeGrand [4] is proposed to determine such a criterion. First

[3] Nonetheless, the effect of ageing on the embrittlement of this grade of uPVC is still much less pronounced than the annealing induced embrittlement reported for PC [8, 22].

a temperature is chosen at which the uPVC pipe should still be ductile. An impact load comparable to that encountered by digging activities is applied on specimens of uPVC pipe material at this temperature. Subsequently, the age of the specimens is increased until a brittle failure is encountered. The thermodynamic state of this brittle specimen corresponds to the critical age. The experimental data presented in this chapter can be used to estimate at which age this transition occurs.

3.9 Conclusions

Instrumented falling weight tests have been used to measure the influence of physical ageing on the ductile-to-brittle transition temperature of uPVC pipes. This transition temperature was hardly influenced for the range of ageing times tested: an increase of only 4 °C was observed after annealing the specimens for $3 \cdot 10^6$ s at 60 °C, equivalent to almost half a million year at the service temperature of uPVC gas pipes. This marginal increase was found to comply at least qualitatively with the description of the evolution of $T_{d \to b}$ with ageing using the hypothesis that the transition from ductile-to-brittle behaviour occurs when the tensile yield stress surpasses a critical, temperature independent stress value. The calculated increase in $T_{d \to b}$ is 0.2 °C for a water pipe grade after 50 years of service at 10 °C. Applying the same hypothesis on the evolution of the yield stress of uPVC gas pipes upon ageing, suggests that the $T_{d \to b}$ for these pipes is much more influenced during service life; an increase of about 7 °C is predicted. The yield stress might therefore be a key parameter in determining the residual lifetime of the uPVC gas pipes that are currently in service.

References

[1] A. Hendriks. Storingsrapportage gasdistributienetten 2008. Technical report, Netbeheer Nederland, **2009**. URL `http://www.energiened.nl/_upload/bestellingen/publicaties/186_315011-Storingsrap`

[2] G. Peilstöcker. Über das Temperaturverhalten von Polykarbonat. *Kunststoffe* 51:509–512, **1961**.

[3] G. Peilstöcker. The temperature behaviour of polycarbonate. *British Plastics* 35:365–369, **1962**.

[4] D.G. Legrand. Crazing, yielding, and fracture of polymers. I. Ductile brittle transition in polycarbonate. *Journal of Applied Polymer Science* 13:2129–2147, **1969**.

[5] J.M. Hutchinson. Physical aging of polymers. *Progress in Polymer Science* 20:703–760, **1995**.

[6] J.H. Golden, B.L. Hammant, and E.A. Hazell. The effect of thermal pretreatment on the strength of polycarbonate. *Journal of Applied Polymer Science* 11:1571–1579, **1967**.

[7] T.E. Brady and G.S.Y. Yeh. Yielding behavior of glassy amorphous polymers. *Journal of Applied Physics* 42:4622–4630, **1971**.

[8] G.A. Adam, A. Cross, and R.N. Haward. The effect of thermal pretreatment on the mechanical properties of polycarbonate. *Journal of Materials Science* 10:1582–1590, **1975**.

[9] A. Cross, R.N. Haward, and N.J. Mills. Post yield phenomena in tensile tests on poly(vinyl chloride). *Polymer* 20:288–294, **1979**.

[10] H.G.H. van Melick, L.E. Govaert, and H.E.H. Meijer. Localisation phenomena in glassy polymers: influence of thermal and mechanical history. *Polymer* 44:3579–3591, **2003**.

[11] K.-H. Illers. Influence of thermal history upon physical properties of PVC. *Journal of Macromolecular Science Physics* B14:471–482, **1977**.

[12] E.B. Rabinovitch and J.W. Summers. The effect of physical aging on properties of rigid polyvinyl chloride. *Journal of Vinyl Technology* 14:126–130, **1992**.

[13] N. Yarahmadi, I. Jakubowicz, and T. Hjertberg. The effects of heat treatment and ageing on the mechanical properties of rigid PVC. *Polymer Degradation and Stability* 82:59–72, **2003**.

[14] E.J. Kramer. Microscopic and molecular fundamentals of crazing. *Advances in Polymer Science* 52/53:1–56, **1983**.

[15] M. Ishikawa, I. Narisawa, and H. Ogawa. Criterion for craze nucleation in polycarbonate. *Journal of Polymer Science: Polymer Physics Edition* 15:1791–1804, **1977**.

[16] M. Ishikawa and I. Narisawa. The effect of heat treatment on plane strain fracture of glassy polymers. *Journal of Materials Science* 18:2826–2834, **1983**.

[17] T.A.P. Engels. *Predicting performance of glassy polymers; Evolution of the thermodynamic state during processing and service life*. Ph.D. thesis, Eindhoven University of Technology, **2008**. URL `http://mate.tue.nl/mate/pdfs/9719.pdf`.

[18] H.G.H. van Melick, O.F.J.T. Bressers, J.M.J. den Toonder, L.E. Govaert, and H.E.H. Meijer. A micro-indentation method for probing the craze-initiation stress in glassy polymers. *Polymer* 44:2481–2491, **2003**.

[19] E.E. Lacatus and C.E. Rogers. The effect of fusion and physical aging on the toughness of poly(vinyl chloride). *Journal of Vinyl Technology* 8:183–188, **1986**.

[20] S. Zerafati and J. Black. Effect of physical aging on the impact retention and heat distortion temperature of vinyl products. *Journal of Vinyl & Additive Technology* 4:240–245, **1998**.

[21] L.-A. Fillot, P. Hajji, C. Gauthier, and K. Masenelli-Varlot. Thermomechanical history effects on rigid PVC microstructure and impact properties. *Journal of Applied Polymer Science* 104:2009–2017, **2007**.

[22] J.T. Ryan. Impact and yield properties of polycarbonate as a function of strain rate, molecular weight , thermal history, and temperature. *Polymer Engineering and Science* 18:264–267, **1978**.

[23] E.T.J. Klompen, T.A.P. Engels, L.E. Govaert, and H.E.H. Meijer. Modelling of the postyield response of glassy polymers: influence of thermomechanical history. *Macromolecules* 38:6997–7008, **2005**.

[24] J.A. Roetling. Yield stress behaviour of polymethylmethacrylate. *Polymer* 6:311–317, **1965**.

[25] J.A. Roetling. Yield stress behaviour of poly(ethyl methacrylate) in the glass transition region. *Polymer* 6:615–619, **1965**.

[26] J.A. Roetling. Yield stress behaviour of isotactic polypropylene. *Polymer* 7:303–306, **1966**.

[27] T. Ree and H. Eyring. Theory of non-Newtonian flow. I. Solid plastic system. *Journal of Applied Physics* 26:794–800, **1955**.

[28] H. Eyring. Viscosity, plasticity, and diffusion as examples of absolute reaction rates. *Journal of Chemical Physics* 4:283–291, **1936**.

[29] C. Bauwens-Crowet and J.C. Bauwens. Effect of thermal history on the tensile yield stress of polycarbonate in the β transition range. *Polymer* 24:921–924, **1983**.

[30] C. Ho Huu and T. Vu-Khanh. Effects of physical aging on yielding kinetics of polycarbonate. *Theoretical and Applied Fracture Mechanics* 40:75–83, **2003**.

[31] Y. Ishida. Dielectric relaxation of high polymers in the solid state. *Journal of Polymer Science. Part A-2, Polymer Physics* 8:1835–1861, **1969**.

[32] L.A. Utracki and J.A. Jukes. Dielectric studies of poly(vinyl chloride). *Journal of Vinyl Technology* 6:85–94, **1984**.

[33] E.R. Harrell, Jr. and R.P. Chartoff. The influence of crystallinity on the beta-transition in poly(vinyl chloride). *Polymer Engineering and Science* 14:362–365, **1974**.

[34] C. Tsitsilianis, M. Tsapatsis, and Ch. Economou. Effects of crystallinity on ageing phenomena in poly(vinyl chloride). *Polymer* 60:1861–1866, **1989**.

[35] T.G. Meijering. The evaluation of the ductility of thermoplastic pipes with an instrumented falling weight test. *Plastics and Rubber Processing and Applications* 5:165–171, **1985**.

[36] C. Bauwens-Crowet, J.C. Bauwens, and G. Homès. Tensile yield-stress behavior of glassy polymers. *Journal of Polymer Science. Part A-2, Polymer Physics* 7:735–742, **1969**.

[37] P.I. Vincent. The tough-brittle transition in thermoplastics. *Polymer* 1:425–444, **1960**.

[38] M. Skibo, J.A. Manson, R.W. Hertzberg, and E.A. Collins. Effects of molecular weight and plasticizer on fatigue crack propagation in PVC. *Journal of Macromolecular Science Physics* B14:525–543, **1977**.

[39] J.A. Juijn, J.H. Gisolf, and W.A. de Jong. Crystallinity in atactic poly (vinyl chloride). *Kolloid-Zeitschrift and Zeitschrift für Polymere* 251:456–473, **1973**.

[40] R.A. Chivers and D.R. Moore. Further developments in the interpretation of signals from instrumented falling weight impact (IFWI). *Measurement Science and Technology* 1:313–321, **1990**.

[41] M. Ishikawa, H. Ogawa, and I. Narisawa. Brittle fracture in glassy polymers. *Journal of Macromolecular Science Physics* B19:421–443, **1981**.

Probing the mechanical properties of uPVC pipes with micro-indentation[1]

Chapter 4

Abstract

The mechanical properties of glassy polymers are known to change in time as a result of physical ageing. During this process the resistance against plastic deformation increases, whereas the resistance against impact decreases, making the material more prone to brittle fracture. This embrittlement limits the lifetime of some polymer products, for example unplasticised poly(vinyl chloride) (uPVC) pipes used in gas distribution systems for which embrittlement can have serious consequences. In this chapter the use of micro-indentation measurements as a tool to determine the condition of uPVC pipe material is studied. The experimental data show a significant increase of the hardness after an ageing treatment. The behaviour is consistent with the known influence of physical ageing on the yield stress of the material. A linear relation between the yield stress and the hardness was observed. This linear relation is confirmed by numerical simulations, albeit not quantitatively. The current state of the material can be determined with the use of micro-indentation measurements, but an increase in the resolution is required before the technique can be put into practice as a tool to determine the residual lifetime of the uPVC gas pipes.

[1]Reproduced from: H.A. Visser, T.C. Bor, M. Wolters, L.C.A. van Breemen, L.E. Govaert, Probing the mechanical properties of uPVC pipes with micro-indentation, in preparation for *Polymer Testing*

4.1 Introduction

The hardness measurement is one of the oldest methods that was used to obtain information about the mechanical properties of a material. The simplest way to determine the hardness of a material is by scratching; a technique which is already in use since the introduction of the Mohs scale in 1822 [1]. In 1882 Hertz [2] published his famous theory on the elastic behaviour of a material subjected to force exerted by a sphere, focusing on the indentation instead of the scratch behaviour. Brinell introduced a hardness measurement based on an indentation test in 1900 [3]. In the course of the 20th century several other hardness tests were introduced, resulting in numerous definitions for the hardness. Typically, a body with a well-defined geometry is pressed into the surface of a material. The ratio between the maximum exerted force and the size of the contact area between the body and the material is a measure for the hardness of the material, i.e. the material's resistance against plastic deformation. The application of hardness tests is not limited to science and engineering; the same principle is used in every day life. A subtle pinch in a piece of fruit gives us, for example, enough information on whether it is ready for consumption. This is in line with a quote of Heinrich Hertz to his parents in 1882 [1]; "Hardness is a property of bodies of which scientific men have as clear, i.e. as vague, a conception as the man in the street."

The resistance against the plastic deformation is not constant during the service life of most glassy polymers. In time, small conformational changes occur within the polymer leading to a change in its mechanical properties such as its yield stress [4]. This process is generally referred to as physical ageing [5], which originates from the fact that glassy polymers are normally not in thermodynamic equilibrium, but display a continuous strive towards it. At elevated temperatures the mobility of the polymer chains is higher, as a result physical ageing occurs at shorter timescales. Besides increasing the yield stress, physical ageing also reduces the impact resistance of polymer glasses [6]. In some applications of polymer products embrittlement limits the lifetime of the product. The current research project focuses on the embrittlement of unplasticised poly(vinyl chloride) (uPVC) pipes, that have been extensively used in the Dutch gas distribution network. In the previous chapter it was shown that physical ageing can induce embrittlement of these pipes. An in-situ measurement from which it is possible to determine the current thermodynamic state of uPVC gas pipes would thus be highly beneficial for the network operators to help developing a replacement strategy. In the development of such a tool it should be taken into

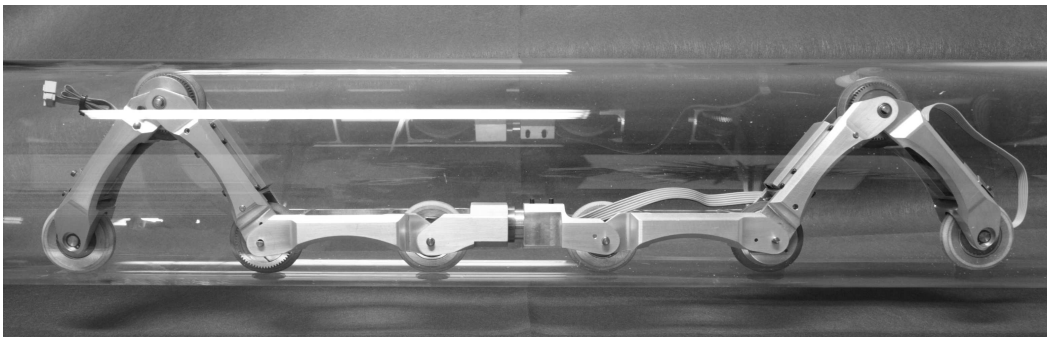

Figure 4.1 *A photograph of the PIRATE autonomous inspection robot in a transparent pipe with a diameter of 63 mm [7] (reproduced with permission).*

account that the variation in the quality of the individual pipes in the network is too large for just a small number of random checks. As a consequence, the condition of a large number of pipes, if not all, should be determined. This rules out destructive testing as it would be cheaper to replace the pipes in the first place. Besides the type of measurement, it is important where the measurement has to be carried out. Measurements on the outer surface of a pipe require excavation activities, which make these measurements nearly as costly as replacement of the pipe. Recently, a prototype of an autonomous inspection robot for a gas distribution network (the PIRATE, shown in Figure 4.1) was presented [7]. The main advantage of such a robot is that measurements can be carried out from the inside of the pipe, circumventing digging activities. Consequently, the measurement device should be small enough to fit on such robots and through the pipe network.

In theory, micro-scale hardness measurements can meet both demands: the size of the indents are small, smaller than for example the scratches imposed on most pipes during installation, which means that these hardness measurements can be considered non-destructive on a macroscopic scale. Hardness meters are relatively compact devices, making future implementation of a hardness measurement on pipe inspection robots possible. Successful application of hardness measurements requires a function between the thermodynamic state and the measured hardness of the polymer. In Chapter 2 a relation between the yield stress and the thermodynamic state was found and in Chapter 3 the influence of a change in thermodynamic state and the ductile to-brittle temperature ($T_{d\rightarrow b}$) was quantified.

The relation between the hardness and the yield stress has been widely acknowledged for metals [8]. Generally the (Vickers) hardness is about three

times the yield stress, but for polymers this relation is less obvious [9–11]. Most hardness measurements determine the contact area during loading from the size of the indent after testing. Because of the visco-elastic mechanical behaviour of polymers, the size of an indent after a measurement is time-dependent, which means that the measurement is influenced by the speed of the operator who carries out the measurement [10]. Consequently, relating the post-mortem size of the indent to the actual size of the contact area between indenter and polymer during the measurement is non-trivial. Therefore, instrumented hardness measurements, referred to as indentation measurements throughout this chapter, where both the force (F) and displacement (h) of the indenter are logged, are more useful in deriving intrinsic mechanical properties of a polymer [12]. A widely employed model to calculate hardness (and the Young's modulus) from a full indentation curve was proposed by Oliver and Pharr [13, 14]. The assumptions in their model are based on the mechanical properties of metals, which makes the model less appropriate for measurements on polymers as some of these assumptions do not comply with polymer specific properties (such as visco-elasticity and, in some cases, a significant contribution of strain hardening).

Another way to retrieve intrinsic material properties from indentation experiments is the use of numerical simulations of the deformation behaviour underneath the indenter tip, employing a constitutive model that describes the intrinsic deformation response of glassy polymers. This approach has gained some interest in recent years [15–17]. A correct description of the intrinsic deformation behaviour (including the influence of physical ageing) of the polymer proves to be the key for quantitative predictions of the indentation behaviour of glassy polymers [18]. In the present study both the Oliver and Pharr method and numerical simulations were employed to confirm whether micro-indentation can indeed be used to probe the thermodynamic state and indirectly the impact behaviour of uPVC pipes.

The chapter starts with an experimental part (Section 4.2 and 4.3) where the influence of physical ageing on the response of uPVC during micro-indentation measurements is presented. Moreover, micro-indentation measurements were carried out on specimens that were subsequently subjected to a tensile test. A relation between the indentation behaviour and the tensile yield stress was found for different thermodynamic states. The results of numerical simulations which confirm the experimentally observed behaviour, are presented in Section 4.4. The chapter concludes with an example in which the residual lifetime of a uPVC pipe is calculated from an indentation test and it is evaluated how accurate the lifetime can be determined with the presented procedure.

4.2 Experimental

4.2.1 Material and specimen preparation

All specimens were taken from a uPVC pipe with a diameter of 160 mm and a wall thickness of approximately 4.1 mm that had been in service for more than 30 years. All indentation experiments were performed on pieces of flattened pipe material. This flattening was realised by heating a piece of pipe up to 100 °C (about 20 °C above its glass transition temperature, T_g), applying a small compressive stress and subsequently cooling the material to room temperature within 5 minutes between metal plates.[2] The indentation experiments were performed on the side that was originally the inner surface of the pipe. Some of the indentation experiments were performed on tensile specimens. The use of tensile specimens makes it possible to combine the results of indentation test data and tensile test data for a single specimen. The tensile specimens were milled from the flattened pieces of the pipe. The gauge section of the specimens is approximately $30\times5\times4.1$ mm^3 and is parallel to the extrusion direction of the original pipe. The annealing treatments were carried out in a convection oven at 40 °C or 60 °C.

Compression tests were performed to characterise the intrinsic behaviour of uPVC at several strain rates. The results are used as input for the constitutive model employed in the numerical simulations. The compression tests were carried out on cylindrical specimens of approximately $\varnothing4\times4$ mm with the axial direction parallel to the extrusion direction. These specimens were manufactured on a lathe from small pieces of pipe.

4.2.2 Test method

All indentation measurements were performed at 21 °C on a CSM Micro-Indentation Tester equipped with either a diamond Berkovich indenter or a diamond spherical tip indenter with a radius of 196 µm. Nine indents were made on each specimen in a square pattern with 1.5 mm inter-distance. For this inter-distance the influence of neighbouring indents was considered to be negligible. During each indent the spherical tip is lowered until a contact force of 20 mN is reached, after which a force controlled signal is applied. The indentation force is

[2] Cooling from the outside means that the surface of the plates is cooled faster. As a consequence the surface of the polymer is "younger" (further away from thermodynamic equilibrium) than the interior of the plate. This difference disappears in time as physical ageing occurs on a logarithmic timescale.

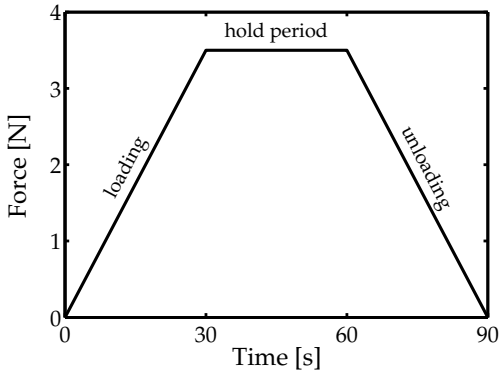

Figure 4.2 *Loading protocol for the indentation experiments.*

then linearly increased to 3.5 N in 30 s (loading), subsequently kept at this force for 30 s (hold period) and linearly decreased to zero in 30 s (unloading). This loading and unloading protocol is shown in Figure 4.2. The displacement of the indenter is recorded during the loading protocol.

All uniaxial tensile experiments were performed on an MTS Elastomer Testing System 810 equipped with a 25 kN force cell. The tensile bars were subjected to an *engineering* strain rate of 10^{-3} s^{-1} at a temperature of 23 °C. The *engineering* yield stress was calculated using the average of the cross-sectional surface areas as measured at three locations in the gauge section.

The compression tests were conducted on an MTS 815 Elastomer Testing Machine equipped with a temperature controlled chamber. Bulging effects were reduced by applying a teflon spray on the surface of the compression plates prior to testing. No bulging was observed up to a true strain of 0.7. The measurements were conducted at a constant true strain rate of 10^{-4} s^{-1}, 10^{-3} s^{-1} or 10^{-2} s^{-1}, all at 25 °C.

4.3 Experimental results

A typical set of force versus displacement (depth of indentation) signals resulting from nine indents on one specimen are shown in Figure 4.3. During loading, the displacement rate of the indenter gradually decreases, as the contact area of the spherical indenter with the flat surface of the specimen gradually increases. After the maximum force is reached, the force is kept constant for an equal amount of time and the displacement of the indenter increases as a result of continued plastic deformation (a creep response). The visco-elastic response of the uPVC

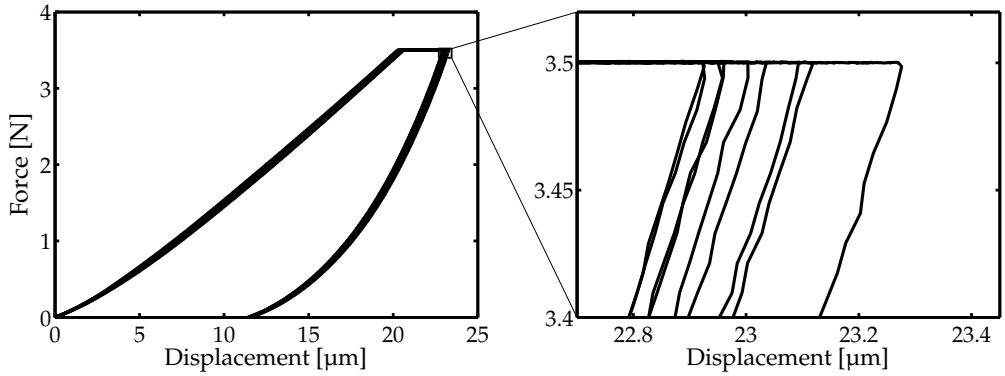

Figure 4.3 *The applied force versus the measured displacement of the indenter for a set of nine indents in an as-manufactured tensile specimen.* ***Left:*** *the full indentation curves.* ***Right:*** *a detail of the indentation curves.*

specimen causes a partial recovery of the indent during unloading, resulting in a significant decrease in depth of the indent (up to 10 μm in this case).

In general, little differences between the individual indentation curves were observed. Larger deviations were found for indents in the vicinity of a weld-line in the uPVC specimen. These weld-lines are a heritage of the extrusion process; during extrusion the polymer flows around the "legs" that connect the mandrel to the extrusion die. The groove in the core of a weld-line can be in the order of 3 μm deep, resulting in a deeper indent for the same force signal. Indenting at surface defects or foreign particles introduced during the flattening procedure of the pipe into a plate also causes significant deviations of the indentation curve. In the present study the indentation curves that differ significantly from the bulk of the indents have been disregarded for the determination of the hardness.

4.3.1 Influence of physical ageing

In Chapters 1 and 2 it was already shown that physical ageing results in an increase in resistance against plastic deformation. Consequently, the yield stress increases for a certain applied strain rate. Moreover, the plastic strain rate, that follows from a certain applied stress, is lower for an aged specimen, resulting in an increase of failure times. During indentation experiments a force is applied on the polymer, leading to a certain stress state and thus a certain plastic deformation rate. Upon ageing this plastic deformation rate can be expected to decrease, leading to lower displacements of the indenter for an identical applied force signal, as observed in [17].

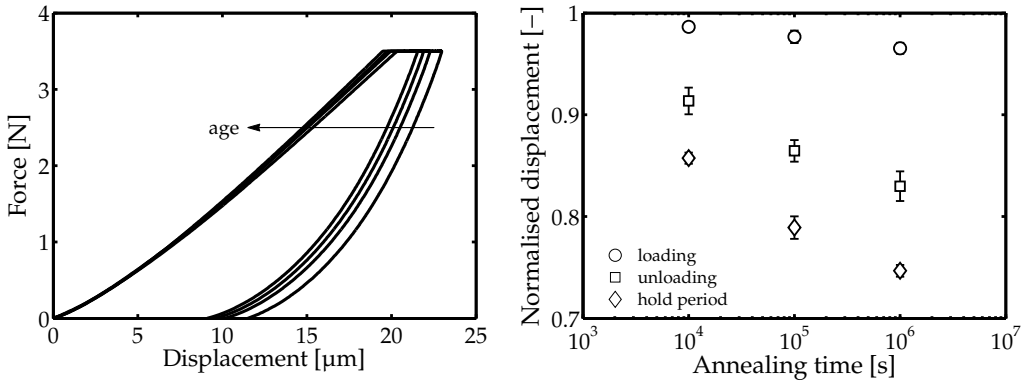

Figure 4.4 *The influence of physical ageing on the indentation behaviour.* ***Left:*** *applied force versus the measured displacement of a typical indent in four tensile bars that differ in thermodynamic state i.e. degree of ageing.* ***Right:*** *the corresponding normalised displacement versus the annealing time at 60 °C. The normalised displacement is calculated by dividing the displacement into the tested specimen by the displacement into the as-manufactured specimen. This is done separately for each segment of the applied force signal.*

Several indentation experiments were carried out on specimens that received different annealing treatments to verify whether the influence of physical ageing as discussed above, manifests itself in the experimental observations. The evolution of the force versus the displacement behaviour upon ageing, as measured with the use of a spherical indenter, is shown in Figure 4.4 (left). In general, the displacement of the indenter is lower after ageing. This difference is most pronounced after the hold period. The influence of physical ageing on each segment of the indentation curve is quantified in Figure 4.4 (right). The figure shows the amount of displacement during each segment of the curve divided by the amount of displacement in the as-manufactured specimen for the corresponding segment. These normalised displacements are plotted as a function of the annealing time at 60 °C. A clear decreasing trend is observed for the normalised displacement of all segments as the annealing time increases. This observation agrees with an increase in resistance against plastic deformation for aged material. The displacement of the indenter during the hold period is most sensitive for ageing. This is a logical consequence from the fact that the deformation during the hold period is mainly plastic, whereas the deformation during loading is partly elastic (which is less influenced by physical ageing).

The goal of this study is to relate the change in indentation behaviour to the change in intrinsic mechanical properties such as the yield stress of uPVC. Therefore, the influence of physical ageing on the indentation behaviour should be quantified. The normalised displacements in Figure 4.4 (right) can, for example, be used as a measure for the influence of physical ageing. Another

possibility is to use the hardness that can be calculated from the indentation curve. Here, the hardness as follows from the analysis proposed by Oliver and Pharr [13, 14], is chosen as a measure for the influence of physical ageing on the indentation response. The calculation procedure is outlined in Appendix 4.A. The hardness is mostly influenced by the displacement after the hold period, which was observed to be most sensitive to physical ageing. It should be emphasised that like the yield stress, the hardness of a polymer is more strongly influenced by the strain rate and temperature as compared to most metals. The experimentally obtained hardness will thus depend on the experimental conditions. Furthermore, the analysis of Oliver and Pharr assumes the material to sink in around the indenter, whereas it is known that polymeric materials can show a reduced amount of sink in or even a pile-up of the material during indentation [19]. As a result, the calculated (projected) contact area is smaller than in reality, causing a higher value of the calculated hardness (via Equation (4A.1)). For the current analysis these issues are not relevant, as the absolute hardness value is not of importance. Only the relative measure is of importance to characterise the evolution of hardness with ageing, and to relate the hardness to the yield stress.

The hardness as calculated from the indentation curves measured with a Berkovich indenter is shown in Figure 4.5 (left). The markers represent the average hardness of the relevant (out of the nine measured) indents, and the error bars indicate the standard deviation. Clearly, the hardness increases significantly with annealing time. Moreover, at higher temperatures the increase in hardness becomes apparent at shorter annealing times. In Chapter 2 similar behaviour

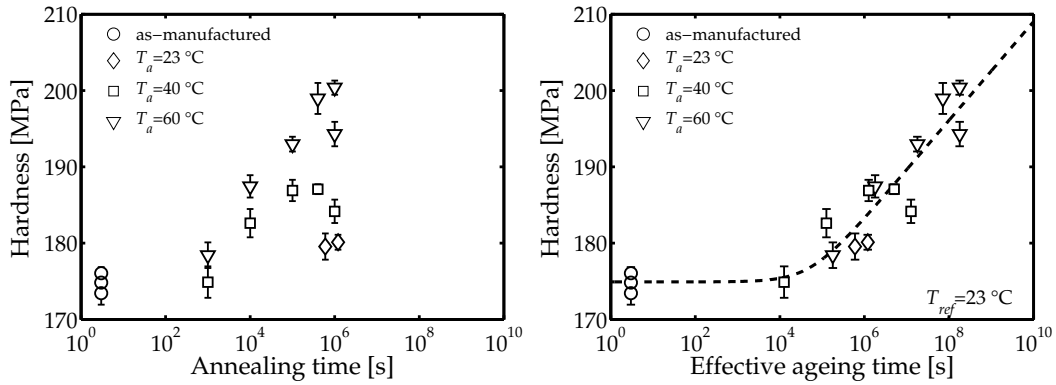

Figure 4.5 *The influence of physical ageing on the hardness of uPVC as measured with a Berkovich indenter.* ***Left:*** *the hardness versus the annealing time for three temperatures.* ***Right:*** *the hardness versus the effective ageing time (at T_{ref}=23 °C) as calculated with Equation (4.1). The dashed line is drawn as a guide to the eye.*

was observed for the tensile yield stress of the same material as a function of the annealing temperature. There, the yield stress data could be shifted towards one mastercurve by applying an Arrhenius-type time-temperature superposition:

$$t_{eff} = t_a \cdot \exp\left(\frac{\Delta U_a}{R} \cdot \left(\frac{1}{T_{ref}} - \frac{1}{T_a}\right)\right) , \tag{4.1}$$

where t_{eff} denotes the effective time, t_a the annealing time, ΔU_a the activation energy for temperature induced physical ageing, R the universal gas constant, T_{ref} a reference temperature at which the mastercurve is plotted and T_a the annealing temperature. An activation energy of 115 kJ/mol was found for the yield stress evolution at a reference temperature of 23 °C. Applying the same activation energy to the hardness data results in a reasonable fit to a mastercurve as shown in Figure 4.5 (right). The dashed line is a guide to the eye with a similar shape as the mastercurve of the yield stress data. Taking into consideration that the hardness measurements are carried out on an unprepared inner surface of a used gas pipe, the hardness evolution resembles the yield stress evolution remarkably well. This opens the possibility to relate a micro-indentation measurement directly with the yield stress of the material.

In the next section micro-indentation measurements are presented that were carried out on tensile specimens, which were subsequently used for a tensile test to determine the yield stress of the material. The results are compared with the behaviour predicted by numerical simulations. Simulation of the deformation underneath a Berkovich indenter requires a large number of elements, because of the singularity at the (sharp) tip and the presence of only one symmetric plane in the indenter shape a 3D mesh is required. Therefore, a spherical indenter is used instead for this series of measurements, which does not impose singularities around the tip during simulations and can be simulated in an axi-symmetrical fashion, significantly reducing computational times.

4.3.2 Relating the hardness to the yield stress

The experimental data presented in Figure 4.5 suggests that the indentation behaviour can be directly related to the yield stress. Additional indentation experiments with the use of a spherical indenter show a similar response. The hardness found with the spherical indenter is significantly lower than the values found with a Berkovich tip. This difference is not caused by physical ageing as the range of thermodynamic states of the tested specimens is equal. The sharper tip of the Berkovich indenter imposes larger strain rates in the material at the

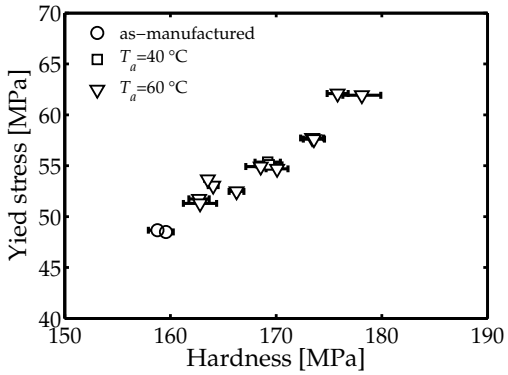

Figure 4.6 *The tensile yield stress versus the hardness as calculated from indentation experiments on tensile specimens with the use of a spherical indenter.*

vicinity of the apex, when compared to the spherical tip. This results in a (locally) increased resistance against deformation explaining the higher hardness.

The tensile specimens used for indentation experiments received an annealing treatment prior to testing, resulting in specimens that differ in thermodynamic state. The resulting relation between the hardness and the tensile yield stress is shown in Figure 4.6. The standard deviation of the calculated hardness for all (relevant) measurements on one specimen is indicated with a horizonal error bar. The results show that the increase in yield stress, resulting from physical ageing, is accompanied by a comparable increase in hardness; the hardness and the tensile yield stress seem to be linearly related within the range of thermodynamic states investigated. Such a linear relation is of importance for the practical application of micro-indentation measurements as a probe for the impact behaviour of uPVC pipes.

It was shown by Van Breemen *et al.* [17] that it is possible to predict indentation experiments quantitatively by numerical simulations. They successfully predicted the influence of physical ageing on flat-tip micro-indentation experiments on polycarbonate and poly(methyl methacrylate). The same model was employed here to support the existence of the experimentally observed relation between the hardness and the yield stress of uPVC.

4.4 Numerical simulations using the EGP-model

In this section numerical simulations on the deformation of uPVC underneath a spherical indenter are described. These simulations have been carried out to verify whether the experimentally observed indentation behaviour complies

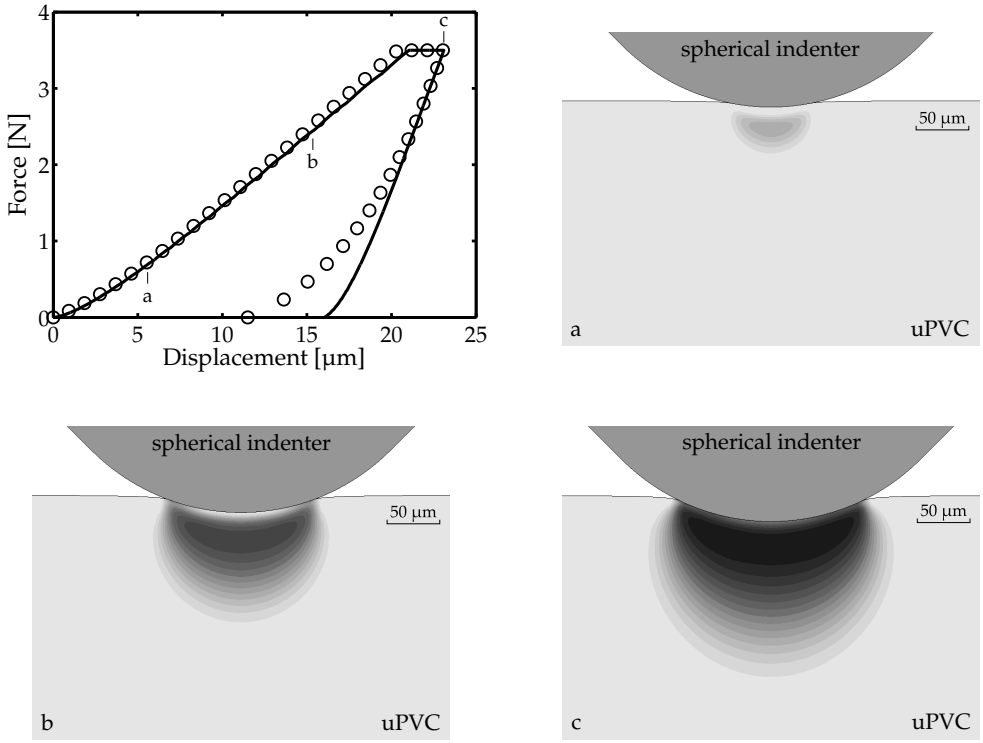

Figure 4.7 *The development of the plastic zone at three stages in the indentation measurement. The images are cross-sections through the centre of the indenter. The grey scales indicate the amount of plastic deformation.* ***Topleft:*** *the force versus displacement curve as calculated using a numerical simulation with the EGP-model (solid line), compared with the experimentally obtained data (markers).*

with the change intrinsic deformation behaviour of the material resulting from physical ageing. The indentation measurements were simulated in MSC.Marc using an axi-symmetric finite element mesh consisting of 3600 linear quad 4 elements (full integration). The intrinsic behaviour is constitutively modelled with the Eindhoven Glassy Polymer (EGP) model [18, 20–22]. As all experiments were carried out at 21 °C the influence of the β-relaxation process on the deformation behaviour becomes significant for strain rates higher than 0.1 s^{-1} (see Chapter 3). Such high strain rates were not expected and only the influence of the α-relaxation process on the intrinsic deformation behaviour was taken into account. A total number of 10 modes was used to accurately describe the nonlinear viscoelastic-plastic behaviour of uPVC. The relaxation spectrum and the values of all parameters used are presented in Appendix 4.B.

The numerically obtained indentation curve for an as-manufactured specimen is shown in Figure 4.7 (topleft) as a solid line. This curve is in excellent quantitative agreement with the experimentally obtained indentation curve (markers) for the loading and hold period. Only the amount of (visco-)elastic recovery visible during the last part of the unloading period is significantly underestimated. This difference might originate from the differences between measurement and simulation: in the simulation the surface is perfectly flat and friction between the indenter and the polymer surface is neglected. These aspects are, however, known to have only a small effect on the force displacement curve, and cannot explain the differences in the unloading curve as observed here. Further research is required to find the physical background of the difference. For the present study only the simulations up to the first part of unloading are of interest, as these parts of the indentation curves are most important in the determination of the hardness of the material.

The text labels in Figure 4.7 (topleft) indicate the force and displacement of the indenter corresponding to the other images in Figure 4.7. These images show a cross-section of the indenter and the loaded specimen and illustrate in which way the plastic zone develops within the specimen during an indentation experiment. The grey scale qualitatively indicates the amount of plastic deformation the material has undergone; the darker areas correspond to a higher degree of plastic deformation. The image at *a* clearly shows that the plastic zone does not initiate at the surface of the material, but somewhat underneath. The zone develops to the side and downwards on continuation of the indentation measurement. After the hold period (at *c*) the plastic zone reaches its maximum size of about 230×170 μm^2 and the zone has developed towards the specimen surface.

The evolution of the simulated normalised displacement of each of the segments of the indentation curve is shown as solid lines in Figure 4.8 (left). Although the predicted evolution of the normalised displacements does not agree quantitatively with the experimental data, the predicted slopes are in reasonable agreement with the experimentally observed ones. The simulated evolution of the hardness is shown as a solid line in Figure 4.8 (right) on top of the experimental data. The hardness of the numerically obtained indentation curves agree reasonably well with the experimentally obtained hardness. Both the tensile yield stress and the hardness were extracted from numerical simulation for uPVC with different thermodynamic states. The linear relation that was found experimentally is confirmed by the numerical simulations. This supports the possibility to use micro-indentation experiments as a probe for the yield stress and thus the thermodynamic state of the uPVC gas pipe material. The slope of

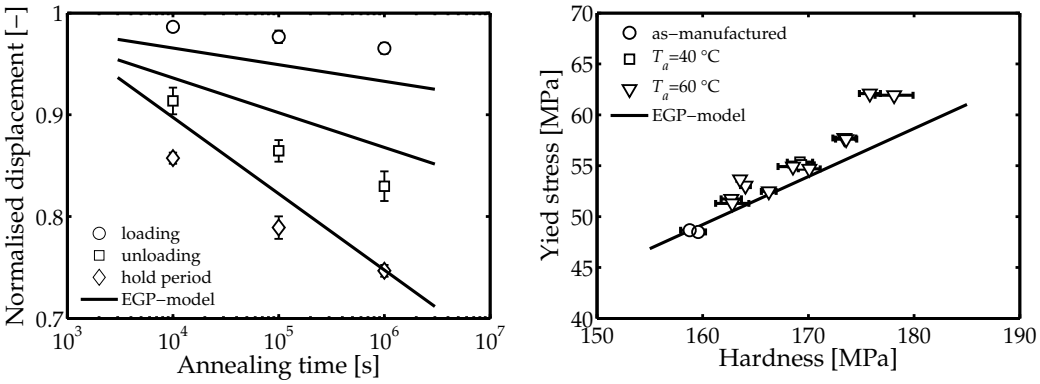

Figure 4.8 *Results of the EGP-model simulation and the experimentally obtained data.* ***Left:*** *reproduction of Figure 4.3 including the indentation curve for an as-manufactured specimen that follows from a numerical simulation with the EGP-model (solid line). Right: reproduction of Figure 4.6 including the relation between the yield stress and the hardness that follows from numerical simulations with the EGP-model (solid line).*

the yield stress versus the hardness for the experimental data is, however, slightly higher than that of the numerically obtained data. The physical background of this difference yet unknown, but might well be related to the difference between the numerical and experimental observations of the unloading curve. In the next section this linear relation between the hardness and yield stress is employed to determine the residual lifetime of uPVC pipes from micro-indentation tests.

4.5 From indentation to residual lifetime

In Chapter 3 it was shown in which way the ductile-to-brittle transition temperature ($T_{d\rightarrow b}$) is related to the present value of the yield stress of a uPVC pipe. The relation between the yield stress and hardness opens the possibility to calculate the residual lifetime of a uPVC pipe from an indentation measurement. The accuracy of this procedure is of importance for the practical application and is evaluated using the following situation.

The precision is determined for the case that a uPVC pipe has a hardness of 170 MPa and the network operator decided to replace the pipe when the $T_{d\rightarrow b}$ reaches -12.5 °C (a purely hypothetical value). The measured hardness value is a mean value from 9 indents. The average of the standard deviation of the hardness values (as measured with the spherical indenter) of all specimens presented in this study was about 1 MPa. This value was taken as the standard deviation of the hardness value here, which is used to calculate the corresponding yield stress

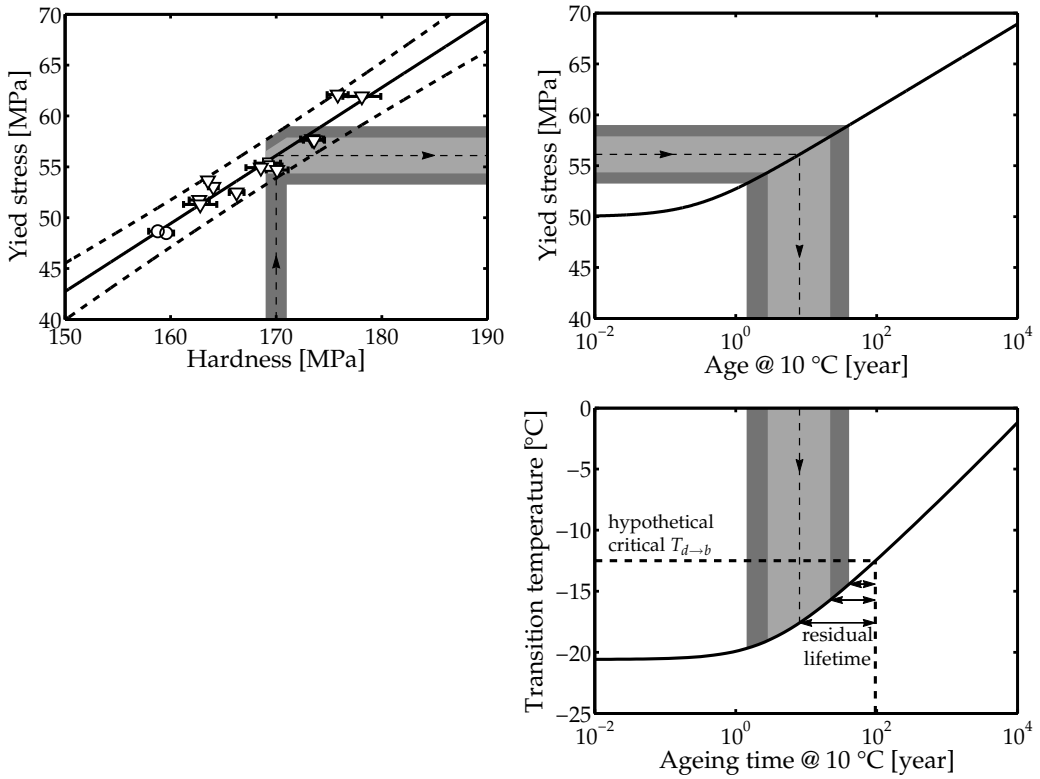

Figure 4.9 *Procedure to obtain the residual lifetime from a hardness measurement based on an assumed hardness of 170 MPa and $T_{d\rightarrow b}$ of -12.5 °C (see text for details). The light grey areas represent the value within the 50% confidence limit and the dark grey areas values within the 95% confidence limit.*

range as shown in Figure 4.9 (topleft). The solid line represents the linear relation between the hardness and the yield stress that corresponds to the best fit to the experimental data. The dashed lines are the 95% confidence limits that were used to calculate the range of values the yield stress is expected to fall within. This range is shown as a dark grey area. The lighter grey area corresponds to the 50% confidence interval. The ranges of the yield stress are translated towards ranges in the ageing time (at T_{ref}=23 °C) with the use of the relation of the yield stress evolution presented in Chapter 2 as shown in Figure 4.9 (topright).[3] The resulting range of the ages can then be compared to the age that corresponds to $T_{d\rightarrow b}$ =-12.5 °C using the evolution of $T_{d\rightarrow b}$ presented in Chapter 3 and shown in Figure 4.9 (bottomright). Depending on a risk assessment, the operator can choose to calculate the residual lifetime of the tested material from the age

[3]The scatter of both the yield stress and $T_{d\rightarrow b}$ evolution is not taken into account here as the focus is on the hardness versus yield stress relation.

corresponding to the mean yield stress, the upper 50% confidence limit yield stress or the upper 95% confidence limit stress.

Both the hardness and the yield stress can be measured with a high accuracy; the hardness was measured with a maximum standard deviation of 1.5 MPa for a hardness value in the range from 150 MPa up to 180 MPa and the yield stress was measured with a standard deviation of about 0.5 MPa in the range from about 45 MPa to 65 MPa. Nonetheless, the hardness versus the yield stress data show significant scatter. The large yield stress range for the 95% confidence limit in Figure 4.9 (topleft) can be mainly attributed to this scatter. The origin of the scatter might be found in local differences on the polymer surface. Whereas the yield stress measurements are related to the bulk behaviour of the polymer, micro-indentation is a local measurement, and thus susceptible for local variations.

It is recommended to perform a large number of additional micro-indentation and tensile measurements to confirm whether the scatter indeed has a statistical background. An increased amount of data might also narrow the confidence interval, increasing the resolution of the determined residual lifetime. A further increase in the resolution might be possible by optimisation of the measurement protocol. For example, the use of a larger indenter or an increased maximum load could decrease the influence of local variations to such an extent that the scatter on the measured relation between hardness and yield stress is reduced.

4.6 Conclusions

In this chapter a study on the use of micro-indentation measurements as a means to determine the condition of uPVC pipe material was described. First the influence of physical ageing on the indentation response was characterised. The evolution of the normalised displacement of each of the indentation segments with ageing corresponds with an increase of the resistance against plastic deformation of the material. The evolution of hardness at different annealing temperatures proved to be similar to that of the tensile yield stress. A mastercurve has been constructed with the use of the same time-temperature superposition relation, employing the same activation energy. This observation suggests a direct relation between the tensile yield stress and the hardness, which is confirmed with indentation data on tensile bars that were also used for tensile testing. The experimentally observed linear relation between the hardness and the yield stress is in qualitative agreement with the relation obtained using numerical simulation of the indentation experiments using the EGP-model.

These observations indicate that micro-indentation can be used for the assessment of the current (thermodynamic) state of uPVC pipe material. The resolution of the procedure is, however, fairly low. Improvements in the resolution would increase the potential of this condition measurement procedure for practical applications.

References

[1] H. O'Neill. *Hardness measurement of metals and alloys*. Chapman and Hall London, **1967**.

[2] H. Hertz. Über die berührung fester elastischer körper. *Journal für die reine und angewandte Mathematik* 92:156–171, **1882**.

[3] A. Wahlberg. Brinell's method of determining hardness and other properties of iron and steel. *Journal of the Iron and Steel Institute* 59:243–298, **1901**.

[4] J.H. Golden, B.L. Hammant, and E.A. Hazell. The effect of thermal pretreatment on the strength of polycarbonate. *Journal of Applied Polymer Science* 11:1571–1579, **1967**.

[5] J.M. Hutchinson. Physical aging of polymers. *Progress in Polymer Science* 20:703–760, **1995**.

[6] D.G. Legrand. Crazing, yielding, and fracture of polymers. I. Ductile brittle transition in polycarbonate. *Journal of Applied Polymer Science* 13:2129–2147, **1969**.

[7] K. Pulles, E. Dertien, H.J. van de Pol, R. Nispeling, and S. Stramigioli. Pirate, the development of an autonomous gas distribution system inspection robot. In: *Proceedings of International Gas Union Research Conference*. Paris, **2008**.

[8] D. Tabor. *The hardness of metals*. Clarendon Press Oxford, **1951**.

[9] S.B. Ainbinder and M.G. Laka. Hardness of polymers. *Mekhanika Polimerov* 2:337–349, **1966**.

[10] P.J. Phillips, R. Ramakrishnan, and P.L.S. Oxlade. Hardness testing of plastics. *Polymer Engineering and Science* 18:869–874, **1978**.

[11] F.J. Baltá Calleja, D.S. Sanditov, and V.P. Privalko. Review: the microhardness of non-crystalline materials. *Journal of Materials Science* 37:4507–4516, **2002**.

[12] B. Darlix, B. Monasse, and P. Montmitonnet. Hardness measurement as a means of determining simultaneously the elastic modulus and yield stress of polymers as a function of temperature. *Polymer Testing* 6:107–120, **1986**.

[13] W.C. Oliver and G.M. Pharr. An improved technique for determining hardness and elastic modulus using load and displacement sensing indentation experiments. *Journal of Materials Research* 7:1564–1580, **1992**.

[14] W.C. Oliver and G.M. Pharr. Measurement of hardness and elastic modulus by instrumented indentation: advances in understanding and refinements to methodology. *Journal of Materials Research* 19:3–20, **2004**.

[15] H.G.H. van Melick, O.F.J.T. Bressers, J.M.J. den Toonder, L.E. Govaert, and H.E.H. Meijer. A micro-indentation method for probing the craze-initiation stress in glassy polymers. *Polymer* 44:2481–2491, **2003**.

[16] L. Anand and N.M. Ames. On modeling the micro-indentation response of an amorphous polymer. *International Journal of Plasticity* 22:1123–1170, **2006**.

[17] L.C.A. van Breemen, T.A.P. Engels, C.G.N. Pelletier, L.E. Govaert, and J.M.J. den Toonder. Numerical simulation of flat-tip micro-indentation of glassy polymers: Influence of loading speed and thermodynamic state. *Philosophical Magazine* 89:677–696, **2009**.

[18] L.C.A. van Breemen. *Contact mechanics in glassy polymers*. Ph.D. thesis, Eindhoven University of Technology, **2009**. URL `http://mate.tue.nl/mate/pdfs/10677.pdf`.

[19] C.G.N. Pelletier, J.M.J. den Toonder, L.E. Govaert, N. Hakiri, and M. Sakai. Quantitative assessment and prediction of contact area development during spherical tip indentation of glassy polymers. *Philosophical Magazine* 8:1291–1306, **2008**.

[20] T.A. Tervoort, R.J.M. Smit, W.A.M. Brekelmans, and L.E. Govaert. A constitutive equation for the elasto-viscoplastic deformation of glassy polymers. *Mechanics of Time-Dependent Materials* 1:269–291, **1997**.

[21] L.E. Govaert, P.H.M. Timmermans, and W.A.M. Brekelmans. The influence of intrinsic strain softening on strain localization in polycarbonate: Modeling and experimental validation. *Journal of Engineering Materials and Technology* 122:177–185, **2000**.

[22] E.T.J. Klompen, T.A.P. Engels, L.E. Govaert, and H.E.H. Meijer. Modelling of the postyield response of glassy polymers: influence of thermomechanical history. *Macromolecules* 38:6997–7008, **2005**.

[23] I.N. Sneddon. The relation between load and penetration in the axisymmetric Boussinesq problem for a punch of arbitrary profile. *International Journal of Engineering Science* 3:47–57, **1965**.

[24] T.A. Tervoort and L.E. Govaert. Strain-hardening behavior of polycarbonate in the glassy state. *Journal of Rheology* 44:1263–1277, **2000**.

[25] H. Eyring. Viscosity, plasticity, and diffusion as examples of absolute reaction rates. *Journal of Chemical Physics* 4:283–291, **1936**.

[26] R.A. Duckett, S. Rabinowitz, and I.M. Ward. The strain-rate, temperature and pressure dependence of yield of isotropic poly(methylmethacrylate) and poly(ethylene terephthalate). *Journal of Materials Science* 5:909–915, **1970**.

[27] R.A. Duckett, B.C. Goswami, L. Stewart, A. Smith, I.M. Ward, and A.M. Zihlif. The yielding and crazing behaviour of polycarbonate in torsion under superposed hydrostatic pressure. *Britisch Polymer Journal* 10:11–16, **1978**.

[28] S. Rabinowitz, I.M. Ward, and J.S.C. Parry. The effect of hydrostatic pressure on the shear yield behaviour of polymers. *Journal of Materials Science* 5:29–39, **1970**.

4.A Appendix: Calculation of the hardness

The hardness is determined from the indentation curve with the use of the procedure proposed by Oliver and Pharr [13, 14]. A typical force versus depth of indenter curve is shown in Figure 4A.1. The indentation hardness (H_{IT}) of the material follows from:

$$H_{IT} = \frac{F_{max}}{A_p}\,, \tag{4A.1}$$

where F_{max} is the force at the moment the maximum indentation depth (h_{max}) is reached (see Figure 4A.1). The projected area of contact (A_p) follows from a geometrical function and the contact depth (h_c):

$$\begin{aligned} A_p &= 2\pi R h_c - \pi h_c^2\,, && \text{(spherical indenter)} \\ A_p &= 24.5 h_c^2\,, && \text{(Berkovich indenter)} \end{aligned} \tag{4A.2}$$

with R the radius of the spherical tip of the indenter. Oliver and Pharr proposed the following procedure to calculate the contact depth (h_c). The contact stiffness (S) is determined from the best fit of the following power law function to the first part of the unloading curve ($0.4F_{max} \leq F \leq 0.98F_{max}$):

$$F = F_{max}\left(\frac{h - h_p}{h_{max} - h_p}\right)^m\,. \tag{4A.3}$$

The permanent depth (h_p) is calculated from a linear fit of the unloading curve at $0 \leq F \leq 0.15F_{max}$. The depth at $0.005F_{max}$ that follows from this linear fit is taken

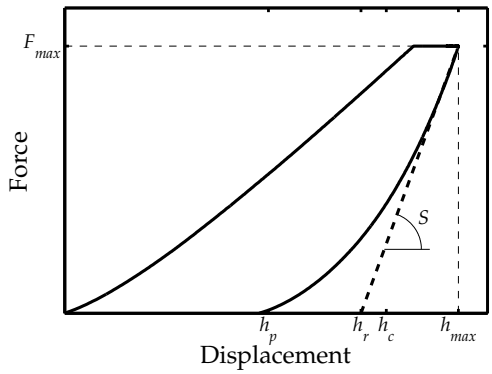

Figure 4A.1 *A typical force versus displacement signal for an indent including the definitions of several parameters used in the Oliver and Pharr method.*

as the permanent depth. The value for m follows from a fitting routine. The value for S is the derivative of Equation (4A.3) at h=h_{max}:

$$S = \frac{mF_{max}}{h_{max} - h_p}. \tag{4A.4}$$

The vertical distance along which contact is made, or contact depth (h_c), follows from Sneddon's [23] expression for the shape of the material surface around the indenter:

$$h_c = h_{max} - \epsilon_{ind} \cdot \frac{F_{max}}{S}, \tag{4A.5}$$

with ϵ_{ind} an indenter geometry dependent constant. In this case for both indenters a value of 0.74 is used. The calculated contact depth (h_c) can be used to calculate the projected contact area (A_p) with Equation (4A.2) and subsequently the hardness with Equation (4A.1).

4.B Appendix: The Eindhoven Glassy Polymer model and the parameters for uPVC

The experimental observations with the micro-indenter and the relation between the yield stress and the calculated hardness is validated with the use of numerical calculations. The Eindhoven Glassy Polymer model [18, 20–22] is employed to describe the intrinsic behaviour of uPVC. The model is reproduced in short here from [18]. In the EGP-model the total stress is split into a driving stress σ_s and a hardening stress σ_r:

$$\sigma = \sigma_s + \sigma_r, \tag{4B.1}$$

where σ_r is modelled employing a neo-Hookean relation [21, 24]:

$$\sigma_r = G_r \tilde{\mathbf{B}}^d. \tag{4B.2}$$

Here G_r is the strain-hardening modulus and $\tilde{\mathbf{B}}^d$ is the deviatoric part of the isochoric left Cauchy-Green strain tensor. The driving stress itself is split into a hydrostatic and a deviatoric stress:

$$\sigma_s = \sigma_s^h + \sigma_s^d\,, \quad \text{with} \quad \sigma_s^h = \kappa(J-1)\mathbf{I} \quad \text{and} \quad \sigma_s^d = \sum_{i=1}^{n} G_i \tilde{\mathbf{B}}_{e,i}^d. \tag{4B.3}$$

Where κ is the bulk modulus, J the volume change ratio, $\mathbf{I}$ the unity tensor, G_i the modal shear modulus and $\tilde{\mathbf{B}}_{e,i}^d$ the modal deviatoric part of the elastic isochoric left Cauchy-Green strain tensor. The superscripts d, h, e and p denote the deviatoric, hydrostatic, elastic and plastic part, respectively. The mode number is denoted with subscript i. The time derivatives capturing the evolution of J and $\tilde{\mathbf{B}}_{e,i}$ are given by:

$$\dot{J} = J\mathrm{tr}(\mathbf{D}) \tag{4B.4}$$

$$\overset{\nabla}{\tilde{\mathbf{B}}}_{e,i} = (\tilde{\mathbf{L}} - \mathbf{D}_{p,i}) \cdot \tilde{\mathbf{B}}_{e,i} + \tilde{\mathbf{B}}_{e,i}(\tilde{\mathbf{L}}^c - \mathbf{D}_{p,i})\,, \tag{4B.5}$$

where $\tilde{\mathbf{L}}$ is the isochoric velocity gradient tensor. The plastic deformation rate tensor $\mathbf{D}_{p,i}$ is related to the deviatoric stress $\sigma_{s,i}^d$ via a non-Newtonian flow rule:

$$\mathbf{D}_{p,i} = \frac{\sigma_{s,i}^d}{2\eta_i(T, \overline{\tau}, p, S)}\,. \tag{4B.6}$$

The viscosities η_i depend on equivalent stress $\overline{\tau}$ and are described by a modified Eyring flow rule [21, 25], in which the pressure dependence (μ) and strain

softening (S) are taken into account [21, 26–28]:

$$\eta_i = \eta_{0,i,ref}(T) \cdot \frac{\frac{\overline{\tau}}{\tau_0}}{\sinh\left(\frac{\overline{\tau}}{\tau_0}\right)} \cdot \exp\left(\frac{\mu p}{\tau_0}\right) \cdot \exp\left(S(\overline{\gamma}_p)\right) , \tag{4B.7}$$

where τ_0 denotes the characteristic stress and $\eta_{0,i,ref}(T)$ the temperature dependent pre-exponential factor, which is given by:

$$\eta_{0,i,ref}(T) = \eta_{0,i,ref} \cdot \exp\left(\frac{\Delta U}{RT}\right). \tag{4B.8}$$

Here ΔU is the activation energy, R the gas constant, T the absolute temperature and $\eta_{0,i,ref}$ the zero-shear viscosities, defined with respect to the reference (unaged) state [22]. The characteristic stress, τ_0, the total equivalent stress, $\overline{\tau}$, and the hydrostatic pressure, p, where the last two depend on the total stress, not on the modal stress, are defined according to:

$$\tau_0 = \frac{kT}{V^*} \quad ; \quad \overline{\tau} = \sqrt{\frac{1}{2}\sigma_s^d : \sigma_s^d} \quad ; \quad p = -\frac{1}{3}tr(\sigma), \tag{4B.9}$$

with k Boltzmann's constant and V^* the activation volume.

The intrinsic strain softening (S) is expressed in the state parameter (S_a), which uniquely defines the current thermodynamic state of the material [22], and the softening function ($R(\overline{\gamma}_p)$),

$$S(\overline{\gamma}_p) = S_a \cdot R(\overline{\gamma}_p) . \tag{4B.10}$$

$R(\overline{\gamma}_p)$ non-linearly depends on the equivalent plastic strain $\overline{\gamma}_p$:

$$R(\overline{\gamma}_p) = \frac{\left(1 + \left[r_0 \cdot \exp(\overline{\gamma}_p)\right]^{r_1}\right)^{\frac{r_2-1}{r_1}}}{\left(1 + r_0{}^{r_1}\right)^{\frac{r_2-1}{r_1}}}, \tag{4B.11}$$

where r_0, r_1 and r_2 are fitting parameters, while the equivalent plastic strain rate ($\dot{\overline{\gamma}}_p$), is coupled to the mode with the highest initial viscosity, referred to as mode 1, since that determines the development of plastic strain $\overline{\gamma}_p$:

$$\dot{\overline{\gamma}}_p = \frac{\overline{\tau}_1}{\eta_1} \quad \text{where} \quad \overline{\tau}_1 = \sqrt{\frac{1}{2}\sigma_{s,1}^d : \sigma_{s,1}^d}. \tag{4B.12}$$

The parameters that are used in this study for uPVC are reproduced in Table 4B.1 and the spectrum of relaxation times is given in Table 4B.2. These parameters

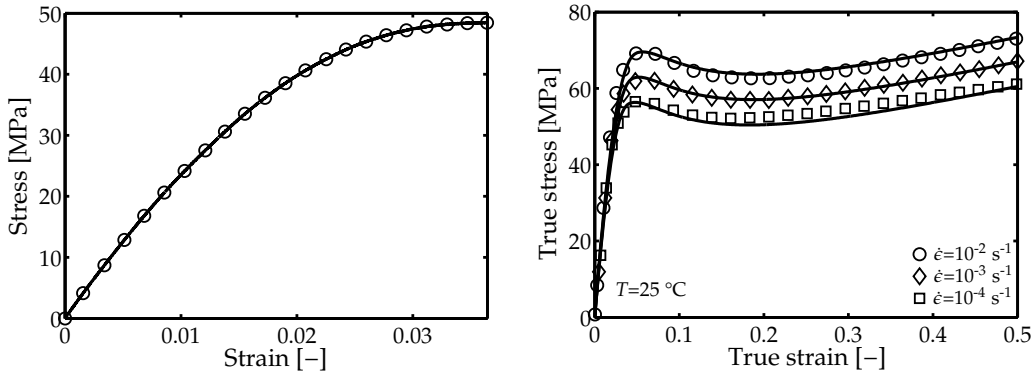

Figure 4B.1 *The experimental data used for the fitting procedure including the result of the best fit.* ***Left:*** *a stress strain curve for an as-manufactured tensile specimen, measured at a strain rate of 10^{-3} s^{-1} (markers) and the curve resulting from the relaxation spectrum denoted in Table 4B.2 (solid line).* ***Right:*** *the intrinsic deformation behaviour of uPVC as measured in uniaxial compression (markers) and the best fit of the constitutive model (solid lines) resulting in the parameters values in Table 4B.1.*

were obtained from a best fit on the true stress versus true strain curves as obtained with compression experiments. The resulting description of the intrinsic behaviour is shown in Figure 4B.1 for three different strain rates. The model shows to describe the intrinsic behaviour of uPVC accurately.

Table 4B.1 *Parameters in the EGP-model for uPVC.*

parameter	value	unit
G_{tot}	871	MPa
V^*	2.76	nm^3
G_r	17.75	MPa
κ	4.0	GPa
μ	0.14	
r_0	0.99	
r_1	50.8	
r_2	-4.00	

Table 4B.2 *Relaxation spectrum for an as-manufactured uPVC specimen.*

mode	$\eta_{0,i,ref}$ [MPa · s]	G_i [MPa]	λ_i [s]
1	$1.45 \cdot 10^9$	$5.03 \cdot 10^2$	$2.89 \cdot 10^6$
2	$2.38 \cdot 10^7$	$8.75 \cdot 10^1$	$2.72 \cdot 10^5$
3	$4.29 \cdot 10^6$	$5.15 \cdot 10^1$	$8.34 \cdot 10^4$
4	$8.86 \cdot 10^5$	$1.43 \cdot 10^1$	$6.21 \cdot 10^4$
5	$7.93 \cdot 10^5$	$4.16 \cdot 10^1$	$1.91 \cdot 10^4$
6	$3.45 \cdot 10^5$	$2.46 \cdot 10^1$	$1.42 \cdot 10^4$
7	$1.69 \cdot 10^5$	$3.89 \cdot 10^1$	$4.35 \cdot 10^3$
8	$4.47 \cdot 10^4$	$4.49 \cdot 10^1$	$9.94 \cdot 10^2$
9	$4.91 \cdot 10^3$	$39.0 \cdot 10^1$	$1.26 \cdot 10^2$
10	$4.19 \cdot 10^2$	$2.63 \cdot 10^1$	$1.59 \cdot 10^1$

Conclusions, recommendations and challenges

Conclusions

In this thesis the framework for a method that can determine the residual lifetime of unplasticised poly(vinyl chloride) (uPVC) gas pipes was developed. The main safety concern to gas distribution companies is brittle fracture behaviour at impact loads. It was argued that physical ageing contributes most to the embrittlement during the service lifetime of uPVC gas pipes. This ageing process is related to a change of the thermodynamic state of the material. It was shown that the thermodynamic state can be directly related to the yield stress (Chapter 2). From Chapter 3 it is learned that since the thermodynamic state is also related to the impact resistance, the yield stress can be employed as a measure for the condition (in this case the impact resistance) of the material.

The experiments performed to determine the yield behavior of uPVC as a function of strain rate and temperature can be exploited to quantitatively predict the time-to-(ductile)failure of uPVC subjected to a certain load. The yield stress behaviour of the polymer can be accurately described with a pressure-modified Eyring reaction rate relation. Combined with a constant critical plastic strain criterion, this description can be employed to quantitatively predict the time-to-(ductile)failure of uPVC subjected to a certain load. The resulting engineering approach can account for the influence of temperature, the loading geometry, the thermo-mechanical history as well as the influence of frequency and stress ratio (in case of a cyclic load). Furthermore, it is possible to determine the long-term hydrostatic strength (LTHS) with the engineering approach using only short-term tests, eliminating the necessity to carry out the conventionally used, expensive, long-term pressurised pipe tests. For this approach to work, it must be assumed that slow crack growth failure does not limit the LTHS, which is the case for uPVC gas pipes as shown in Chapter 2.

The process of physical aging accelerates at elevated temperatures and under applied loads. Consequently, the increase in yield stress with ageing becomes apparent at shorter time scales, when uPVC is stored at elevated temperatures or

when the material is subjected to a (tensile) stress. The accelerated ageing kinetics can be described with an Arrhenius and a reaction rate type relation. Incorporating the ageing description in the engineering approach enables quantitative predictions of the so-called endurance limit observed in the long-term ductile failure behaviour of uPVC under static loading conditions.

Unplasticised PVC specimens that are subjected to a cyclic load can in some cases display a different type of failure kinetics: fatigue crack growth. Extrapolations from fatigue crack growth failure data show that (slow) crack growth failure is not expected to occur within the service lifetime of a uPVC gas pipe operated at a constant pressure.

The rate of physical ageing of a recently produced water pipe grade uPVC is significantly lower than that of a uPVC gas pipe produced several decades ago. Consequently, the ageing induced increase of the ductile-to-brittle transition temperature, and thus the amount of embrittlement, of the water pipe grade is less pronounced than the increase that can be expected for the uPVC gas pipe grade.

Finally, the potential of micro-indentation measurements as a means to determine the yield stress of uPVC in a macroscopically non-destructive manner has been shown in Chapter 4. Since the yield stress is related to both thermodynamic state and impact behaviour, the residual lifetime of uPVC gas pipes can be estimated from the measured hardness.

Still, additional research is required to put the residual lifetime procedure, that was proposed in this thesis, into practice. Some matters of interest for further research are given in the next section.

Recommendations

An old GIVEG-standard was used as a starting point for determining the critical thermodynamic state at which uPVC pipes become too brittle. This standard describes a falling weight test in which a pipe segment should not fail at a temperature of 0 °C. For characterisation of the influence of physical ageing on the impact behaviour of uPVC as described in Chapter 3 a similar, but instrumented, setup was selected. The selected setup requires a large amount of pipe material for the characterisation procedure, which was not available for the pipe grade used in Chapter 1 and 2. The experiments were, therefore, performed on uPVC pipes that were recently produced for water distribution purposes. On hindsight it would have been of interest to use a different type of impact test (for example a Charpy test) for which only a small amount of material is required.

This would have made it possible to characterise the impact behaviour of the gas pipe grade that was used for all other experiments throughout this thesis. Furthermore, the critical thermodynamic state for the gas pipe grade can best be determined by performing the selected impact test at a constant, predetermined temperature on specimens at different thermodynamic states. The mechanical properties corresponding to the state at which the pipes behave (too) brittle can be used as a criterion.

The impact experiments on the water pipe grade revealed a remarkable difference between the ageing behaviour of the two pipe grades used. In Chapter 3 several reasons for this difference have been put forward (difference in crystallinity, anti-plasticisation effect). The viability of each of these reasons has to be verified. Doing so requires a more physical approach. It would especially be of interest to know whether such differences in ageing kinetics can also be expected in the uPVC pipe grades used in the gas network. If so, these differences should be accounted for in determining the residual lifetime. Unpublished results of experimental work, carried out within the present research project, suggests that some differences between the pipes originating from different suppliers might be present. Some tensile experiments were carried out on two other pieces of uPVC pipe material originating from pipes with an outer diameter of 60 mm and 110 mm. The 110 mm pipe showed identical ageing behaviour as the pipe investigated throughout this thesis and had an ageing activation volume of 113 kJ/mol (opposed to a value of 115 kJ/mol found in Chapter 2). Not enough experiments were carried out on the 60 mm pipe to accurately determine its activation volume, but the ageing effects seemed less severe than for the other types of pipe. Additional (mechanical) experiments are required to verify this observation.

The engineering approach presented in Chapter 1 and extended with ageing kinetics in Chapter 2 was employed to predict the time-to-failure of uPVC specimens subjected to both constant and dynamic loads. Whereas the constant load experiments were predicted quantitatively, the failure time predictions for the dynamic loads were somewhat on the conservative side. The ductile fatigue failure data can be predicted accurately by using a 20% higher value for the activation volume. It is of interest to find out whether this difference in activation volume has a physical background or if it is an experimental artefact, such as (local) hysteretic heating of the specimens.

One of the main assumptions in this work is that the impact resistance limits the residual lifetime of uPVC gas pipes. This means that failure as a result of slow crack growth is not considered as a process that causes failure within the expected service lifetime of uPVC gas pipes. Extrapolation of preliminary results of fatigue crack growth measurements presented in Chapter 2, showed that this assumption

is justified for gas pipes. If installed correctly, these pipes only bear a small (constant) load during their service life. The location of the transition from yield failure towards slow crack growth failure in the creep rupture curve of uPVC is only roughly estimated and additional fatigue crack growth measurements at constant stress ratios should be carried out to confirm and increase the accuracy of the extrapolation procedure. Fatigue crack growth rate experiments could be carried out at a range of stress ratios (R). Measurements at increased temperatures could be useful to enable fatigue crack growth measurements up to, or at least close to, R=1 within experimentally acceptable timescales. The results can be used to determine the function that should be used to extrapolate the fatigue crack growth data at room temperature towards R=1. Furthermore, if it is indeed possible to measure the slow crack growth rate (thus at R=1) at elevated temperatures, it might also be possible to measure the location of the transition from yield to crack growth failure in a creep rupture plot at this temperature. The slow crack growth predictions based on the fatigue crack growth measurements can then be verified. These additional measurements are not just of interest for determining the slow crack growth rate more accurately. The measurements can also be used to model the crack growth rate in uPVC water pipes, which operate at pressures up to 6 bar and are also subjected to a fatigue load: water hammer, caused by closure of valves, results in oscillations of the operating pressure. Fatigue crack growth can therefore occur in water distribution pipes. This is confirmed by failure data as spontaneous ruptures have been reported in the water distribution network. Based on this observation one can conclude that monitoring the evolution of the yield stress alone is probably not sufficient for water distribution pipes. Therefore it is of interest to study the crack growth kinetics into more depth as proposed above.

Challenges

The indentation measurements presented in Chapter 4 were carried out in a laboratory under well defined testing conditions. Putting the same tests into practice by employing an autonomous robot to carry out the measurement within a gas pipe which is still in service is obviously more challenging. The measurement should be more robust to minimise the influence of changes in temperature, dust on the pipe's inner surface, gas condensate at the bottom of the pipe, et cetera. A potential solution lies in the principle of a Poldi hardness tester, where a steel ball is pressed simultaneously into both a reference bar with a known hardness and the specimen. Comparison of the resulting indent in the specimen and reference bar reveals whether the specimen has a higher or

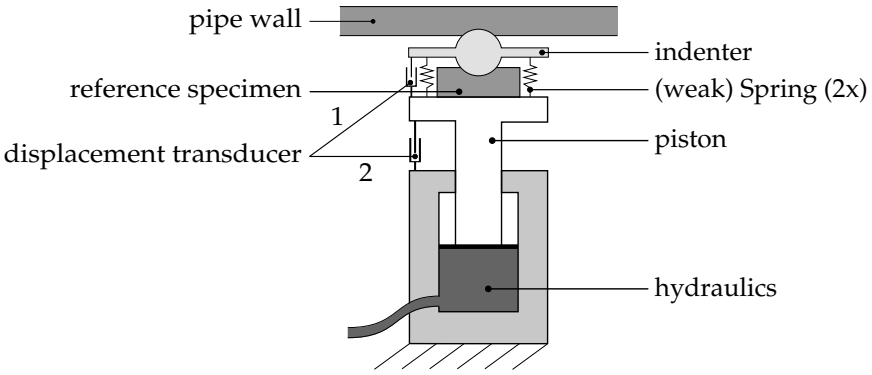

Figure 1 *Schematic representation of a differential indentation device.*

lower hardness than the reference bar. As already stated in the introduction of Chapter 4, post mortem measurement of an indent is troublesome for polymers. Therefore, the use of a differential indentation device is proposed.

The principle of the proposed differential indentation device is shown schematically in Figure 1. During measurement a hydraulic system causes the piston to move upwards until the ball reaches the surface of the pipe wall. Increasing the pressure inside the piston to a predefined value causes an indentation of the ball in both the pipe wall and the reference specimen with an equal load. The displacement of the piston and the ball are recorded separately. The signals make it possible to calculate the displacement of the ball into the reference sample (equal to the displacement of transducer 1) and the displacement of the ball into the pipe wall (equal to the difference between the displacement of transducer 2 and the displacement of transducer 1). The difference in displacement can be used as a measure for the residual lifetime of the pipe. If a piece of uPVC at the critical thermodynamic state is chosen as the reference specimen, the pipe should be taken out of service if the displacement of the ball into the pipe wall is smaller than the displacement of the ball into the reference specimen.

The difference in yield stress between the pipe wall and the reference sample that can still be distinguished depends on the radius of the ball, the maximum force applied and the precision of the displacement transducers. As an illustration of the precision that can be reached with the proposed device, the precision is estimated for a ball with a radius of 2.5 mm. A ball of this size minimises local effects, whilst keeping the required indentation force reasonably low. For a maximum force of 300 N the ball penetrates about 115 µm into a specimen with a hardness of 170 MPa. The linear relation between the yield stress and hardness

was found to have a slope of about 0.67 MPa/MPa in Figure 4.6. Assuming the displacements can be measured with a precision of 1 µm, a difference of about 1 MPa in the yield stress can be distinguished.

Obviously, further research is required to optimise the geometry, force range, accuracy of the device and overcome problems such as how to differentiate between elastic and plastic deformation of the pipe wall. Moreover, indentation measurements on several different pieces of excavated uPVC gas pipes should be carried out to get an idea about the hardness range and differences that can be expected in the gas distribution network. These recommendations can be used as a promising start towards the practical realisation of an in situ non-destructive residual lifetime assessment method for uPVC gas pipes.

Dankwoord

Het is algemeen geaccepteerd dat het dankwoord het meest gelezen stuk tekst in een proefschrift is. Dat is jammer (er staat niks nieuws in), maar begrijpelijk. Het is wat luchtiger dan de rest van het boekje en het geeft antwoord op de vraag of jouw belangrijke bijdrage aan het boekje genoemd wordt. Om te bevorderen dat ook de rest van de bladzijden voldoende daglicht krijgen heb ik voor de fanatici een aantal "eastereggs" in dit boekje verstopt. Elke eerste vinder die zich per e-mail (zie boekenlegger) meldt, krijgt een presentje. Dat gezegd hebbende wil ik nu overgaan op het specifiek bedanken van een aantal mensen die een onmisbare bijdrage hebben geleverd aan mijn onderzoek en daarmee aan de totstandkoming van dit proefschrift.

Allereerst wil ik Mannes Wolters bedanken. Hij heeft het voor mij mogelijk gemaakt om dit onderzoek uit te voeren. Zijn interesse en betrokkenheid in het onderzoek hebben mij erg gemotiveerd. Daarnaast heeft hij door regelmatig de rol als advocaat van de duivel op zich te nemen, ervoor gezorgd dat ik kritisch bleef kijken naar de resultaten en de gemaakte keuzes. Mannes bedankt!

Remko Akkerman, ik vind het bewonderenswaardig hoe je altijd weer precies op de juiste momenten de juiste bijdrage weet te leveren. Verder wil ik je bedanken voor de prettige sfeer die je in de vakgroep Productie Technologie weet neer te zetten.

In het eerste jaar van mijn promotieonderzoek ben ik op bezoek gegaan bij Leon Govaert in Eindhoven en er vervolgens niet meer weg gegaan. Zijn ideeën, creativiteit en vooral zijn enthousiasme omtrent de polymeertechnologie is op vrijwel elke bladzijde van dit boekje terug te vinden. Bedankt Leon, en help me even; het was R.M. Louis de 13^{de} toch?

Het is inmiddels wel duidelijk dat ik een uitgebreid team van begeleiders had. Daarbij mag de begeleiding van Ton Bor zeker niet worden vergeten. Door zijn metaalkundige achtergrond bekeek hij de zaken vaak vanuit een ander perspectief. Daarmee wist hij problemen vrijwel altijd te laten verdwijnen als sneeuw voor de zon. Hopelijk zien we in mei 2010 de sneeuw inderdaad voor de zon verdwijnen tijdens het jaarlijkse fietstochtje in zuid-Frankrijk.

Naast de hiermee benoemde begeleiders had ik ook nog een begeleidingsgroep (het kon niet op). Per sponsor kwam er twee à drie keer per jaar een afgevaardigde naar Enschede om de voortgang en de onderzoekslijn te bespreken. Deze input vanuit het bedrijfsleven was voor mij de reden om juist voor dit promotieonderzoek te kiezen en was onmisbaar voor de inhoud van het boekje zoals deze voor je ligt. Paul Latta, Roger Janssen, Wim van Erp, Bart Vogelzang, Hans van der Vegt, Eelco Trietsch, Martin Meerkerk en Roger Loop bedankt voor jullie kritische blik vanuit de praktijk.

Ik wil iedereen waarmee ik gedurende mijn promotieonderzoek ben opgetrokken bedanken voor de schitterende tijd die ik heb gehad in mijn tijd als promovendus. Daarnaast wil ik een aantal mensen meer specifiek bedanken. Laurent: bedankt voor het aanwakkeren van het Mud & Foam vuur in mij, het uitstapje in de wereld van de breukmechanica en de experimentele ondersteuning (lees flanzen). Tom: bedankt voor de spoedcursus "Experimenteren en modeleren met polymeren". Lambert: bedankt voor het uitvoeren van de numerieke simulaties die in hoofstuk 4 zijn beschreven, de hulp bij de interpretatie van deze resultaten en al die andere zaken waarvoor ik altijd bij je kon aankloppen. Norbert en de Theo's: bedankt voor de praktische ondersteuning bij het flanzen. Sjef: bedankt voor het maken van de prupkes en alle andere PVC gerelateerde proef- en hulpstukken. Joris: bedankt voor het zetten van de eerste stappen in de scheurgroeimetingen waardoor hoofdstuk 2 een stuk leuker is geworden. Belinda, Debbie, Tanja, Marleen, Yvon en Alice: bedankt voor het regelen van zaken waar ik, net als menig ander promovendus, zo min mogelijk mee te maken wilde hebben. Marlous: bedankt voor je interesse in de PVC gasleidingen en het leuke afstudeerwerk dat je hebt uitgevoerd. Gerrit, Erik en Walter: bedankt voor de gastvrijheid en hulp in het Tribologielab. Datzelfde geldt voor de heer "van Marsi", alleen dan voor het Multiscale-lab. Bart en Sam: bedankt voor het uitvoeren van een aantal van de in dit boekje beschreven experimenten. Durk: bedankt voor het kritisch doorlezen van het concept en de jaarlijkse Texelse schuimen. Ashok: bedankt voor de Engelse correcties. Sjoerd: tijd om de dank voor de niet altijd smakelijke, maar wel altijd gezellige mensa-hap terug te geven. Nicht @nnet: bedankt voor de leuke buitenlandse excursies. Neef Joost: bedankt voor de inspirerende lunches. Barry en Wouter: bedankt voor het aan mijn zijde staan de 22ste. Peter: bedankt voor het opsturen van vergeten documenten. Dit geldt ook voor Wouter en Sebastiaan in de gevallen dat ik iets in Enschede had vergeten. Fred & Ed (al.): bedankt voor het aantrekkelijk maken van beleggen. Wim: je oven doet het nog steeds, bedankt! Bram: bedankt voor de inspiratie als ik even vast zat met schrijven. Esther: bedankt voor de tips & tricks van de kenner, het opdoen van de nu broodnodige kluservaring en de kennismaking met Fritsie. Anton, Elena, Clemens, Marcoon, Joost P., Sjoerd en neef Joost:

bedankt voor de gastvrijheid in mijn tijd als nomade. T.J. Idema: bedankt voor het bijna schrijven van een ongetwijfeld schitterend voorwoord. Alle collega's in Enschede, Eindhoven en Arnhem: bedankt voor alle hulp en gezelligheid!

Een speciaal woord van dank voor mijn ouders. Met hen is het immers voor mij allemaal begonnen. Jullie dachten me niet te kunnen helpen met het afronden van mijn boekje, maar het is jullie erg goed gelukt. Bedankt voor jullie altijd aanwezige stimulans en wat al niet meer.

De laatste woorden van dank gaan, zoals traditie dit voorschrijft, naar mijn vriendin Inge. Bedankt dat je, ondanks jouw onmogelijke werktijden (zie stelling 8), me toch altijd weer op de juiste momenten hebt weten te steunen. Ik weet niet of het symbolisch is dat we precies de week dat ik dit proefschrift afrond dan toch eindelijk echt gaan samenwonen, maar ik weet wel dat ik er heel veel zin in heb!

Roy
Nijmegen, december 2009